UNIVERSITY OF CALIFORNIA,
IRVINE

Mitochondrial Zn^{2+} accumulation in ischemic neuronal injury: evidence from *in vitro* models and evaluation for delayed interventions

DISSERTATION

submitted in partial satisfaction of the requirements
for the degree of

DOCTOR OF PHILOSOPHY

in Anatomy & Neurobiology

by

Sunggoan Ji

Dissertation Committee:
Professor John H Weiss, Chair
Associate Professor David Christian Lyon
Professor Edwin S Monuki

2020

DEDICATION

To my grandfather, who nurtured me with kindness as a young boy and whose tragic disease started my interest in the neurosciences and medicine

TABLE OF CONTENTS

LIST OF FIGURES

ACKNOWLEDGMENTS

This work was made possible by the financial supports from NIH, the American Heart Association, and UCI Grad Division. Permission to use copyrighted materials in published manuscripts has been granted per the policies of the respective journals.

First of all, I would like to thank my advisor Dr. John Weiss. While he has been instrumental in shaping my view as a scientist, from cell culture, imaging, to manuscript and grant writing, the most important lesson I will carry with me will be his teaching that research is not about just finding solutions or cures, it is about asking the right questions.

Beyond Dr. Weiss, I have been fortunate enough to meet and learn from great mentors, both in the lab bench and in the wards. I would like to thank Dr. Yama Akbari for the advice he gave me during my graduate phase and the rigorous clinical training he gave me in the wards. To Dr. Edwin Monuki, for his mentorship starting almost immediately from the moment I started medical school. To Dr. David Lyon, for being a constant figure as a graduate advisor. And to Dr. Alena Savonenko and Dr. Bronwen Martin, who mentored me during my undergraduate years.

Thank you to my friends all over the world, many of whom are like family to me and whose friendship I feel privileged to have been part of.

And lastly, to my family, my greatest supporters. I would not be where I am currently without my parent's sacrifices to give their children a chance to gain an education in the United States to improve our life. To my brother, who despite his silence and cool demeanor, has always been proud of and supportive of me. And finally, to my wife Maarika. Without her support and love during these times have been unconditional to the extent that I cannot imagine having completed this without her presence by my side.

CURRICULUM VITAE

Sunggoan 'Sung' Ji

Education

MD/PhD University of California Irvine, Anatomy & Neurobiology — Present
Medical Scientist Training Program
Committee: John H Weiss MD PhD (chair),
Edwin Monuki MD PhD, David Lyon PhD

MS Johns Hopkins University, Molecular & Cellular Biology — May 2010
"The effects of energy restriction and excess on the HPA axis"
Principal Investigator: Bronwen Martin, PhD

BS Johns Hopkins University, Molecular & Cellular Biology — May 2009
General and departmental honors in Molecular and Cellular Biology
Dean's List every semester

Honors and Awards

American Heart Association Predoctoral Fellowship — 2016 - 2018
Stipend and research support for 2 years ($53,688)

UC Irvine MSTP student of the year Award — 2017
Recognition for the highest contribution to the program of the year

University of California Irvine, Graduate Bridge Funding — 2015 - 2016
Bridge funding prior to receiving fellowship

Post-baccalaureate Intramural Research Training Award — 2010 - 2011
Full time research opportunity awarded to recent graduates
Stipend support

Research Experience

University of California Irvine, Irvine CA — June 2013 – May 2018
Graduate Student (Researcher), John H Weiss MD PhD

- Cellular neuroscience
- Primary neuron culture
- Fluorescent imaging microscopy
- 5 publications, 1 submitted

University of California Irvine, Irvine CA June 2012 – August 2012
Rotation Student, Tallie Z Baram, MD PhD

- Neurobiology of epilepsy
- Behavioral test
- Immunofluorescence assay
- 2 publications

National Institute on Aging, Baltimore MD June 2008 – March 2011
Postbaccalaureate Trainee, Bronwen Martin PhD

- Neuroendocrinology
- Behavioral test
- Animal husbandry
- 7 publications

Johns Hopkins University, Baltimore MD Oct 2006 – May 2008
Research Assistant, Alena Savonenko MD PhD

- Neuropathology of Alzheimer's Disease
- Behavioral test
- Animal husbandry

Teaching Experience

University of California Irvine, Irvine CA May 2013 – Present
Teaching Assistant, Medical Neuroscience (for medical students only)

- Worked with course director Ana Solodkin organize weekly review session
- Held weekly office hours

Johns Hopkins University, Baltimore MD August 2009 to May 2010
Teaching Assistant, General Biology I – II (with labs)

- Led weekly lab section consisting of 30 – 40 students
- Held weekly office hours
- Scored examinations

Work Experience

Cornell University, Ithaca NY August 2019 – Present
Scientific editor, for the laboratory of Esak Lee PhD, Assistant Professor

- Edit manuscripts, grant applications, and any other materials for clarity and grammatical correctness
- 5 – 6 hours of work

Publications

1. **Ji SG**, Medvedeva YV, Weiss JH.
Zn^{2+} entry through the mitochondrial calcium uniporter is a critical contributor to mitochondrial dysfunction and neurodegeneration.
Exp Neurol. 2020;325:113161. doi:10.1016/j.expneurol.2019.113161

2. Yin HZ, Wang HL, **Ji SG**, Medvedeva YV, Tian G, Bazrafkan AK, Maki NZ, Akbari Y, Weiss JH.
Rapid Intramitochondrial Zn2+ Accumulation in CA1 Hippocampal Pyramidal Neurons After Transient Global Ischemia: A Possible Contributor to Mitochondrial Disruption and Cell Death.
J Neuropathol Exp Neurol. 2019 May 9. pii: nlz042. doi: 10.1093/jnen/nlz042

3. **Ji SG,** Medvedeva YV, Wang HL, Yin HZ, Weiss JH.
Mitochondrial Zn^{2+} Accumulation: A Potential Trigger of Hippocampal Ischemic Injury.
Neuroscientist. 2018 May 1:1073858418772548. doi: 10.1177/1073858418772548.

4. **Ji SG**, Weiss JH.
Zn^{2+}-induced disruption of neuronal mitochondrial function: Synergism with Ca^{2+}, critical dependence upon cytosolic Zn^{2+} buffering, and contributions to neuronal injury.
Exp Neurol. 2018 Apr;302:181-195. doi: 10.1016/j.expneurol.2018.01.012. Epub 2018 Jan 24.

5. Medvedeva YV, **Ji SG**, Yin HZ, Weiss JH.
Differential Vulnerability of CA1 versus CA3 Pyramidal Neurons After Ischemia: Possible Relationship to Sources of Zn^{2+} Accumulation and Its Entry into and Prolonged Effects on Mitochondria.
J Neurosci. 2017 Jan 18;37(3):726-737. doi: 10.1523/JNEUROSCI.3270-16.2017.

6. Lee TC, Frangos SN, Torres M, Winckler B, **Ji SG**, Dow E.
Integrating Undergraduate Patient Partners into Diabetes self-management education: Evaluating a free clinic pilot program for the Underserved.
J Health Care Poor Underserved. 2016;27(4):1689-1708.

7. Maras PM, Molet J, Chen Y, Rice C, **Ji SG**, Solodkin A, Baram TZ.
Preferential loss of dorsal-hippocampus synapses underlies memory impairments provoked by short, multimodal stress.
Mol Psychiatry. 2014 Mar 4. doi: 10.1038/mp.2014.12.

8. Clausen A, McClanahan T, **Ji SG**, Weiss JH.
Mechanisms of Rapid Reactive Oxygen Species Generation in Response to Cytosolic Ca^{2+} or Zn^{2+} Loads in Cortical Neurons.
PLoS One. 2013 Dec 10;8(12):e83347. doi:10.1371/journal.pone.0083347

9. Cope JL, Regev L, Chen Y, Korosi A, Rice CJ, **Ji S**, Rogge GA, Wood MA, Baram TZ.
Differential contribution of CBP:CREB binding to corticotropin-releasing hormone expression in the infant and adult hypothalamus.
Stress. 2013 Jul 5

10. Cai H, Cong WN, **Ji S**, Rothman S, Maudsley S, Martin B.
Metabolic dysfunction in Alzheimer's disease and related neurodegenerative disorders.
Curr Alzheimer Res. 2012 Jan;9(1):5-17. Review.

11. Hallböök T, **Ji S**, Maudsley S, Martin B.
The effects of the ketogenic diet on behavior and cognition.
Epilepsy Res. 2012 Jul;100(3):304-9. Epub 2011 Aug 27.

12. Shin YK, Martin B, Kim W, White CM, **Ji S**, Sun Y, Smith RG, Sévigny J, Tschöp MH, Maudsley S, Egan JM.
Ghrelin is produced in taste cells and ghrelin receptor null mice show reduced taste responsivity to salty (NaCl) and sour (citric acid) tastants.
PLoS One. 2010 Sep 14;5(9):e12729. doi: 10.1371/journal.pone.0012729.

13. White CM, **Ji S**, Cai H, Maudsley S, Martin B.
Therapeutic potential of vasoactive intestinal peptide and its receptors in neurological disorders.
CNS Neurol Disord Drug Targets. 2010 Nov;9(5):661-6. Review.

14. Martin B, **Ji S**, Maudsley S, Mattson MP.
"Control" laboratory rodents are metabolically morbid: why it matters.
Proc Natl Acad Sci U S A. 2010 Apr 6;107(14):6127-33. Epub 2010 Mar 1.

15. Martin B, Shin YK, White CM, **Ji S**, Kim W, Carlson OD, Napora JK, Chadwick W, Chapter M, Waschek JA, Mattson MP, Maudsley S, Egan JM.
Vasoactive intestinal peptide-null mice demonstrate enhanced sweet taste preference, dysglycemia, and reduced taste bud leptin receptor expression.
Diabetes. 2010 May;59(5):1143-52. Epub 2010 Feb 11.

16. Martin B, Dotson CD, Shin YK, **Ji S**, Drucker DJ, Maudsley S, Munger SD.
Modulation of taste sensitivity by GLP-1 signaling in taste buds.
Ann N Y Acad Sci. 2009 Jul;1170:98-101.

17. Martin B, **Ji S**, White CM, Maudsley S, Mattson MP. (2009). Dietary Energy Intake, Hormesis, and Health. In Mark P Mattson, Edward J Calabrese (Ed.), Hormesis: A revolution in biology, toxicology and medicine (pp. 123-137). New York: Springer.

Presentations

"Zn^{2+} entry through the mitochondrial calcium uniporter (MCU) contributes critically to mitochondrial dysfunction and neurodegeneration after neuronal Zn^{2+} loading and ischemia"
Sung G Ji, Yuliya V Medvedeva, John H Weiss
Society for Neuroscience, 2018

"Zn^{2+} induced mitochondrial dysfunction: dependence upon disruption of buffering, synergism with Ca^{2+} and contributions to neuronal injury in vitro and in vivo"
Sung G Ji, Yuliya V Medvedeva, Hong Z Yin, John H Weiss
Society for Neuroscience, 2017
Biophysical Society, 2018

"Zn^{2+} triggered mitochondrial dysfunction depends upon entry via the mitochondrial Ca^{2+} uniporter"
Sung G Ji, John H Weiss
Society for Neuroscience, 2016

"Mechanisms of Rapid Reactive Oxygen Species Generation in Response to Cytosolic Ca^{2+} or Zn^{2+} Loads in Cortical Neurons."
Clausen A, McClanahan T, Ji SG, Weiss JH.
University of California, Irvine Third International Epilepsy Research Center Symposium, 2014

ABSTRACT OF THE DISSERTATION

Mitochondrial Zn^{2+} accumulation in ischemic neuronal injury: critical dependence upon entry through the mitochondrial calcium uniporter and the potential of delayed interventions

By

Sunggoan Ji

Doctor of Philosophy in Anatomy & Neurobiology

University of California, Irvine, 2019

Professor John H Weiss, Chair

Ischemic stroke is a major cause of death and disabilities worldwide, and it has been long hoped that improved understanding of relevant injury mechanisms would yield targeted neuroprotective therapies. While Ca^{2+} overload during ischemia-induced glutamate excitotoxicity has been identified as a major contributor, failures of glutamate targeted therapies to achieve desired clinical efficacy have dampened early hopes for the development of new treatments. However, additional studies examining possible contributions of Zn^{2+}, a highly prevalent cation in the brain, have provided new insights that may help to rekindle the enthusiasm. In this thesis, we discuss findings yielding clues as to sources of the Zn^{2+} that accumulates in many forebrain neurons after ischemia, and mechanisms through which it mediates injury, specifically highlighting the growing evidence of important Zn^{2+} effects on mitochondria. First, using brief high (90 mM) K^+/Zn^{2+} exposures to mimic neuronal depolarization and extracellular Zn^{2+} accumulation as may accompany ischemia *in vivo*, we examined effects of disrupted cytosolic Zn^{2+} buffering and/or the presence of Ca^{2+}, and made several observations: **1.** Mild disruption of

cytosolic Zn^{2+} buffering—while having little effects alone—markedly enhanced mitochondrial Zn^{2+} accumulation and dysfunction (including loss of $\Delta\Psi_m$, ROS generation, swelling and respiratory inhibition) caused by relatively low (10 – 50 μM) Zn^{2+} with high K^+. **2.** The presence of Ca^{2+} during the Zn^{2+} exposure decreased cytosolic and mitochondrial Zn^{2+} accumulation, but markedly exacerbated the consequent dysfunction. **3.** Paralleling effects on mitochondria, disruption of buffering and presence of Ca^{2+} enhanced Zn^{2+}-induced neurodegeneration. We also use recently available MCU knockout mice to examine how the deletion of this channel impacts deleterious effects of Zn^{2+}. In cultured cortical neurons from MCU knockout mice, we find significantly reduced mitochondrial Zn^{2+} accumulation. Correspondingly, these neurons were protected from both acute and delayed Zn^{2+}-triggered mitochondrial dysfunction, including mitochondrial reactive oxygen species generation, depolarization, swelling and inhibition of respiration. Furthermore, when toxic extramitochondrial effects of Ca^{2+} entry were moderated, both cultured neurons (exposed to Zn^{2+}) and CA1 neurons of hippocampal slices (subjected to prolonged oxygen glucose deprivation to model ischemia) from MCU knockout mice displayed decreased neurodegeneration. Finally, to examine the therapeutic applicability of these findings, we added a Zn^{2+} chelator or MCU blocker after Zn^{2+} exposure in wildtype neurons (to induce post-insult MCU blockade). This significantly attenuated the delayed evolution of both mitochondrial dysfunction and neurotoxicity. Taken together, these data support the hypothesis that mitochondrial Zn^{2+} accumulation is a critical contributor to ischemic neurodegeneration that could be targeted for neuroprotection.

INTRODUCTION

Ischemic stroke: the role of Ca^{2+}

Ischemic stroke is a leading cause of disability and death worldwide, reflecting the extreme sensitivity of brain to even brief (several minutes) disruption of blood flow. Despite extensive efforts to understand the basis of this unique vulnerability with the aim of developing neuroprotective interventions, attempts to date have failed, with the maintenance and prompt restoration of perfusion being the only presently available therapeutic approach.

Considerable evidence implicates a role for "excitotoxicity" (neuronal damage triggered by excessive release of the excitatory neurotransmitter glutamate) occurring in conditions including ischemia, prolonged seizures and trauma. Excitotoxic mechanisms have been extensively investigated, and a critical early finding was that brief strong activation of highly Ca^{2+} permeable NMDA type glutamate receptors (**NMDAR**) results in delayed Ca^{2+} dependent neurodegeneration (Choi, 1987; Choi et al., 1988). After the brief exposure, intracellular Ca^{2+} levels recover for a period of time before undergoing a sharp and sustained rise (termed "**Ca^{2+} deregulation**") that is strongly correlated with cell death (Randall and Thayer, 1992).

It is also apparent that oxidative mechanisms contribute to the neuronal injury, induced after production of the reactive oxygen species (**ROS**; including superoxide and nitric oxide) (Lafon-Cazal et al., 1993; Sattler et al., 1999).

Mitochondria have been implicated as important targets of Ca^{2+} effects. Ca^{2+} enters mitochondria through a specific channel (the mitochondrial Ca^{2+} uniporter, **MCU**), and

under normal circumstances, physiological mitochondrial Ca^{2+} rises help to regulate mitochondrial metabolic function by matching ATP production to need (Nicholls and Budd, 2000). Mitochondria are also important buffers of large cytosolic Ca^{2+} loads (Wang and Thayer, 1996; White and Reynolds, 1997). However, with excess accumulation, Ca^{2+} can disrupt mitochondrial function, with effects including increased superoxide production (Dugan et al., 1995; Reynolds and Hastings, 1995), and opening of a large conductance inner membrane channel (the mitochondrial permeability transition pore; **mPTP**), that can lead to mitochondrial swelling and the release of cytochrome C and other pro-apoptotic peptides (Nicholls and Budd, 2000). Recent studies have also demonstrated the importance of another distinct mechanism of excitotoxic superoxide generation, via Ca^{2+} dependent activation of the superoxide-generating cytosolic enzyme NADPH oxidase (**NOX**) (Brennan et al., 2009; Clausen et al., 2013), and it is likely that depending upon conditions both sources can contribute.

However, despite considerable early hope and some promising results in animals, use of NMDAR antagonists (to prevent Ca^{2+} mediated injury and deregulation) have yielded little benefit in human studies (Hoyte et al., 2004; Ikonomidou and Turski, 2002), necessitating a further search for new targets yielding better efficacy.

Zn^{2+}: a distinct ionic contributor to brain injury

Zn^{2+} is a critical and highly prevalent cation in all tissues. It is particularly prevalent in brain, which has an overall Zn^{2+} content estimated to be 100-200 μM, and is especially high in certain limbic and forebrain regions including hippocampus, amygdala and cortex (Frederickson, 1989). Despite the high total Zn^{2+}, virtually all of it is bound or sequestered; while precise measurements are difficult (as it can bind numerous ligands with a wide

range of affinities), it is agreed that free intracellular Zn^{2+} levels are subnanomolar (Colvin et al., 2010; Maret, 2015). Reflecting its importance in all tissues, there are two families of transporters (with >20 variants identified to date) dedicated to movement of Zn^{2+} between compartments, with the Zrt-, Irt-like protein (**ZIP**) family moving Zn^{2+} into cytosol, and the Zn^{2+} transporter (**ZnT**) family moving Zn^{2+} from cytosol out of the cell or into subcellular compartments (Kambe et al., 2014). In neurons, most ($\sim$ 90%) of the Zn^{2+} is bound to or associated with proteins, and it is an integral component of numerous enzymes, transcription factors and structural proteins (Frederickson, 1989).

Synaptic Zn^{2+}: a modulator of neurotransmission and contributor to injury

A distinct and critical pool of brain Zn^{2+} is that which is sequestered within presynaptic vesicles of some excitatory neurons. This pool of free or loosely bound Zn^{2+} is visualized by histochemical procedures like Timm's silver sulfide staining or labeling with Zn^{2+} sensitive fluorescent dyes, and is often referred to as chelatable or "histochemically reactive" Zn^{2+} (Frederickson, 1989; Frederickson et al., 1992). This Zn^{2+} has a distinctive distribution, generally corresponding with areas of greatest total Zn^{2+}; high levels are found in hippocampus (particularly the dentate granule cells and their "mossy fiber" projections, accounting for the distinctive appearance of hippocampus after Timm's staining), as well as in cortex and amygdala. In these neurons, the Zn^{2+} appears to be loaded into vesicles at millimolar concentrations by the vesicular Zn^{2+} transporter, **ZnT3** (Cole et al., 1999). It is further evident that this Zn^{2+} is co-released with glutamate upon stimulation (Assaf and Chung, 1984; Howell et al., 1984; Sloviter, 1985), and peak levels at synapses may reach into the 100 μM range with strong activation (Ueno et al., 2002; Vogt et

al., 2000), constituting about a 10,000-fold increase over physiologic resting level of extracellular Zn^{2+} (Frederickson et al., 2006).

The identification of populations of forebrain excitatory neurons containing substantial quantities of presynaptic vesicular Zn^{2+} begs understanding of the actions and effects of synaptically released Zn^{2+}. While much is not known, Zn^{2+} has complex effects on extracellular receptors, antagonizing NMDAR currents via both voltage dependent and voltage independent mechanisms; electrophysiological studies have demonstrated Zn^{2+} release from mossy fibers to provide tonic inhibition of NMDAR on CA3 pyramidal neurons (Vogt et al., 2000). In addition, Zn^{2+} has effects on GABA and glycinergic receptors, as well as on a Zn^{2+} sensing G-protein linked metabotropic receptor, and synaptic Zn^{2+} likely has roles in forms of synaptic plasticity (Sensi et al., 2011).

Observations that ischemia, prolonged seizures and brain trauma resulted in loss of chelatable Zn^{2+} labeling in presynaptic pools (most evident in the mossy fibers), and its appearance in somata of injured neurons led to the suggestion that synaptic Zn^{2+} release and its translocation through channels into postsynaptic neurons contributed to their degeneration in these conditions (Frederickson et al., 1989; Suh et al., 2000; Tonder et al., 1990). Indeed, this idea was markedly strengthened by observations that application of an extracellular Zn^{2+} chelator decreased both the postsynaptic Zn^{2+} accumulation and subsequent neurodegeneration (Calderone et al., 2004; Koh et al., 1996; Yin et al., 2002).

Paralleling observations of neuronal Zn^{2+} accumulation after seizures or ischemia *in vivo*, studies in neuronal culture models documented the potent toxic effects of Zn^{2+} and sought to examine its mechanisms. One early aim was to identify the routes through which synaptically released Zn^{2+} can enter post-synaptic neurons to trigger injury. These studies

found Zn^{2+} to permeate three distinct channels through which Ca^{2+} also permeates: (1) NMDAR (Koh and Choi 1994); (2) L-type voltage gated Ca^{2+} channels (**VGCC**) (Freund and Reddig, 1994; Kerchner et al., 2000; Weiss et al., 1993); and (3) atypical Ca^{2+} permeable AMPA type glutamate receptors ("**Ca-AMPAR**"); whereas most AMPA receptors are Ca^{2+} impermeable, these lack the GluA2 subunit in their tetrameric structure, and are only present in substantial numbers on small subpopulations of neurons. Our lab found these Ca-AMPAR to be highly Zn^{2+} permeable (Jia et al., 2002; Yin and Weiss, 1995). However, direct comparison of these routes indicated substantial differences in their Zn^{2+} permeabilities, and corresponding differences in the potency with which Zn^{2+} entry through each of them triggers injury. Consistent with its effective antagonism of NMDAR currents, very little Zn^{2+} permeates NMDARs. Ubiquitously expressed VGCC showed an intermediate permeability, and the selectively expressed Ca-AMPAR had the greatest Zn^{2+} permeability (Sensi et al., 1999).

While brief moderate Zn^{2+} exposures to depolarized neurons resulted in sufficient Zn^{2+} entry through VGCC to trigger extensive degeneration over the subsequent day (Weiss et al., 1993), several considerations led us to believe that entry through Ca-AMPAR might be of particular importance. First, despite their selective expression (in contrast to the VGCC, they are present in large numbers only on ~13% of neurons in cortical cultures, and preferentially found in dendrites of some pyramidal neurons) (Lerma et al., 1994; Ogoshi and Weiss, 2003; Sensi et al., 1999; Yin et al., 1994; Yin et al., 1999), they permit substantially greater rates of Zn^{2+} entry, and, when present, are concentrated at postsynaptic membranes where the highest levels of extracellular Zn^{2+} are likely achieved. Furthermore, early Zn^{2+} accumulation has been found to trigger a delayed increase in

numbers of Ca-AMPAR in many forebrain neurons 2-3 days after transient ischemia (due to decreased expression of GluA2), a factor that likely contributes to delayed neurodegeneration (Calderone et al., 2004; Gorter et al., 1997). Indeed, supporting the significance of this route, a Ca-AMPAR antagonist attenuated Zn^{2+} accumulation and injury both in a slice model of acute ischemia (Yin et al., 2002), and when delivered late after transient global ischemia *in vivo* (Noh et al., 2005). However, this does not mean VGCC are not important. Although VGCC are not concentrated specifically at synapses, entry through this route would likely occur under pathologic conditions in which extracellular Zn^{2+} accumulation is accompanied by widespread neuronal depolarization. Also, VGCC activity increases with age (Thibault and Landfield, 1996), possibly increasing the contribution of this route in aging populations most at risk of brain ischemia.

The generation of ZnT3 knockout mice, which are entirely lacking in chelatable presynaptic Zn^{2+} (Cole et al., 1999), provided a valuable tool to test the presumption that presynaptic Zn^{2+} release and its translocation into postsynaptic neurons accounted for the injurious postsynaptic Zn^{2+} accumulation. Consistent with this idea, when ZnT3 knockouts were tested in a prolonged kainate seizure model, the knockouts showed modestly decreased Zn^{2+} accumulation and injury in CA3 pyramidal neurons (which are innervated by the very densely Zn^{2+} containing mossy fibers). Surprisingly, however, Zn^{2+} accumulation and injury were markedly *increased* in CA1 pyramidal neurons of the knockouts, indicating an additional source of Zn^{2+} that did not depend upon synaptic release and translocation (Lee et al., 2000).

Zn^{2+} binding proteins: buffers of Zn2+ loads or sources of non-synaptic Zn2+ accumulation (or both)?

Metallothioneins (**MT, I-IV**), are cysteine rich peptides with multiple Zn^{2+} binding sites that play critical roles in buffering Zn^{2+} within cells (MT-III being the predominant neuronal isoform), making them likely candidate sources for the non-synaptic neuronal Zn^{2+} accumulation (Maret, 1995). Zn^{2+} binding to MT's is highly sensitive to environmental conditions, with metabolic aberrations associated with pathological conditions (specifically oxidative stress and acidosis) destabilizing binding, resulting in release of free Zn^{2+} into cytosol (Jiang et al., 2000; Maret, 1995). A seminal observation that simple application of a disulfide oxidant to cultured neurons was capable of causing cytosolic Zn^{2+} rises that could trigger delayed neurodegeneration provided the first *proof of principle* that simple mobilization of Zn^{2+} from intracellular buffers could result in neurodegeneration (Aizenman et al., 2000). A subsequent study overexpressing MT-III found that depending upon conditions it could have divergent effects, either buffering excess Zn^{2+} that enters the cell (and thereby diminishing its toxic effects), or providing a source of injurious Zn^{2+} mobilization, under conditions of oxidative stress (Malaiyandi et al., 2004).

Indeed, use of MT-III knockout mice (as well as double MT-III / ZnT3 knockouts) helped clarify the respective contributions of synaptic vs MT-III bound Zn^{2+} in the kainate seizure model. In contrast to the increased Zn^{2+} accumulation seen in ZnT3 knockouts in CA1 neurons, Zn^{2+} accumulation and injury in MT-III knockouts were decreased in CA1, consistent with a dominant contribution of mobilization from MT-III. Conversely, these were increased in CA3 of MT-III knockouts, consistent with synaptic "translocation"

predominating, with MT-III in CA3 serving a protective role by helping to buffer Zn^{2+} entering the neurons (Lee et al., 2003).

Might these differences in sources of injurious Zn^{2+} accumulation be a factor contributing to their differential disease susceptibilities, with CA3 neurons preferentially degenerating after recurrent limbic seizures (associated with repetitive firing of the Zn^{2+} rich mossy fibers) and CA1 neurons undergoing delayed degeneration after transient ischemia (Ben-Ari et al., 1980; Sugawara et al., 1999)?

Discrimination of Ca^{2+} and Zn^{2+} reveals distinct contributions

Despite the emerging evidence for contributions of Zn^{2+}, there is still much evidence for important Ca^{2+} contributions in excitotoxicity associated conditions, and it is probable that both ions contribute. However, early attempts to discriminate their contributions were confounded by the fact that until relatively recently, there were no available Zn^{2+}-selective indicators. Furthermore, it became apparent that some effects that had been attributed to Ca^{2+} might actually be partly Zn^{2+} mediated, since available Ca^{2+} indicators bound and responded to Zn^{2+} with higher affinity than Ca^{2+} (Cheng and Reynolds, 1998), and fluorescence increases detected by a "Ca^{2+} indicator" in a slice model of ischemia (that would previously have been assumed to reflect Ca^{2+} rises) were found to be substantially diminished by selective Zn^{2+} chelation (Stork and Li, 2006). The development of Zn^{2+} selective indicators provided a breakthrough in attempts to study Zn^{2+}-specific effects and discriminate them from those of Ca^{2+}. Furthermore, using a high affinity Zn^{2+} indicator in

combination with a low affinity Ca^{2+} indicator, it became possible to simultaneously track changes in both ions (Devinney et al., 2005). Our lab used this approach to simultaneously track changes in both Zn^{2+} and Ca^{2+} in single pyramidal neurons in hippocampal slices subjected to oxygen glucose deprivation (**OGD**). Interestingly, our lab found that cytosolic Zn^{2+} rises both preceded and contributed to the onset of terminal Ca^{2+} deregulation events, which still occurred but were significantly delayed by the presence of a Zn^{2+} chelator (Medvedeva et al., 2009). This provided new evidence that Zn^{2+} accumulation might be an early event in the ischemic injury cascade, the appropriate targeting of which might provide therapeutic benefit. As discussed further below, clues from this and other early studies suggested that mitochondria might be an important target for these early Zn^{2+} effects.

Mitochondria: a critical target of Zn^{2+}

Paralleling studies of Ca^{2+}, studies over several decades have highlighted ways in which Zn^{2+} impacts mitochondrial function. Below, I review the evolution of these data, leading up to our proposition that mitochondrial Zn^{2+} accumulation may be an important early step in the ischemic injury cascade of many neurons. Specifically, as it occurs upstream from terminal Ca^{2+} deregulation, its targeting may provide benefits distinct from those provided by attenuation of Ca^{2+} entry (via NMDAR blockade).

Isolated mitochondria: Evidence of potent Zn^{2+} effects

A number of studies dating back over 50 years have found that Zn^{2+} can enter mitochondria, inducing effects including swelling, and inhibition of respiration with high potency (Brierley, 1967; Skulachev et al., 1967). Over the subsequent decades, with growing awareness that Zn^{2+} is a pathophysiologically important ion that contributes to neuronal injury, there has been an increasing interest in determining how Zn^{2+} impacts mitochondria. Zn^{2+} was found to enter mitochondria specifically through the MCU (Saris and Niva, 1994), and to trigger opening of the mPTP (Wudarczyk et al., 1999). Other studies found potent (submicromolar) Zn^{2+} inhibition of the bc1 complex of the electron transport chain and of the TCA cycle α-ketoglutarate dehydrogenase enzyme complex (Brown et al., 2000; Link and von Jagow, 1995). Highlighting the complexity of Zn^{2+} effects on mitochondria, prior studies by us have found low (submicromolar) exposures to induce loss of mitochondrial membrane potential ($\boldsymbol{\Delta\Psi_{mito}}$), decreased ROS production and increased O_2 consumption (consistent with uncoupling of the electron transport from ATP synthesis), while slightly higher levels increased ROS generation and decreased O_2 consumption (consistent with inhibition of electron transport) (Sensi et al., 2003). A subsequent study reported Zn^{2+}, after entry through the MCU, to induce irreversible inhibition of major thiol oxidoreductase enzymes involved in energy production and antioxidant defense, an effect that appeared to be linked to mPTP opening (Gazaryan et al., 2007).

Using isolated brain mitochondria, our lab found Zn^{2+} (10-100 nM) to potently induce swelling, that appeared to depend upon Zn^{2+} entry through the MCU and opening of the mPTP (Jiang et al., 2001). Our group further found that although Zn^{2+} triggered mitochondrial swelling with far greater potency than Ca^{2+}, the effects of these ions were

synergistic, with greater swelling when Ca^{2+} was also present (Jiang et al., 2001). Indeed, a number of other studies have also suggested that the presence of Ca^{2+} may critically modulate effects of Zn^{2+} on isolated mitochondria. Specifically, Ca^{2+} was found to markedly enhance Zn^{2+} entry through the MCU (Saris and Niva, 1994), and Zn^{2+} triggered mPTP opening of de-energized (but not energized) mitochondria was found to be Ca^{2+} dependent (Wudarczyk et al., 1999). Interestingly, a relatively recent study exposed purified and substrate attached mitochondria using buffers pre-treated to ensure complete elimination of Ca^{2+}, and found Zn^{2+} to have weak depolarizing effects with no evidence of its entry into mitochondria (Devinney et al., 2009). Of possible relevance, the MCU and associated regulatory peptides were recently identified and two regulatory peptides (MICU1 and 2), appear to sense Ca^{2+}, inhibiting MCU opening when Ca^{2+} is near resting levels (<100-200 nM) and promoting opening when Ca^{2+} is elevated, thus conferring a sigmoid shaped Ca^{2+} level / conductance relationship to the channel (De Stefani et al., 2015; Kamer and Mootha, 2015; Marchi and Pinton, 2014). Indeed, Ca^{2+} dependence of MCU opening to permit Zn^{2+} entry could help to explain apparent synergism between Ca^{2+} and Zn^{2+} effects on mitochondria.

Thus, it is apparent that Zn^{2+} effects on mitochondria are complex and a better definition of its mechanisms and how its entry is regulated by the MCU are rich areas for further investigation. Yet, the potency of its effects, taken together with the high levels of Zn^{2+} present in neurons, highlight the strong potential for Zn^{2+} to contribute to mitochondrial dysfunction in disease.

Cell culture studies: Neuronal Zn^{2+} entry results in mitochondrial accumulation and dysfunction contributing to cell death

Culture studies permit investigation of Zn^{2+} effects in the neuronal environment, bringing us a step closer to understanding possible effects in diseases like ischemia. Above, I introduced studies examining routes through which synaptic Zn^{2+} could enter neurons, and reported evidence for particularly rapid entry through selectively expressed Ca-AMPAR, with slower entry through VGCC. Sensi et al., subsequently examined effects of this Zn^{2+} entry, and found brief Ca-AMPAR activation, in the presence of 100-300 μM Zn^{2+}, to induce rapid loss of $\Delta\Psi_{mito}$ and ROS generation that persisted for at least an hour after the exposure, consistent with the potent neurotoxicity of these exposures. Identical kainate exposures with physiological (1.8 mM) Ca^{2+}, but no Zn^{2+}, triggered smaller and transient episodes of ROS generation. However, if Zn^{2+} and Ca^{2+} were both present during the exposure, the ROS production was significantly greater than with Zn^{2+} alone, again indicating synergistic effects of these ions (Sensi et al., 1999; Sensi et al., 2000).

In other studies, our group induced smaller Zn^{2+} loads, via similar brief Zn^{2+} exposures under depolarizing conditions, to trigger entry through VGCC (rather than Ca-AMPAR). Although still causing considerable delayed neurotoxicity (Weiss et al., 1993), these exposures did not cause the acute ROS generation and loss of $\Delta\Psi_{mito}$ seen with rapid entry through Ca-AMPAR (Sensi et al., 1999; Sensi et al., 2000). This, along with similar findings by others, have led to questions as to the likelihood that mitochondria constitute important targets of Zn^{2+} effects in disease (Pivovarova et al., 2014). However, despite the absence of rapid ROS production, our group found these brief episodes of Zn^{2+} entry

through VGCC to have distinct and long lasting effects on mitochondria, with low (50-100 μM) exposures resulting in Zn^{2+} accumulation within mitochondria persisting for at least 2 hours after the exposure along with partial loss of $\Delta\Psi_{mito}$ (Sensi et al., 2002); similar brief exposures with 300 μM Zn^{2+} (and 1.8 mM Ca^{2+}) triggered mitochondrial swelling, and delayed release of apoptotic mediators (cytochrome C and apoptosis inducing factor) (Jiang et al., 2001), possibly consistent with more slowly evolving cell death occurring after these exposures.

Notably, cytosolic Zn^{2+} accumulation results not only from entry of extracellular Zn^{2+}, but also upon mobilization from cytosolic pools like MT-III, and studies of the effects of strong cytosolic Zn^{2+} mobilization alone also have found it to induce effects on mitochondria, contributing to loss of $\Delta\Psi_{mito}$ and delayed degeneration (Bossy-Wetzel et al., 2004; Sensi et al., 2003). In addition, recent studies have highlighted possible contributions of such Zn^{2+} mobilization and consequent mitochondrial dysfunction to the Ca^{2+} dependent excitotoxic injury cascade (Granzotto and Sensi, 2015). In pathologic conditions like ischemia or seizures, where synaptic Zn^{2+} release and mobilization from cytosolic buffers both occur, it is likely that both sources contribute to mitochondrial dysfunction.

Slice and in vivo studies support contributions of mitochondrial Zn^{2+} to ischemic neuronal injury

Although the studies discussed above demonstrate that exogenously applied Zn^{2+} can impact mitochondria and contribute to neuronal injury, this does not indicate that endogenous Zn^{2+} actually does so in ischemia. However, recent studies in more

pathophysiologically relevant ischemia models provide compelling evidence that mitochondria are indeed important targets of endogenous Zn^{2+} effects. Specifically, in one study, addition of extracellular Zn^{2+} chelators shortly after brief ischemia reduced the subsequent mitochondrial release of pro-apoptotic peptides (Calderone et al., 2004). In another *in vivo* study, Zn^{2+} was found to accumulate in mitochondria within 1 hour after transient ischemia, contributing to the opening of large, multi-conductance outer membrane channels (Bonanni et al., 2006). However, whereas these studies demonstrate that Zn^{2+} contributes to mitochondrial dysfunction after *in vivo* ischemia, they do not address therapeutically crucial questions including the source and time course of the Zn^{2+} accumulation, and potential avenues for beneficial interventions.

To examine these issues, Medvedeva have undertaken studies using hippocampal slice OGD models, a paradigm that models aspects of *in vivo* ischemia while permitting precise control of the microenvironment and detailed measurement of cellular responses. Our early studies in this model found cytosolic Zn^{2+} rises to precede and contribute to the onset of delayed Ca^{2+} deregulation and cell death during prolonged, lethal OGD (Medvedeva et al., 2009), with evidence for early Zn^{2+} entry into mitochondria. Subsequent studies provided strong evidence that Zn^{2+} entry specifically through the MCU is a critical early step, triggering mitochondrial dysfunction (including ROS production) that contributes to the occurrence of acute Ca^{2+} deregulation and degeneration of CA1 neurons (Medvedeva and Weiss, 2014).

Aims of present thesis

While much has been uncovered about the importance of both extracellular and intracellular sources of Zn^{2+} to neuronal injury, little is known about the respective contributions of each of these sources to mitochondrial dysfunction; indeed, only few studies to date have begun to explore the idea that the integrity of cytosolic buffering may critically modulate the effects of exogenous Zn^{2+} entry on mitochondrial function in cultured neurons (Clausen et al., 2013; Sensi et al., 2003). Furthermore, as most early studies were carried out in Ca^{2+} free media to ensure observation of Zn^{2+} specific effects, there is debate about the respective contributions of Ca^{2+} and Zn^{2+} to mitochondrial dysfunction observed *in vivo*, with some proposing synergy between these ions (Gazaryan et al., 2007; Jiang et al., 2001; Sensi et al., 2000) while others see little evidence for Zn^{2+} contributions (Devinney et al., 2009; Pivovarova et al., 2014). Furthermore, despite numerous studies suggesting the critical role of MCU in Zn^{2+}-triggered injury, past studies elucidating the role of the MCU in Zn^{2+} effects were limited to the use of pharmacologic MCU blockers which lack complete specificity (Tapia and Velasco, 1997). Consequently, one cannot be certain that beneficial effects are specifically due to MCU blockade.

The present thesis seeks to address these questions by modeling early Zn^{2+} dependent events in ischemic neuronal injury to quantitatively examine how disrupted cytosolic Zn^{2+} buffering and the presence of Ca^{2+} modulate the consequences of moderate exogenous Zn^{2+} loads on mitochondrial function and cell death. To this aim, we use brief high K^+/Zn^{2+} exposures (to mimic neuronal depolarization and extracellular Zn^{2+} accumulation as may accompany ischemia *in vivo*), and find that both disrupted buffering and the presence of Ca^{2+} strongly increase the impact of low Zn^{2+} exposures on

mitochondrial function and cell death, with greater synergistic effects when combined. These findings support the hypothesis that slow Zn^{2+} entry into depolarized neurons could well contribute to mitochondrial dysfunction and neurodegeneration *in vivo*.

Furthermore, we took advantage of the recent availability of MCU knockout (**KO**) mice (Pan et al., 2013) to assess the role of MCU specifically in Zn^{2+}-induced mitochondrial dysfunction and neuronal injury. Our findings in both cultured cortical neurons and hippocampal slices provide further support to the hypothesis that Zn^{2+} entry into the mitochondria through the MCU plays a critical role in promoting early and prolonged mitochondrial dysfunction—as well as the consequent neurodegeneration—and that delayed MCU blockade can specifically attenuate these contributions to injury.

And finally, we examined the therapeutic potentials of these findings by applying delayed interventions targeting Zn^{2+} accumulation or MCU blockade. We found Zn^{2+} chelation after the Zn^{2+} load diminishes both mitochondrial ROS generation and cell death, and that delayed MCU blockade via pharmacologic MCU blockers could attenuate the downstream, deleterious effects of Zn^{2+} on mitochondria supporting the idea that delayed interventions targeting mitochondrial Zn^{2+} could provide therapeutic benefits.

CHAPTER 1

Methodology

In this chapter, we discuss the various methodologies—including sample preparation and experimental techniques—that were used to address the questions discussed above.

Ethics statement

All procedures for the current study were approved by the Institutional Animal Care and Use Committee of the University of California Irvine, and in accordance with the recommendations from the Guide for the Care and Use of Laboratory Animals of the National Institutes of Health.

Animals

Mice lacking Mitochondrial Calcium Uniporter (Ccdc109a [Mcu], IST11669F8; Texas A&M Institute for Genomic Medicine) were bred from homozygous breeding pairs. Genotype was validated with protocol as detailed previously (Pan et al., 2013), using the following primers: HP3' (CCATCTGTTCCTGACCTTGA), IST11669F8-F (GGAGTTAAGTCATGAGCTGC), and IST11669F8-R (CTGGCTTAGTTGGCAGAGTT). CD-1 mice (used as control and wildtype) were ordered from Charles River (Crl:CD1[ICR]).

Reagents and indicators

Materials for culture maintenance (Minimum Essential Media [**MEM**], fetal bovine serum, glutamine, and horse serum) and for imaging (Newport Green, FluoZin-3 AM, MitoTracker Green, Pluronic F-127, Fura-FF) were purchased from Life Technologies (Grand Island, NY). Other reagents for experiments (2,2'-dithiodipyridine [**DTDP**], Carbonyl cyanide-p-trifluoromethoxyphenylhydrazone [**FCCP**], Rhodamine 123 [**Rhod123**], Ruthenium Red [**RR**], and N-methyl-D-aspartate [**NMDA**]) were purchased from Sigma-Aldrich (St. Louis, MO). Hydroethidine (**HEt**) was purchased from Assay Biotech (Sunnyvale, CA), MK-801 from Abcam, Apocynin from Acros Organics (Morris Plains, NJ), and XF Base Medium (minimal Dulbecco's Modified Eagle's Medium) from Agilent Technologies (Santa Clara, CA). All other chemicals and reagents were purchased from common commercial sources.

Media

For culture growth and/or maintenance, the following media were used: "Maintenance media" (MEM supplemented with 25 mM glucose), "growth media" (maintenance media supplemented with 10% heat-inactivated horse serum 2 mM glutamine), and "plating media" (growth media supplemented with 10% fetal bovine serum). For imaging experiments and/or Zn^{2+} exposures, HEPES-buffered media (consisting of the following [in mM]: 120 NaCl, 5.4 KCl, 0.8 $MgCl_2$, 20 Hepes, 15 glucose, 10 NaOH, in pH 7.4; with either 0 mM $CaCl_2$ [0 mM Ca^{2+} HSS] or 1.8 mM $CaCl_2$ [1.8 mM Ca^{2+} HSS]) were used, and kept at room temperature unless specified otherwise. To prepare hippocampal slices, isolated brains were maintained in the "preparation solution" (consisting of the following [in mM]: 220 sucrose, 3 KCl, 1.25 NaH_2PO_4, 6 $MgSO_4$, 26

$NaHCO_3$, 0.2 $CaCl_2$, 10 glucose, and 0.42 ketamine, kept in pH 7.35, maintained at 310 mOsm, and equilibrated with 95% O_2/5% CO_2). The hippocampal slices were maintained in artificial cerebral spinal fluid (ACSF; consisting of the following [in mM]: 126 NaCl, 3 KCl, 1.25 NaH_2PO_4, 1 $MgSO_4$, 26 $NaHCO_3$, 2 $CaCl_2$, 10 glucose, kept in pH 7.35, maintained at 310 mOsm with sucrose, and equilibrated with 95% O_2/5% CO_2).

Neuronal culture preparation

Mixed cortical neuronal cultures were prepared as described previously (Yin et al., 1994). Briefly, neocortical regions from CD-1 or MCU KO mouse embryos (15 – 16 gestational day; mixed gender) were isolated and cells suspended in plating media. The neuronal suspension was then plated on previously established astrocytic monolayers (of the same genotype) on glass-bottomed dishes, Seahorse XF24 cell culture microplates, or culture-treated 24 well microplates. 2 – 3 days after plating, culture was treated with 10 μM cytosine arabinoside for 24 hrs (to stop non-neuronal cell division), and media was switched to growth media. Cells were kept in 5% CO_2/37ºC incubator for at least 10 days prior to experiment. To prepare astrocytic monolayers, the same protocol was used with the following changes: 1) neocortical tissues from postnatal mice (1 – 3 days old; mixed gender) from CD-1 or MCU KO mice were used, 2) plating media was supplemented with epidermal growth factor (10 ng/ml), and 3) suspended cells were plated on poly-D-lysine and laminin-coated glass-bottomed dishes, culture treated 24 well microplates, and Seahorse XF24 cell culture microplates.

Zn^{2+} exposure

Cultured neurons were placed in either 0 mM Ca^{2+} or 1.8 mM Ca^{2+} HSS prior to starting all experiments. After 10 min baseline and pre-treatment with 60 μM DTDP ± 500 μM Apocynin (if indicated), Zn^{2+} and/or Ca^{2+} loading was induced. To permit ion influx, neurons were exposed to indicated levels of Zn^{2+} (0 – 300 μM) and/or 1.8 mM Ca^{2+} in 90 mM K^+ HSS ("high K^+"; HSS modified with 90 mM K^+ and Na^+ adjusted to 35 mM to maintain osmolarity) for 5 min to depolarize neurons, inducing Zn^{2+} and/or Ca^{2+} entry through VGCC. NMDA antagonist MK-801 (10 μM)—used to inhibit Ca^{2+} entry through NMDAR—was added during all Zn^{2+} and/or Ca^{2+} exposures (even when Ca^{2+} was not present during the experiment) to maintain consistency. After 5 min Zn^{2+} and/or Ca^{2+} exposure in high K^+, neurons were washed 3 times in HSS (60 μM DTDP ± 500 μM apocynin or 10 μM RR, as indicated). If the experiment involved incubation, cultured neurons were washed 3 times into maintenance media and kept in the 5% CO_2/37ºC incubator until needed. When attempting to best model the events that may occur during ischemic conditions, the following standardized paradigm was used when indicated (10 min pre-exposure to 60 μM DTDP, followed by 5 min 100 μM Zn^{2+} + high K^+ + MK-801, followed by 3x wash into DTDP, all in 1.8 mM Ca^{2+} HSS; termed "ischemic Zn^{2+} exposure").

Quantitative imaging studies

Neuronal cultures aged 10 – 16 days *in vitro* (DIV) were placed on the stage of a Nikon Diaphot inverted microscope equipped with 75 Watts Xenon-lamp, a filter wheel controlled by a computer, a 40x (1.3 numerical aperture) epifluorescence oil-immersion objective along with the following fluorescence cubes: a green FITC (Ex: 480 nm, dichroic:

505 nm, Em: 535 nm) and a red TRITC fluorescence cube (Ex: 540 nm, dichroic: 565 nm, Em: 605 nm). Emitted signals were captured every min with a Sensys Photometrics intensified charge-coupled device camera, and converted digitally by the MetaFluor software (Version 7.0, Molecular Devices LLC, Sunnyvale, CA). Gain and exposure of the camera were adjusted to obtain baseline fluorescence level of 200 – 300 arbitrary units of a 12-bit signal output of 4,096 for all fluorophores. For imaging, only fields with at least 20 healthy looking cells (non-clustered neurons with robust processes) were used. For analysis, background fluorescence (the lowest value in a neuron-free region of the field) was subtracted from images, and fluorescence measurement for each neuron (F_x) was normalized to the average fluorescence intensity of the 10 min baseline measure (F_0) to trend normalized fluorescence over time (F_x/F_0). The F_x/F_0 of each cell in the field was averaged to produce a value constituting one experiment repetition.

Cytosolic Zn^{2+}

Either low affinity cytosolic Zn^{2+} indicator Newport Green diacetate ($K_d \sim 1$ μM, Ex: 490 nm, Em: 530 nm; using a green FITC fluorescence cube) or the high affinity cytosolic Zn^{2+} indicator FluoZin-3 AM ($K_d \sim 15$ nM, Ex: 494 nm, Em: 516 nm; using a green FITC fluorescence cube) was used to quantify neuronal Zn^{2+} levels. Cultured neurons were loaded with 5 μM Newport Green or FluoZin-3 in 0 mM Ca^{2+} HSS containing 0.2% Pluronic F-127 and 1.5% dimethlyl sulfoxide (in the dark room, at room temperature) prior to use for experiments. FCCP (1 μM) was added at the experiment to release mitochondrially sequestered Zn^{2+}, permitting estimate of degree of mitochondrial Zn^{2+} accumulation.

Mitochondrial membrane potential

Mitochondrial membrane potential sensitive indicator Rhod123 (Ex: 507 nm, Em: 529 nm; using a green FITC fluorescence cube) was used to quantify mitochondrial depolarization. Neurons were used for imaging after loading the cultures with 2 μM Rhod123 in 1.8 mM Ca^{2+} HSS for 30 min (in the dark room, at room temperature). Rhod123 is a positively charged dye which accumulates in mitochondria, where its fluorescence is quenched. With mitochondrial depolarization, the Rhod123 sequestered in the mitochondria gets released, resulting in increase in Rhod123 fluorescence intensity (Duchen et al., 2003). FCCP (1 μM; 5 min) was added at the end of each experiment to induce maximal mitochondrial depolarization, permitting measure of maximal Rhod123 ΔF.

Reactive oxygen species

Superoxide sensitive dye HEt (Ex: 510-560 nm; Em: > 590 nm; using a red TRITC fluorescence cube) was used to quantify ROS generation. Neurons were used for imaging after loading the cultures with 5 μM HEt in 0 mM or 1.8 mM Ca^{2+} HSS for 30 min (in the dark room, at room temperature). As HEt is oxidized into highly fluorescent ethidium, ROS generation is quantified as the HEt fluorescence increase.

Mitochondrial respiration assay

Mitochondrial respiration was assessed by measuring changes in O_2 consumption rate (**OCR**) using the Seahorse XF24 Extracellular Flux Analyzer, as described previously with adjustments (Yao et al., 2009). Briefly, neurons plated on top of astrocytic monolayers on Seahorse XF24 Cell Culture Microplates were exposed to the ischemic Zn^{2+} exposure, washed into DTDP for 20 min, and incubated for 2 hrs (in maintenance media and % CO_2/37ºC incubator). After completing the incubation, cultures were washed into XF Base

Medium (supplemented with 2 mM glutamine, 15 mM glucose, and 1 mM sodium pyruvate), and maintained at 37ºC for 1 hr prior to starting the Seahorse XF24 assay. The machine measures the OCR of cells during baseline and after the sequential exposure to 1 μM oligomycin, 2 μM FCCP, and antimycin A/rotenone (both at 1 μM). The concentrations of mitochondrial inhibitors were determined empirically, with FCCP specifically adjusted to induce approximately 1.5x the baseline. Prior to each experiment, all culture wells were visually inspected (to ensure equal distribution of cells) and randomly assigned to treatment groups. All calibration instructions were followed according to the manufacturer's protocols, and Seahorse XF24 program and Wave software were used to run the assay and analyze the data respectively. We carried prior validation study confirming astrocytes make minimal contributions to observed OCR and its changes, as our cultured neurons are plated on top of astrocyte monolayers (as discussed above).

Confocal imaging of mitochondrial morphology

Mitochondrial morphology was assessed as described previously (Ji and Weiss, 2018). Briefly, confocal microscopy was performed using an inverted stage Nikon Eclipse Ti chassis microscope with a Yokogawa CSUX spinning disk head. Images were observed at 1000x oil-immersion objective (1.49 numerical aperture) using a Hamamatsu electromultiplying CCD camera. Field was scanned sequentially with excitation (488 nm) via a Coherent sapphire laser source synchronized with the camera, and emission monitored with a 525 (50) nm filter. Images were acquired using the MicroManager Image Acquisition software (ver 1.52). After cultured neurons were exposed to the ischemic Zn^{2+} exposure paradigm (discussed above) + 20 min wash + 12 hr incubation (in maintenance

media at 37°C/5% CO_2), cultures were loaded with 200 nM MitoTracker Green (Ex: 490 nm, Em: 516 nm) in 1.8 mM Ca^{2+} HSS for 30 min at room temperature in the dark, and then switched into 1.8 mM Ca^{2+} HSS for the imaging. Only healthy appearing neurons with intact outer membranes (as could be visualized via brightfield imaging) were chosen for imaging. Camera gain, laser intensity, and exposure times were adjusted to make MitoTracker Green fluorescence intensity 1.5 – 2 times that of the background fluorescence value. Heat fan was used to maintain imaging rig at 37ºC. Images acquired were blinded, and lengths and width of distinct mitochondria measured manually in the ImageJ software. The values were used to calculate length/width (L/W) ratio of individual mitochondria, which were then averaged to produced one average L/W ratio representing one repetition of an experiment.

Neurotoxicity Assessment

Neurotoxicity was examined in cultured neurons plated on 24 well microplates at 14 – 16 DIV. Briefly, neurons were switched into their HSS (0 or 1.8 mM Ca^{2+}), and exposed to 60 μM DTDP (10 min), Zn^{2+} ± Ca^{2+} (in high K^+ and 10 μM MK-801, as discussed above; 5 min) and 10 μM RR (20 min), with concentration as detailed above. After the exposures and treatment, cultures were washed in maintenance media and kept in 37°C/5% CO_2 for 24 hrs, at which cell death was quantified with by lactate dehydrogenase (LDH) efflux assay as described (Koh and Choi, 1987). In all experiments, the background LDH present in the media was subtracted by measuring the level in the sham wash protocol, used as negative control. LDH values of cultures exposed to 300 μM NDMA for 24 hrs (paradigm that destroys most neurons while sparing glia) were set as positive control. All wells were

visually inspected to estimate degree of cell death, which was compared to quantification from LDH assay, for validation.

Hippocampal slices oxygen-glucose deprivation

Acute hippocampal slices were prepared as described previously (Medvedeva et al., 2009). Briefly, brains from 25 ± 3 days old mice were rapid removed after anesthesia with isoflurane and kept in the ice-cold preparation solution. Hippocampal slices were cut with Leica VT1200 vibratome at 300 μm thickness and placed in ACSF. After slices were equilibrated in ACSF for 1 hr at 34ºC, slices were switched into oxygenated ACSF in room temperature for ≥1 hr prior to use.

Slices were mounted on the stage of an upright microscope (BX51WI; Olympus), placed in a flow-through chamber (RC-27L chamber with plastic slice anchor; Warner Instruments), and perfused with the oxygenated ACSF (2 ml/min). To measure intracellular Ca^{2+} dynamics, Fura FF ($K_d \sim 6$ μM) was loaded in individual hippocampal pyramidal neurons with fluorescent indicators using a patch pipette held in the whole cell configuration at – 60 mV for 5 min. After pipette withdrawal, the injected cell was left to recover for 20 min prior to experiment. Fluorescence was alternately excited at 340(20)/380(20) nm via 40× water-immersion objective using a xenon light source (Sutter Instruments) and emitted fluorescence was collected at 532(40) nm using a cooled CCD camera (Hamamatsu). All filters are band pass with bandwidths indicated in parentheses. Images were taken every 15 or 30 s, background subtracted, and analyzed using the MetaFluor software. Changes in Ca^{2+} levels are displayed as the ratio of background subtracted Fura FF emission intensities upon excitation at 340 and 380 nm ("340/380 ratio").

To model ischemic injury, slices were placed in hypoxic-hypoglycemic condition (via oxygen-glucose deprivation [**OGD**]). ACSF was changed to the same solution lacking glucose (and replaced with sucrose to maintain osmolarity) and bubbled with 95% N_2/5% CO_2. OGD was continued for ≥ 15 min and maintained until causing Ca^{2+} deregulation.

Statistical analysis

All values on traces are displayed as mean ± standard error of the mean (SEM), and on bars displayed as mean + SEM. All experiments were interleaved and have been repeated ≥ 3 times. All comparisons reflect matching sets of cell cultures or slices from the same set of dissections or slice preparation, and all efforts were made to match biologic variables between comparisons. Two-tailed student's t-test was used to assess significance for groups of two, and one-way ANOVA used for groups ≥ 3.

CHAPTER 2

Zn^{2+}-induced neuronal injury: synergism with Ca^{2+} and critical dependence upon cytosolic Zn^{2+} buffering

In this chapter, we model early Zn^{2+} dependent events in ischemic neuronal injury to quantitatively examine how disrupted cytosolic Zn^{2+} buffering and the presence of Ca^{2+} modulate the consequences of moderate exogenous Zn^{2+} loads on mitochondrial function and cell death. Using brief high (90 mM) K^+/Zn^{2+} exposures to mimic neuronal depolarization and extracellular Zn^{2+} accumulation as may accompany ischemia *in vivo*, we made several observations: **1.** Mild disruption of cytosolic Zn^{2+} buffering—while having little effects alone—markedly enhanced mitochondrial Zn^{2+} accumulation and dysfunction (including loss of $\Delta\Psi_m$, ROS generation, swelling and respiratory inhibition) caused by relatively low (10 – 50 μM) Zn^{2+} with high K^+. **2.** The presence of Ca^{2+} during the Zn^{2+} exposure decreased cytosolic and mitochondrial Zn^{2+} accumulation, but markedly exacerbated the consequent dysfunction. **3.** Paralleling effects on mitochondria, disruption of buffering and presence of Ca^{2+} enhanced Zn^{2+}-induced neurodegeneration. Taken together, these data lend credence to the idea that in pathologic states that impair cytosolic Zn^{2+} buffering, slow uptake of Zn^{2+} along with Ca^{2+} into neurons via VGCC can disrupt the mitochondria and induce neurodegeneration.

Slow Zn^{2+} translocation through VGCC induces only mild mitochondrial dysfunction

As discussed above, neuronal Zn^{2+} accumulation contributes to delayed neurodegeneration in pathological conditions like ischemia. One likely important source of

this Zn^{2+} is co-release (with glutamate) from presynaptic terminals, and its entry into postsynaptic neurons (**"translocation"**) via various routes (including VGCC and Ca-AMPAR). Inside neurons, Zn^{2+} can enter mitochondria and disrupt their function (Clausen et al., 2013; Jiang et al., 2001; Sensi et al., 2003; Sensi et al., 2002; Sensi et al., 2000). While mitochondrial Ca^{2+} accumulation has long been considered the major contributor to their dysfunction in ischemia (Halestrap, 2006; Nicholls and Budd, 2000), clues have emerged that Zn^{2+} may also be an important contributor (Bonanni et al., 2006; Calderone et al., 2004; Medvedeva et al., 2017; Medvedeva et al., 2009; Medvedeva and Weiss, 2014), particularly after rapid influx through highly Zn^{2+} permeable Ca-AMPAR (Jia et al., 2002; Sensi et al., 1999a; Yin and Weiss, 1995). However, although brief exposure of cultured neurons to Zn^{2+} under depolarizing conditions (triggering entry largely through VGCC) led to considerable delayed degeneration (Weiss et al., 1993), this induced only mild acute effects on mitochondria (Pivovarova et al., 2014; Sensi et al., 1999a), raising uncertainty as to contributions of slower Zn^{2+} translocation to mitochondrial dysfunction in disease conditions.

Present studies seek to further clarify whether and under what circumstances low to moderate extracellular Zn^{2+} accumulation and its slower entry into neurons can impact the mitochondria and promote neuronal injury. We chose to model Zn^{2+} translocation by inducing entry through the VGCC, as may occur in ischemia with extracellular Zn^{2+} accumulation around depolarized neurons, because VGCC are ubiquitously expressed (unlike Ca-AMPAR, which are only present on some neurons) and permit slower entry, resulting in more uniform and moderate Zn^{2+} loads. Our first aim was to extend prior studies by quantitatively examining the relationship between extracellular Zn^{2+} exposure,

cytosolic and mitochondrial Zn^{2+} accumulation, and the consequent acute mitochondrial dysfunction.

Neurons were loaded with the low affinity cytosolic Zn^{2+} indicator Newport Green ($K_d \sim 1$ μM) (Sensi et al., 1999a) in 0 Ca^{2+} HSS (to ensure observation of Zn^{2+}-specific effects). After measuring baseline fluorescence for 10 min, cultures were exposed to 25, 75, or 300 μM Zn^{2+} with high (90 mM) K^+ for 5 min, washed into 0 Ca^{2+} HSS for 5 min, then treated to the mitochondrial protonophore, carbonyl cyanide 4-(trifluoromethoxy)phenylhydrazone (**FCCP**, 1 μM) for 10 min. FCCP dissipates the proton gradient across the inner mitochondrial membrane, resulting in rapid loss of mitochondrial membrane potential (**$\Delta\Psi_m$**) and release of mitochondrially sequestered Zn^{2+} (Clausen et al., 2013; Medvedeva et al., 2017; Sensi et al., 2003; Sensi et al., 2002). Thus, the rise in cytosolic Zn^{2+} after FCCP (assessed as Newport Green fluorescence change; **Newport Green ΔF**) reflects the amount of Zn^{2+} that had been taken up into mitochondria. Our findings indicate a direct relationship between the magnitude of the exogenous Zn^{2+} load with both the degree of cytosolic Zn^{2+} rise and the consequent Zn^{2+} uptake into mitochondria (**Fig 2.1A**), with high K^+/300 μM Zn^{2+} exposure resulting in far greater cytosolic and mitochondrial Zn^{2+} accumulation than the 25 or 75 μM exposures.

We next sought to examine the acute consequences of these mitochondrial Zn^{2+} loads on $\Delta\Psi_m$ and reactive oxygen species (**ROS**) generation. To assess changes in $\Delta\Psi_m$, we used the cationic indicator Rhodamine 123 (**Rhod123**), which accumulates in mitochondria in proportion to their $\Delta\Psi_m$ (where its fluorescence is quenched); upon loss of $\Delta\Psi_m$, Rhod123 is released into the cytosol and the fluorescence increases (**Rhod123 ΔF**) (Duchen et al., 2003). ROS generation was assessed using the superoxide preferring oxidant sensitive

indicator, hydroethidine (**HEt**), which is oxidized by superoxide radicals into the highly fluorescent compound, ethidium. The fluorescence of ethidium is amplified upon its binding to DNA, providing high sensitivity and resulting in predominant visualization of the signal in the nucleus (Bindokas et al., 1996). Because the oxidized ethidium accumulates, the rate of fluorescence increase indicates ROS production rate, and the increase in HEt fluorescence (**HEt ΔF**) over baseline reflects total ROS production. Rhod123 and HEt loaded cultures were exposed to Zn^{2+} in high K^{+} and washed into 0 Ca^{2+} HSS, similarly as above. After the 300 μM Zn^{2+} exposures, we detected modest loss of $\Delta\psi_m$ (as indicated by Rhod123 ΔF prior to FCCP-induced maximal depolarization) and ROS production (as indicated by HEt ΔF); the 25 and 75 μM Zn^{2+} exposures had little effects (**Fig 2.1B**). Of note, although Zn^{2+} exposure has been found to cause delayed activation of the superoxide generating enzyme NADPH oxidase (**NOX**) (Noh and Koh, 2000), our prior studies indicated that ROS production with acute Zn^{2+} loads is predominantly of mitochondrial origin (Clausen et al., 2013; Sensi et al., 1999a). Thus, above data suggest that while neuronal Zn^{2+} entry through VGCC (modeling slow Zn^{2+} translocation) induces dose dependent mitochondrial Zn^{2+} accumulation, acute mitochondrial dysfunction was only detected with the strongest (300 μM) Zn^{2+} exposures.

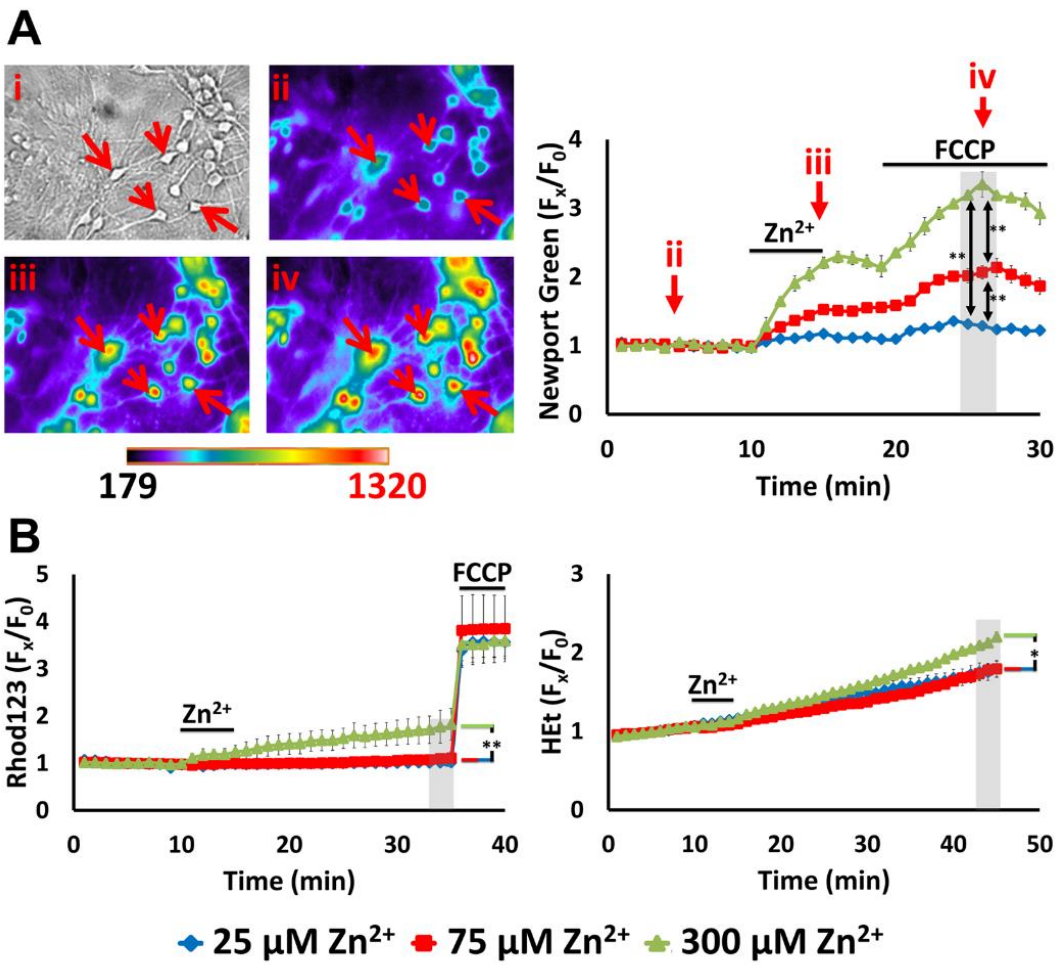

Figure 2.1. High K^+/Zn^{2+} exposures induce dose-dependent mitochondrial Zn^{2+} uptake but only mild acute dysfunction.

A. High K^+/Zn^{2+} exposures cause dose-dependent mitochondrial Zn^{2+} accumulation. Cultures were loaded with the low affinity cytosolic Zn^{2+} indicator Newport Green ($K_d \sim 1$ μM), exposed to 90 mM K^+ (high K^+) with Zn^{2+} (25, 75, 300 μM) for 5 min in 0 Ca^{2+} HSS, followed by wash into 0 Ca^{2+} HSS for additional 5 min prior to application of FCCP (1 μM). **Left:** Representative images: Brightfield image (**i**) shows appearance of neurons at baseline, and pseudocolor images show Newport Green fluorescence from the same field at baseline (**ii**), 5 min after high K^+/300 μM Zn^{2+} exposure (**iii**), and 5 min after FCCP (**iv**). (Arrows highlight the same neurons in these images.) **Right:** Traces show time course of Newport Green ΔF (background subtracted and normalized to baseline [F_x/F_0]; arrows indicate the time points illustrated in the images), and represent means ± standard error of the mean (SEM) of 6 experiments, ≥ 120 neurons. Grey bar indicates time points of comparison (** indicates $p < 0.01$ by one-way ANOVA with Tukey post hoc). Note the Zn^{2+} exposure concentration-dependent mitochondrial Zn^{2+} accumulation, indicated by the increase in ΔF after FCCP

B). These exposures only induce mild mitochondrial dysfunction: Cultures were loaded with the $\Delta\Psi_{mito}$ sensitive indicator, Rhod123, or the superoxide preferring ROS indicator, HEt, and exposed to high K^+/Zn^{2+} for 5 min, followed by wash into 0 Ca^{2+} HSS, as above. After 20 min, FCCP (1 μM) was applied to Rhod123-loaded cultures to induce full loss of $\Delta\Psi_m$. Traces show time course of Rhod123 ΔF (**left**) or HEt ΔF (**right**), normalized to baseline values (after background subtraction, as above; F_x/F_0), and represent mean ± SEM 6 experiments, ≥ 120 neurons. Grey bars indicate time points of comparison (* indicates $p < 0.05$, ** indicates $p < 0.01$, by one-way ANOVA with Tukey post hoc). Note that only 300 μM Zn^{2+} exposure induced discernable effects.

Critical role of cytosolic buffering in Zn^{2+}-triggered mitochondrial dysfunction

We next sought to examine the degree to which endogenous Zn^{2+} buffering, likely in large part via MTs, impacts Zn^{2+} dependent modulation of mitochondrial function. Indeed, whereas Zn^{2+} mobilization from cytosolic buffers appears able to impact mitochondrial function and trigger slow Zn^{2+} dependent injury even in the absence of exogenous Zn^{2+} entry (Aizenman et al., 2000; Sensi et al., 2003), there has been little quantitative assessment of these effects. To disrupt endogenous Zn^{2+} buffering, we used the disulfide compound 2,2-dithiodipyridine (DTDP) which oxidizes the sulfhydryls linking Zn^{2+} to cysteines, thus releasing bound Zn^{2+} from buffering proteins (like MTs) and preventing the released Zn^{2+} from being bound again (Aizenman et al., 2000; Maret and Vallee, 1998; Sensi et al., 2003).

To assess Zn^{2+} release from the buffers and its ability to enter mitochondria, we loaded cells (in 0 Ca^{2+} HSS) with the higher affinity Zn^{2+} indicator, FluoZin-3 ($K_d \sim 15$ nM) (Gee et al., 2002; Sensi et al., 2003), and monitored changes in fluorescence before and after application of 100 μM DTDP and subsequent addition of FCCP. In agreement with our prior observations (Sensi et al., 2003), this fairly high DTDP exposure caused a prompt but relatively modest Zn^{2+} rise, followed by a further sharp rise in cytosolic Zn^{2+} upon FCCP exposure, indicating robust mitochondrial Zn^{2+} accumulation (likely due to strong disruption of cytosolic buffering). With lower (60 μM) DTDP, we still observed an acute cytosolic Zn^{2+} rise and mitochondrial Zn^{2+} uptake, but these were markedly diminished, consistent with impaired—but not fully disrupted—Zn^{2+} buffering (**Fig 2.2A**).

To examine acute effects of these DTDP exposures on mitochondria, we used the $\Delta\Psi_m$ indicator Rhod123 and the ROS indicator HEt, as above. With continuous exposure to

100 μM DTDP, we noted a gradual increase in Rhod123 ΔF that progressed to subtotal loss of $\Delta\psi_m$ within 40 min (as indicated by lack of response to FCCP), and a rise in HEt ΔF indicative of increased ROS production. In contrast, with 60 μM DTDP, there was little Rhod123 or HEt ΔF (**Fig 2.2B**). Finally, to validate the Zn^{2+} dependence of these DTDP effects, we repeated strong (100 μM) DTDP exposures in the presence or absence of the membrane permeable Zn^{2+} chelator, N,N,N,N-tetrakis(2-pyridylmethyl)ethane-1,2-diamine (**TPEN;** 20 μM, applied 10 min before and with DTDP). TPEN application provided near complete block of both the Rhod123 and HEt ΔF, indicating that the acute effects of the DTDP exposure on mitochondrial function are largely Zn^{2+} dependent, likely resulting from movement of Zn^{2+} from the endogenous buffers into the mitochondria (**Fig 2.2C**). As prior studies found that DTDP can induce Ca^{2+} release from endoplasmic reticulum (McCord and Aizenmann, 2013), we assess changes in Ca^{2+} levels in response to 60 and 100 μM DTDP, and found no significant difference (data not shown), further supporting Zn^{2+} dependence of DTDP effects. Thus, these results confirm and extend prior studies (Sensi et al., 2003), and indicate dose dependent effects of protracted mobilization of endogenous Zn^{2+} stores on mitochondria, even in the absence of extracellular Zn^{2+} influx.

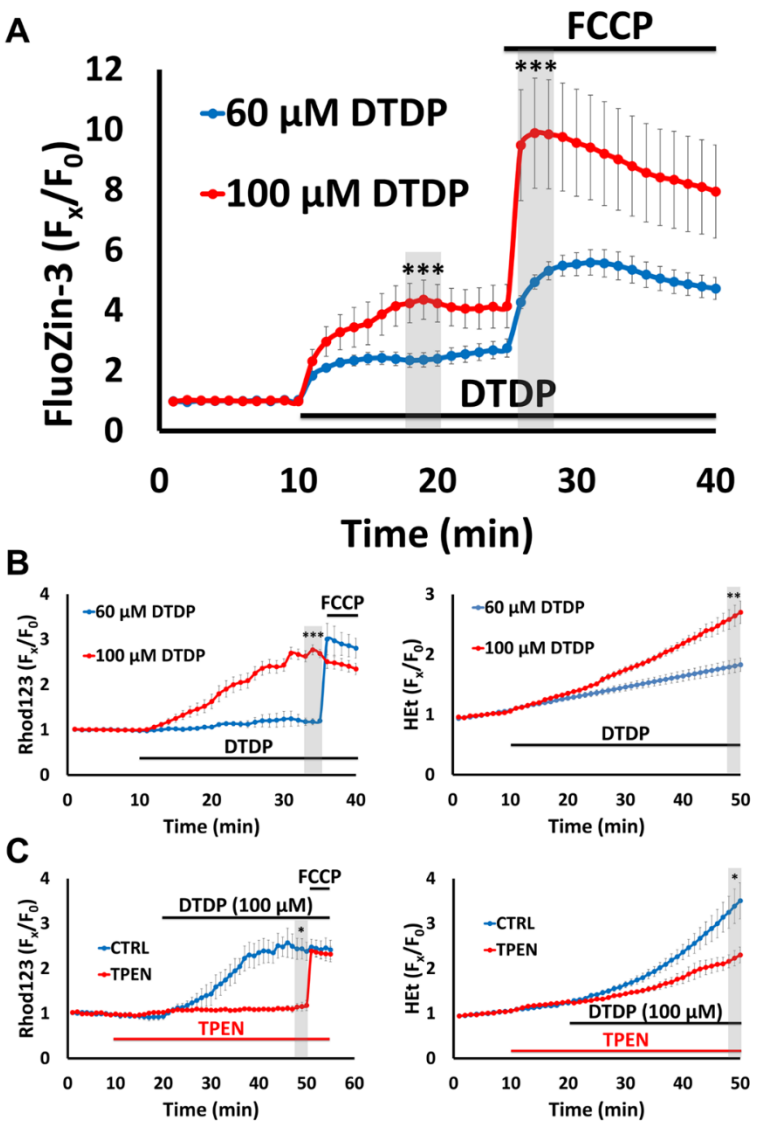

Figure 2.2. Disruption of cytosolic Zn^{2+} buffering leads to Zn^{2+}-dependent mitochondrial dysfunction. Cultures were loaded with the high affinity Zn^{2+} indicator FluoZin-3 ($K_d \sim 15$ nM), Rhod123 or HEt in 0 Ca^{2+} HSS, then exposed to DTDP (60 or 100 µM; to disrupt cytosolic Zn^{2+} buffering), with FCCP (1 µM) or TPEN (20 µM) applied as indicated. Traces represent mean ± SEM F_x/F_0 values for each indicator and represents ≥ 5 experiments consisting of ≥ 100 neurons. Grey bars indicate time points of comparison (* indicates $p < 0.05$, ** indicates $p < 0.01$, *** indicates $p < 0.001$, by two-tailed t-test).

A). DTDP induces dose-dependent cytosolic Zn^{2+} release and mitochondrial Zn^{2+} accumulation: FluoZin-3 loaded neurons were exposed to DTDP followed by addition of FCCP, as indicated. Note the dose dependent effects of DTDP, with 100 µM causing both greater cytosolic Zn^{2+} rise and mitochondrial Zn^{2+} loading (as indicated by the FCCP-induced ΔF) than 60 µM.

B). Disruption of buffering via DTDP can induce mitochondrial dysfunction: Rhod123- (**left**) or HEt- (**right**) loaded neurons were subjected to the indicated DTDP and FCCP exposures. Note that the 100 µM DTDP exposure resulted in substantial loss of $\Delta\Psi_{mito}$ within 25 min (as indicated by the minimal response to FCCP) and significant ROS production, while 60 µM DTDP had far smaller effects.

C). DTDP effects on mitochondria are Zn^{2+}-dependent: Rhod123- (**left**) or HEt- (**right**) loaded neurons were exposed to 100 µM DTDP ± Zn^{2+} chelator TPEN (applied 10 min before DTDP), followed by FCCP (only in Rhod123 loaded cultures), as indicated. Note that TPEN largely eliminated the DTDP induced loss of $\Delta\Psi_{mito}$ (**left**) and markedly attenuated the ROS production (**right**).

While above findings help clarify the degree to which the integrity of cytosolic Zn^{2+} buffering can impact mitochondria, disruption of buffering (due to acidosis/oxidative stress) would most likely occur concurrently with extracellular Zn^{2+} accumulation (largely from vesicular release) in pathological conditions like ischemia. Thus, we next sought to examine how relatively low extracellular Zn^{2+} accumulation (at levels that may occur in ischemia) can impact mitochondria when cytosolic Zn^{2+} buffering is impaired. To this aim, we combined two exposures that each caused little acute mitochondrial dysfunction when applied alone (modest Zn^{2+} entry triggered by 5 min high K^+ exposure with 50 μM Zn^{2+}, and partial disruption of buffering induced by 60 μM DTDP), and compared the consequences with those of a far greater exogenous Zn^{2+} exposure alone (high K^+/300 μM Zn^{2+} in the absence of DTDP; **see Fig 2.1B, .2.2B**). Using Newport Green, Rhod123, and HEt to assess mitochondrial Zn^{2+} loading, loss of $\Delta\psi_m$ and ROS generation respectively (as in **Fig 2.1**), we found these exposures to induce similar levels of acute mitochondrial Zn^{2+} accumulation (as indicated by the similar Newport Green ΔF upon adding FCCP; **Fig 2.3A**), but the combined exposure caused markedly greater loss of $\Delta\psi_m$ and ROS generation than the higher Zn^{2+} exposure alone (**Fig 2.3B, C**). Furthermore, the loss of $\Delta\psi_m$ and ROS generation occurring after the high K^+/50 μM Zn^{2+}/DTDP exposure are not transient, but appeared to progress at a near constant rate (as indicated by the slope of the Rhod123 and HEt ΔF traces) for the duration of the recording period.

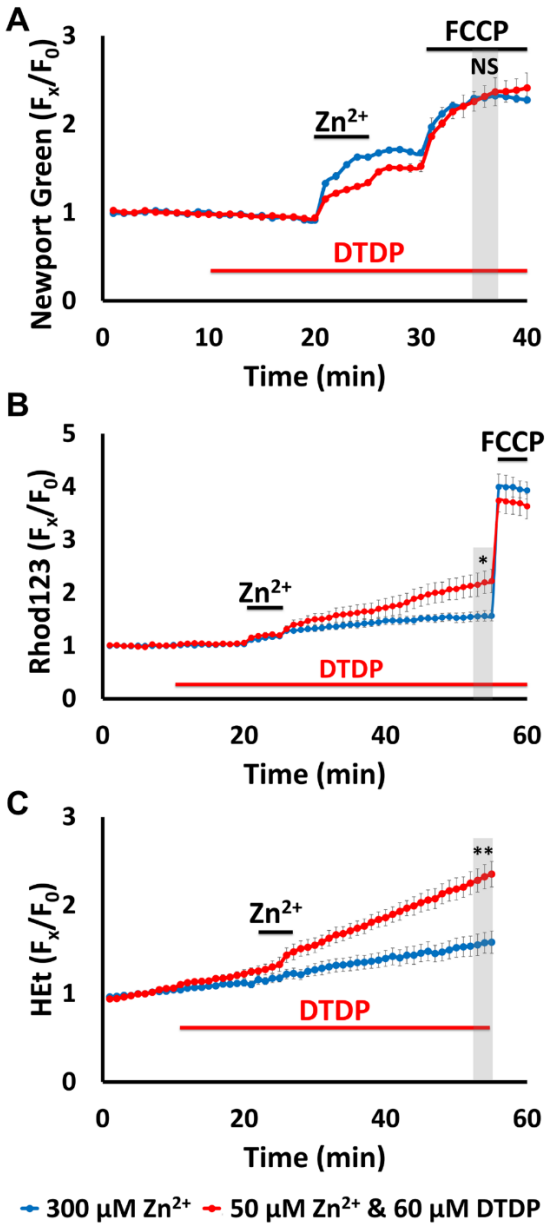

Figure 2.3. Impaired cytosolic Zn^{2+} buffering markedly enhances the acute impact of Zn^{2+} exposures on mitochondria.
Cultures were loaded with Newport Green, Rhod123, or HEt in 0 Ca^{2+} HSS, and exposed to high K^+/300 µM Zn^{2+} alone (**blue**), or to high K^+/50 µM Zn^{2+} with 60 µM DTDP (applied as indicated; **red**); FCCP (1 µM) was added as indicated. Traces represent mean ± SEM F_x/F_0 values for each dye and represents 6 experiments consisting of ≥ 120 neurons. Grey bars indicate time points of comparison (NS indicates No Significance, * indicates $p < 0.05$, ** indicates $p < 0.01$, by two-tailed t-test).
A). Low exogenous Zn^{2+} exposure to neurons with impaired buffering results in similar degrees of mitochondrial uptake as much higher Zn^{2+} exposure with intact buffering: Note the similar magnitudes of mitochondrial Zn^{2+} loading caused by the high K^+/300 µM Zn^{2+} (**blue**) and the high K^+/50 µM Zn^{2+}/DTDP exposures.
B, C). However, the lower Zn^{2+} exposure with impaired buffering results in greater mitochondrial dysfunction: Rhod123 (**B**) or HEt (**C**) loaded neurons were exposed as indicated. Note that the 50 µM Zn^{2+}/DTDP exposure induced markedly greater loss of $\Delta\psi_m$ and ROS generation than 300 µM Zn^{2+} alone.

Prior studies have estimated that neurons exposed to high K^+/300 μM Zn^{2+} reaches free cytosolic Zn^{2+} levels in the 100s of nM range (a significant increase, given that resting free resting free cytosolic Zn^{2+} levels are estimated to be in the 10-100 pM range) (Canzoniero et al., 1999; Sensi et al., 1999; Colvin et al., 2010; Frederickson et al., 2005; Maret, 2015). However, rather than a transient increase, DTDP likely prolongs the duration of this concentration. Thus, despite similar degrees of acute mitochondrial Zn^{2+} accumulation, the greater and longer-lasting mitochondrial dysfunction triggered by the lower Zn^{2+} exposure with DTDP likely reflects a greater persistence of the Zn^{2+} within the mitochondria, triggered by both release of bound Zn^{2+} and an impaired ability to buffer the Zn^{2+} entering neurons.

Finally, we examined the Zn^{2+} exposure dependence of the combined high K^+/Zn^{2+}/60 μM DTDP exposures by comparing effects obtained using 50 μM Zn^{2+} with those occurring with lower (10 μM) Zn^{2+} exposures. Not surprisingly, the effects were strongly dose dependent, with the higher exposure causing more mitochondrial Zn^{2+} accumulation (**Fig 2.4A**) and greater acute effects on $\Delta\psi_m$ and ROS generation (**Fig 2.4B, C**). Interestingly, the difference was greater for the ROS generation, with both exposures only causing partial loss of $\Delta\psi_m$. In sum, above data indicate that even partial disruption of cytosolic Zn^{2+} buffering can significantly exacerbate the impact of neuronal Zn^{2+} entry on mitochondria, and thus is likely to be a critical determinant of the extent of Zn^{2+}-triggered mitochondrial disruption after ischemia.

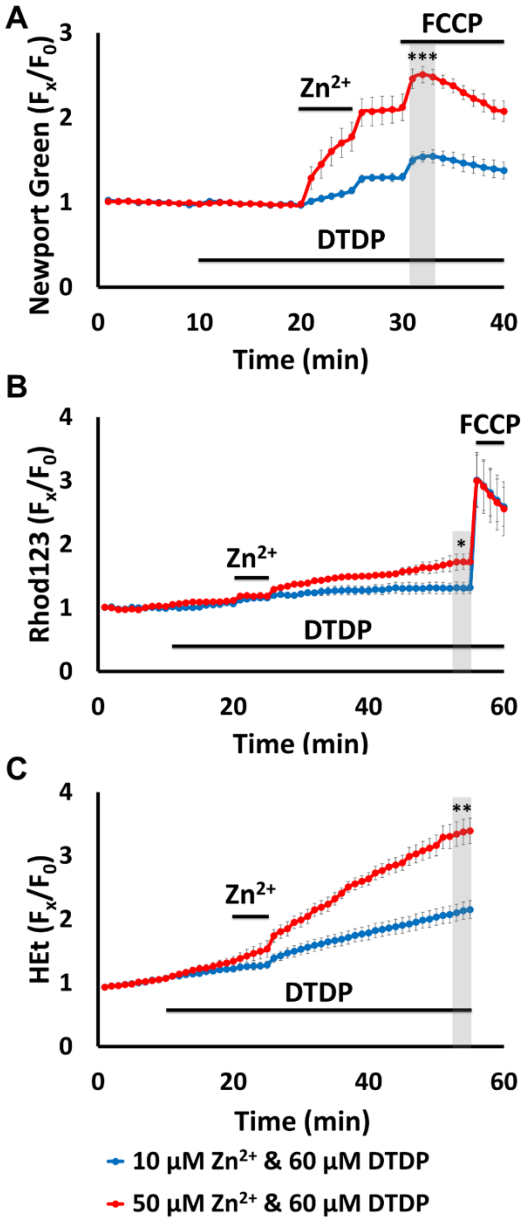

Figure 2.4. Zn^{2+} exposure dose-dependence of mitochondrial Zn^{2+} loading and acute dysfunction in neurons with impaired buffering.
Cultures were loaded with Newport Green, Rhod123 or HEt in 0 Ca^{2+} HSS, and exposed to high K^{+} with 10 (**blue**) or 50 (**red**) µM Zn^{2+} in 60 µM DTDP. FCCP (1 µM) was added as indicated. Traces represent mean ± SEM F_x/F_0 values for each dye and represents 6 experiments consisting of ≥ 120 neurons. Grey bars indicate time points of comparison (* indicates $p < 0.05$, ** indicates $p < 0.01$, *** indicates $p < 0.001$, by two-tailed t-test).
A). Zn^{2+} exposure induces dose-dependent mitochondrial Zn^{2+} loading in neurons with disrupted buffering: Note the dose dependency of the cytosolic Zn^{2+} rise and mitochondrial Zn^{2+} uptake, with the 50 µM Zn^{2+} exposure causing far greater Zn^{2+} uptake than the 10 µM Zn^{2+}.
B, C). Mitochondrial dysfunction reflects the extent of Zn^{2+} accumulation: Rhod123 (**B**) or HEt (**C**) loaded neurons were exposed as indicated. Note that the 50 µM Zn^{2+} exposure induced far greater loss of $\Delta\psi_m$ and ROS generation than 10 µM Zn^{2+}. Further note that despite causing relatively strong ROS generation, 50 µM Zn^{2+} still only caused modest loss of $\Delta\psi_m$.

Ca^{2+} reduces Zn^{2+} uptake but exacerbates consequent mitochondrial dysfunction

Above experiments (like many prior studies of Zn^{2+} effects) were carried out in Ca^{2+} free media, to ensure Zn^{2+}-specificity of effects. However, as Ca^{2+} is always present *in vivo*, we felt it crucial to next examine effects of Zn^{2+} in the presence of physiologic (1.8 mM) levels of Ca^{2+}. First, to assess effects of Ca^{2+} on cytosolic and mitochondrial Zn^{2+} accumulation, Newport Green loaded cultures were subjected to a range of Zn^{2+} loads (high K^+/300 μM Zn^{2+} alone, or high K^+ with 10 or 50 μM Zn^{2+}/60 μM DTDP) for 5 min in 0 or 1.8 Ca^{2+} HSS. The NMDA antagonist, MK-801 (10 μM) was added during these exposures to prevent rapid Ca^{2+} influx through highly Ca^{2+} permeable NMDAR. In each of these conditions, the presence of Ca^{2+} decreased both the cytosolic Zn^{2+} rises (likely reflecting competition for entry through VGCC) (Kerchner et al., 2000; Weiss et al., 1993) and the mitochondrial Zn^{2+} uptake (assessed as the ΔF upon application of FCCP; **Fig 2.5A**).

Despite above findings of reduced mitochondrial Zn^{2+} loading in the presence of Ca^{2+}, some prior studies have suggested that these ions may have synergistic effects on mitochondrial function (Gazaryan et al., 2007; Jiang et al., 2001; Sensi et al., 2000). Thus, we next used Rhod123 and HEt loaded cultures to examine how the presence of Ca^{2+} influences Zn^{2+} effects on $\Delta\psi_m$ and ROS generation. To assess possible synergism, we first examined the low end of the Zn^{2+} exposure range (high K^+ with 10 μM Zn^{2+}/60 μM DTDP) that caused little loss of $\Delta\psi_m$ and ROS generation in 0 Ca^{2+} HSS (**Fig 2.4B**). In a new set of experiments. cultures were exposed to high K^+/60 μM DTDP (with 10 μM MK-801) in the presence of either 10 μM Zn^{2+}, 1.8 mM Ca^{2+} or with both Zn^{2+} and Ca^{2+}. In addition, as NOX activation has been reported to contribute, along with mitochondria, to acute Ca^{2+} triggered ROS generation (unlike acute Zn^{2+} triggered ROS, which appears mostly to be of

mitochondrial origin, as discussed above), the NOX inhibitor apocynin (500 μM) was added in HEt loaded cultures to prevent ROS generation due to Ca^{2+} dependent activation of this enzyme (Brennan et al., 2009; Clausen et al., 2013). While the high K^+ exposures with either the 10 μM Zn^{2+} or 1.8 mM Ca^{2+} alone had little acute impact on the mitochondria, the combined exposure resulted in substantially greater loss of $\Delta\psi_m$ and ROS generation (**Fig 2.5B**), further supporting that Ca^{2+} and Zn^{2+} synergistically impact the mitochondria. To ensure that these effects were not due to additional ion loading via entry through the Ca-AMPAR (which permit more rapid influx than VGCC, as discussed above), we did additional control experiments with the AMPA channel antagonist 2,3-dihydroxy-6-nitro-7-sulfamoyl-benzo(F)quinoxaline (NBQX; 10 μM) present during Ca^{2+} and/or Zn^{2+} exposures (Sensi et al., 1999a). We found that addition of NBQX made no difference in our findings (data not shown), in line with our prior study that Ca-AMPAR are expressed only in a small subset (~ 13%) of cultured cortical neurons (Yin et al., 1994) and further supporting that the observed enhanced effects were due to synergy.

Finally, we examined the dose dependence of loss of $\Delta\psi_m$ and ROS generation at the high end of the exposure range, in light of our prior observations (**Fig 2.4B, C**) that high K^+/50 μM Zn^{2+}/60 μM DTDP exposures caused substantial ROS generation but rather modest loss of $\Delta\psi_m$. Rhod123 and HEt loaded cultures were exposed to high K^+ with Zn^{2+} (50 or 300 μM) and 1.8 mM Ca^{2+} in 60 μM DTDP (with MK-801, and apocynin added in HEt loaded cultures as above). Whereas both of these exposures caused similar strong and persistent ROS generation, there was a clear dose dependency on the loss of $\Delta\psi_m$, with the 50 μM Zn^{2+} exposure still causing only partial loss of $\Delta\psi_m$, while the "maximal" (and likely supraphysiological) 300 μM Zn^{2+} exposure triggered near complete loss of $\Delta\psi_m$ (**Fig 2.5C**).

This highlights the ability of mitochondria to maintain at least partial $\Delta\psi_m$ despite quite strong Zn^{2+} loads that cause strong and persistent ROS generation.

Thus, despite the presence of Ca^{2+} in the extracellular fluid resulting in decreased cytosolic and mitochondrial Zn^{2+} accumulation, it markedly increases the consequent Zn^{2+} effects on the mitochondria, highlighting strong synergism of these 2 cations. Indeed, the degree of synergism is sufficient that even a quite brief and low extracellular Zn^{2+} exposure (5 min, 10 μM Zn^{2+}) applied under pathophysiologically relevant conditions (with Ca^{2+} present in depolarized neurons with partially impaired Zn^{2+} buffering) triggered substantial acute effects on the mitochondria.

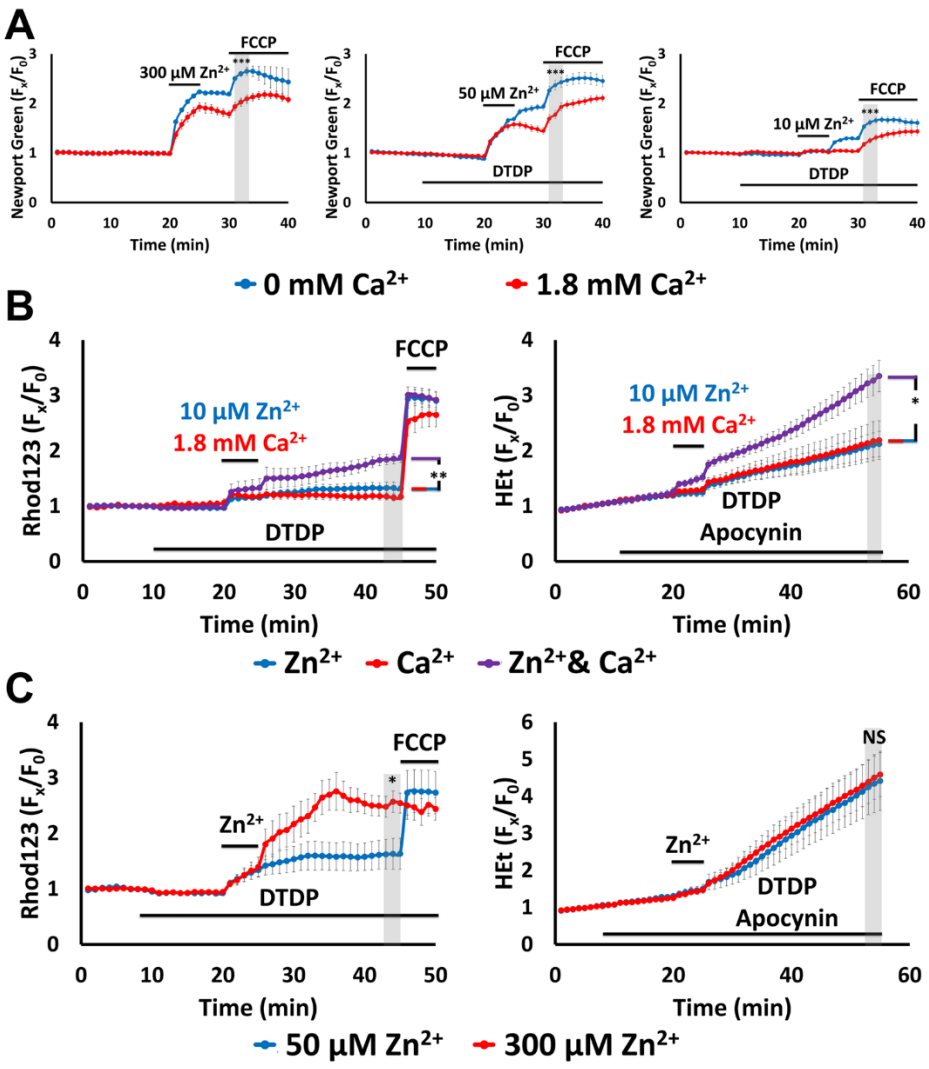

Figure 2.5. Ca^{2+} attenuates mitochondrial Zn^{2+} accumulation despite exacerbating the consequent dysfunction.

Cultures were loaded with Newport Green, Rhod123 or HEt in 0 or 1.8 Ca^{2+} HSS, and exposed to high K^+ with 300, 50,10 or 0 µM Zn^{2+} (as indicated, along with 10 µM MK-801, to inhibit Ca^{2+}-entry via NMDAR activation); DTDP (60 µM), FCCP (1 µM) and/or apocynin (500 µM) were added as indicated. Traces represent mean ± SEM F_x/F_0 values for each dye and represents ≥ 5 experiments consisting of ≥ 120 neurons. Grey bars indicate time points of comparison (NS indicates No Significance, * indicates $p < 0.05$, ** indicates $p < 0.01$, *** indicates $p < 0.001$, by two-tailed t-test [**A, C**] or by one-way ANOVA with Tukey post hoc [**B**]).

A). Presence of Ca^{2+} decreases neuronal and mitochondrial Zn^{2+} uptake: Note that presence of Ca^{2+} attenuated both cytosolic Zn^{2+} rise during the exposure and FCCP-induced mitochondrial Zn^{2+} release.

B). Ca^{2+} and Zn^{2+} synergistically induce mitochondrial dysfunction: Neurons loaded with Rhod123 (**left**) or HEt (**right**) were exposed to high K^+/DTDP/MK-801 with 10 µM Zn^{2+} (**blue**), 1.8 mM Ca^{2+} (**red**) or with both Zn^{2+} and Ca^{2+} (**purple**) for 5 min, then washed as indicated. Apocynin was added to HEt-loaded neurons (**right**) to inhibit contributions from Ca^{2+}-dependent NOX activation. Note that despite relatively little effects from Ca^{2+} and Zn^{2+} individually, together they induced significant mitochondrial dysfunction.

C). Overwhelming mitochondrial Zn^{2+} loading induces rapid mitochondrial depolarization: Neurons loaded with Rhod123 (**left**) or HEt (**right**) in 1.8 Ca^{2+} HSS were exposed to high K^+/DTDP/MK-801/Ca^{2+}, with 50 (**blue**) or 300 µM (**red**) Zn^{2+} for 5 min, followed by wash as indicated. Note that 300 µM Zn^{2+} induced greater loss of $\Delta\Psi_m$ than 50 µM Zn^{2+}, despite both inducing similar levels of ROS generation.

Mitochondrial Zn^{2+} accumulation induces rapid swelling and disruption of mitochondrial respiration

Above findings lend credence to the hypothesis that neuronal Zn^{2+} entry contributes to mitochondrial dysfunction in pathological conditions like ischemia. However, whereas the measures employed thus far (loss of $\Delta\psi_m$ and ROS production) are valuable indices of acute disruption, they are not indicative of long lasting mitochondrial dysfunction or loss of viability that may ultimately lead to neurodegeneration.

To address this, we first examined acute changes in mitochondrial morphology triggered by Zn^{2+} loads. While mitochondria are mostly rod shaped, in pathological conditions like ischemia, both Ca^{2+} and Zn^{2+} can trigger either transient or irreversible morphologic changes, including swelling (Brustovetsky et al., 2002; Halestrap, 2006; Jiang et al., 2001; Sugawara et al., 1999).

To assess mitochondrial morphology, cultures were loaded with the fluorescent mitochondrial marker, MitoTracker Green (200 nM), and neuronal mitochondria examined using confocal microscopy at 1000x (as described in Material and methods). This marker has the advantages that it covalently binds to mitochondrial proteins (and thus stays in neuronal mitochondria despite loss of $\Delta\psi_m$) and maintains fluorescence in oxidative environments (Buckman et al., 2001; Jiang et al., 2001). Cultures were exposed as indicated to high K^+/MK-801 with Zn^{2+} and/or Ca^{2+} (± DTDP) and images acquired at baseline, after the 5 min Zn^{2+}/Ca^{2+} exposure, and, finally, 10 min after wash (into HSS ± DTDP) (as indicated in **Fig 2.6A, B**). We examined effects of 60 μM as well as 100 μM DTDP, to assess possible consequences of Zn^{2+} loads with both partial and near maximal disruption of cytosolic buffering, as might occur during episodes of strong *in vivo* ischemia.

To assess morphological changes, images were blinded to experimental condition and time point, and imported into Image J software, where the lengths and widths of distinct mitochondria were measured manually (see Material and methods); data are expressed as mean length/width (**L/W**) ratios normalized to baseline values (which ranged from 4-8; mean 5.9 ± 0.3).

There were distinct differences triggered by the different exposures (**Fig 2.6C**): 1). Exposure to high K^+/1.8 mM Ca^{2+} alone caused a significant swelling of mitochondria evident at the end of the 5 min exposure, that had largely recovered after 10 min wash. 2). High K^+ with 300 μM Zn^{2+} alone, or with 50 μM Zn^{2+}/60 μM DTDP (both in 0 Ca^{2+} HSS) did not cause swelling evident at the end of the exposure, but mild swelling was evident 10 min later in both treatments. 3). High K^+/50 μM Zn^{2+}/100 μM DTDP exposures in 0 Ca^{2+} HSS caused marked swelling at the end of the exposure that substantially progressed over the subsequent 10 min; with Ca^{2+} present, the swelling at both time points was even greater, with extreme rounding up of mitochondria that may be indicative of irrecoverable damage. Of note, we found little morphological changes after 10 min pre-treatment with DTDP (60 or 100 μM in 0 or 1.8 Ca^{2+} HSS) prior to Zn^{2+} exposure (data not shown), further supporting the need for contributions from both extracellular Zn^{2+} entry and intracellular Zn^{2+} mobilization to potently impact the mitochondria. In summary, these data suggest distinct effects of these ions, with Ca^{2+} being an effective trigger of acute transient—but largely recoverable—swelling, while Zn^{2+} induces swelling of slower onset, that, when "strengthened" (by DTDP and synergism with Ca^{2+}) appears to be strongly progressive after termination of the exposure.

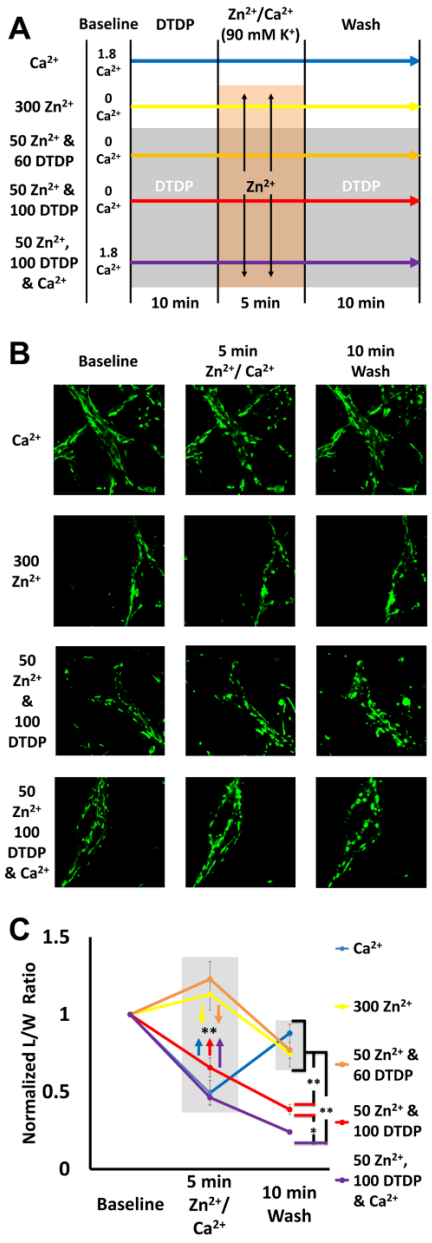

Figure 2.6. Effects of Ca^{2+}, Zn^{2+}, and disruption of cytosolic Zn^{2+} buffering on mitochondrial morphology.

A). Experiment schematic: Neurons loaded with the mitochondrial dye MitoTracker Green (200 nM) were placed in 0 or 1.8 Ca^{2+} HSS, then exposed to DTDP (60 or 100 µM; where indicated), high K^+/MK-801 with Zn^{2+} (0, 50, or 300 µM) and/or 1.8 mM Ca^{2+}, followed by wash into HSS ± DTDP, as described.

B). Representative images: Confocal images (1000x) were taken at baseline, 5 min after Zn^{2+} and/or Ca^{2+} exposure, and 10 min after wash.

C). Zn^{2+} and Ca^{2+} induce different patterns of morphology change: The length and width of individual mitochondria were measured blindly, and length/width (L/W) ratios calculated and normalized to baseline. Values for baseline, 5 min after exposure, and after 10 min wash are displayed. Traces show mean ± SEM normalized L/W ratio for each time point, each representing ≥ 5 experiments consisting of ≥ 50 mitochondria (* indicates $p < 0.05$, ** indicates $p < 0.01$, by one-way ANOVA with Tukey post hoc). Note that while the Ca^{2+} induces a rapid but transient morphologic change, Zn^{2+} triggers more progressive changes (that increase with the degree of Zn^{2+} loading).

We next sought to examine delayed effects of the Zn^{2+} exposures on mitochondrial respiration. Indeed, as the main function of mitochondria is energy production, which is dependent upon the integrity of the electron transport chain, we felt it critical to assess such effects, which, in contrast to loss of $\Delta\psi_m$ and ROS production, provide a direct measure of the disruption of mitochondrial respiratory capacity after an insult. For these studies, we made use of a device (the Seahorse XF24 analyzer) which measures the O_2 consumption rate (**OCR**) in cultures at baseline and in response to sequential application of the following drugs: (1) the ATP synthase inhibitor, oligomycin (1 μM), which prevents dissipation of the proton gradient across the inner membrane due to ATP synthesis, leading to membrane hyperpolarization and slowing of electron transport; the decrease in OCR upon its application provides an estimate of the portion of O_2 consumption contributing to ATP production; (2) FCCP (2 μM), which dissipates the proton gradient, uncoupling the electron transport chain, yielding maximal oxidative capacity and OCR, and; (3) combined application the complex I blocker, rotenone, and the complex III blocker, antimycin A (both 1 μM), to fully inhibit the electron transport chain, and blocking all mitochondrial respiration (**Fig 2.7A**) (Brand and Nicholls, 2011).

We carried out two sets of experiments. The first aimed to examine synergism between effects of Zn^{2+} and Ca^{2+} (via exposure to high K^+/MK-801 with 300 μM Zn^{2+}, 1.8 mM Ca^{2+}, or both Zn^{2+} and Ca^{2+} **Fig 2.7B left**), while the second aimed to examine the degree to which disruption of cytosolic Zn^{2+} buffering can exacerbate Zn^{2+}-triggered respiratory inhibition (via exposure to high K^+/MK-801 with 300 μM Zn^{2+}, 100 μM DTDP alone, 10 μM Zn^{2+} + DTDP, all in 0 Ca^{2+} HSS; **Fig 2.7C left**). When present, DTDP was added 10 min prior to, during and for 20 min after the high K^+ exposures, to ensure strong

disruption of buffering at the time of and for a period after the Zn^{2+} loading. Our findings were generally consistent with those above, examining Zn^{2+} effects on $\Delta\psi_m$, ROS generation, and mitochondrial morphology. Specifically, whereas OCR after high K^+ exposures with either 300 μM Zn^{2+} or 1.8 mM Ca^{2+} alone was not different from that of control (wash into 1.8 Ca^{2+} HSS), with combined Zn^{2+} and Ca^{2+} exposure, both the basal and the maximal uncoupled OCR (upon FCCP exposure) were substantially decreased (by ~ 50%) (**Fig 2.7B right**). Similarly, whereas OCR after exposure to either 100 μM DTDP or high K^+/300 μM Zn^{2+} alone was little different from that of control (wash into 0 Ca^{2+} HSS), exposure to high K^+/10 μM Zn^{2+}/DTDP caused almost complete inhibition of respiration (**Fig 2.7C right**). Of note, these effects on respiration were long-lasting, persisting even at the time of FCCP application (>2 h after the high K^+/Zn^{2+} exposures).

In sum, these findings further support the hypothesis that mitochondrial Zn^{2+} accumulation (enhanced and prolonged by disrupted cytosolic Zn^{2+} buffering), can act synergistically with Ca^{2+} to disrupt mitochondrial function. The intense swelling and long lasting respiratory inhibition caused by the low Zn^{2+} exposures with 100 μM DTDP (but not by DTDP alone) lend further credence to the idea that Zn^{2+}-triggered mitochondrial dysfunction may be irreversible and contribute to neuronal death in pathological conditions.

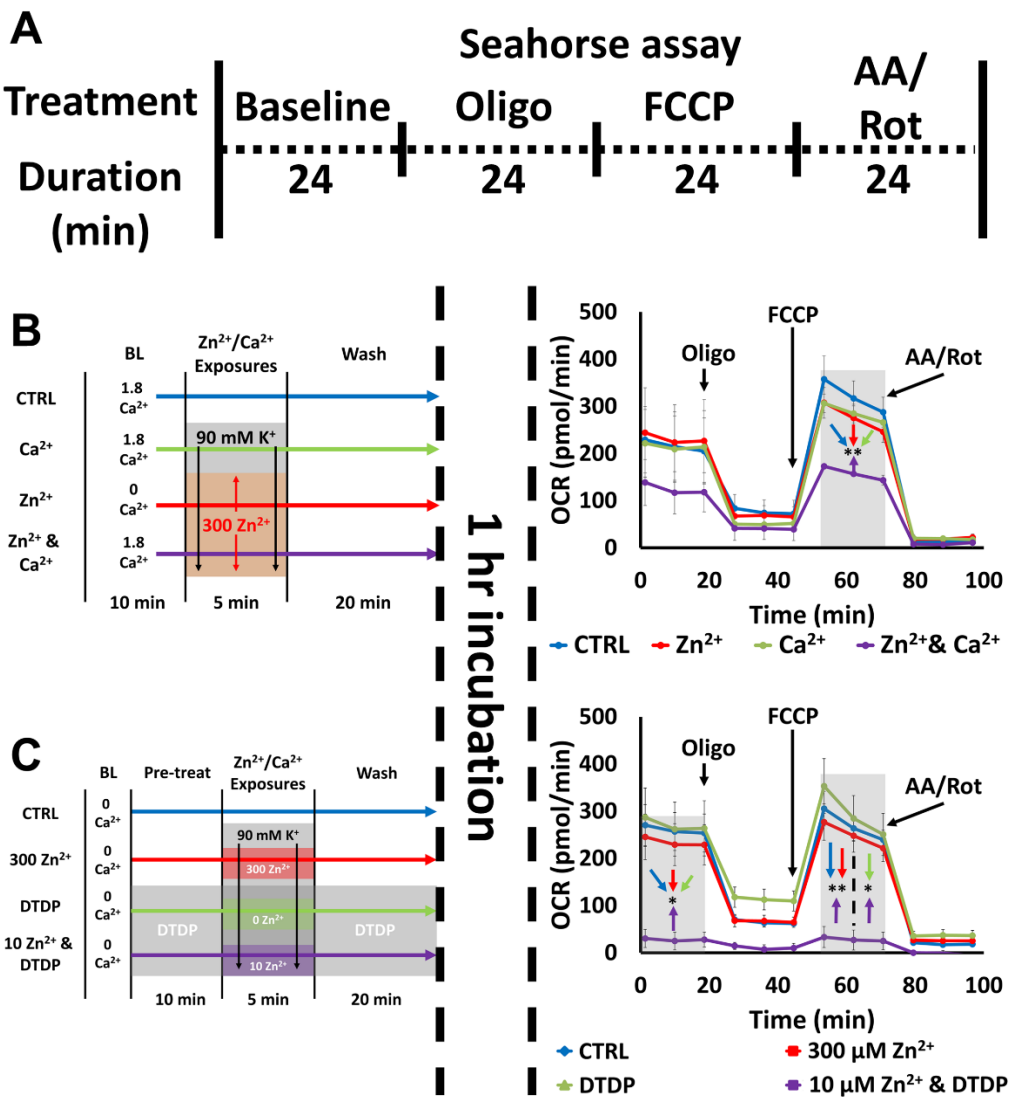

Figure 2.7. Zn^{2+}-induced inhibition of mitochondrial respiration: synergy with Ca^{2+} and effects of disrupted buffering.

A). Schematic of experiment: Neurons were exposed to a series of treatments (detailed in **B** and **C**, left), incubated for 1 hr, then placed in the Seahorse assay, which measures O_2 consumption rate (OCR) at baseline and after sequential application of oligomycin (**Oligo**; 1 µM), FCCP (2 µM), and antimycin A & rotenone (**AA/Rot**; both 1 µM) to characterize various respiratory parameters. Traces (**B** and **C**, right) show time course of OCR and represent mean ± SEM of 3 – 4 wells of cultured neurons, with arrows indicating time point at which mitochondrial inhibitors were added. Grey bars indicate time points of comparison (* indicates $p < 0.05$, ** indicates $p < 0.01$, by one-way ANOVA with Tukey post hoc).

B). Ca^{2+} and Zn^{2+} synergistically inhibit mitochondrial respiration: Neurons were placed in 0 or 1.8 Ca^{2+} HSS, exposed to high K^+/MK-801 with 300 µM Zn^{2+}, 1.8 mM Ca^{2+} or both Zn^{2+} and Ca^{2+} as described (**left**). After 1 hr incubation OCR was measured (**right**). Note that simultaneous exposure to Zn^{2+} and Ca^{2+} induced significant inhibition of mitochondrial respiration, despite the ions having minimal effects individually.

C). Disrupted Zn^{2+} buffering significantly exacerbates Zn^{2+} effects on mitochondrial respiration: Neurons were placed in 0 Ca^{2+} HSS, exposed to DTDP (100 µM; where indicated), high K^+/MK-801 with Zn^{2+} (300, 10 or 0 µM, as indicated; **left**). After 1 hr incubation OCR was measured (**right**). Note the near complete inhibition of mitochondrial respiration by 10 µM Zn^{2+} exposure with DTDP.

Mitochondrial Zn^{2+} accumulation contributes to dose-dependent cell death

While above studies showing pronounced mitochondrial swelling and long lasting respiratory inhibition might predict that these effects would contribute to subsequent neurodegeneration, they are not in themselves indicative of cell death. We thus felt it important to carry out neurotoxicity studies, to more directly address the cytotoxic consequences of the mitochondrial effects (**Fig 2.8**).

Three sets of studies—generally paralleling those on mitochondrial respiration (**Fig 2.7**)—were carried out to assess the importance of both Zn^{2+}-Ca^{2+} synergy and integrity of cytosolic Zn^{2+} buffering to delayed neurodegeneration. In the first set, cultures were exposed to high K^+/MK-801 with 300 μM Zn^{2+}, 1.8 mM Ca^{2+}, or both Zn^{2+} and Ca^{2+} for 5 min (**Fig 2.8A**). In the second set, cultures were pre-exposed to 100 μM DTDP prior to 5 min high K^+/MK-801 with 0, 50 or 100 μM Zn^{2+} (± Ca^{2+}), followed by 10 min washout into DTDP (**Fig 2.8B**). In the third set, cultures were pre-exposed to 100 μM DTDP prior to 5 min high K^+/MK-801 with 50 μM Zn^{2+} + Ca^{2+}, followed by 10 min washout into DTDP (**Fig 2.8C**). In all sets, neurons were transferred to MEM (supplemented with 25 mM glucose) and returned to the incubator for 24 hrs (or 2 hrs in **Fig 2.8C**, as described) after which neuronal injury was assessed via direct morphological examination and by lactate dehydrogenase (LDH) efflux assay (as described in Material and methods). Our findings are again consistent with above studies on mitochondrial function, with Ca^{2+} strongly enhancing Zn^{2+} triggered cell death (in neurons with both intact and disrupted buffering), and with Zn^{2+} exposure inducing dose-dependent injury under conditions of strongly disrupted buffering (**Fig 2.8A, B**).

We have also assessed cell death at 2 hrs, matching the time of the substantial respiratory inhibition seen above (**Fig 7C**), and find that toxicity at this early point is less than half seen at 24 hrs (**Fig 2.8C**), suggesting cell death is not an immediate consequence of mitochondrial dysfunction but rather a slowly progressing, downstream event. While these findings do not directly prove that Zn^{2+} induced mitochondrial dysfunction caused the cell death, the similarity of effects for both mitochondrial dysfunction and neurodegeneration strongly suggest a link between the two.

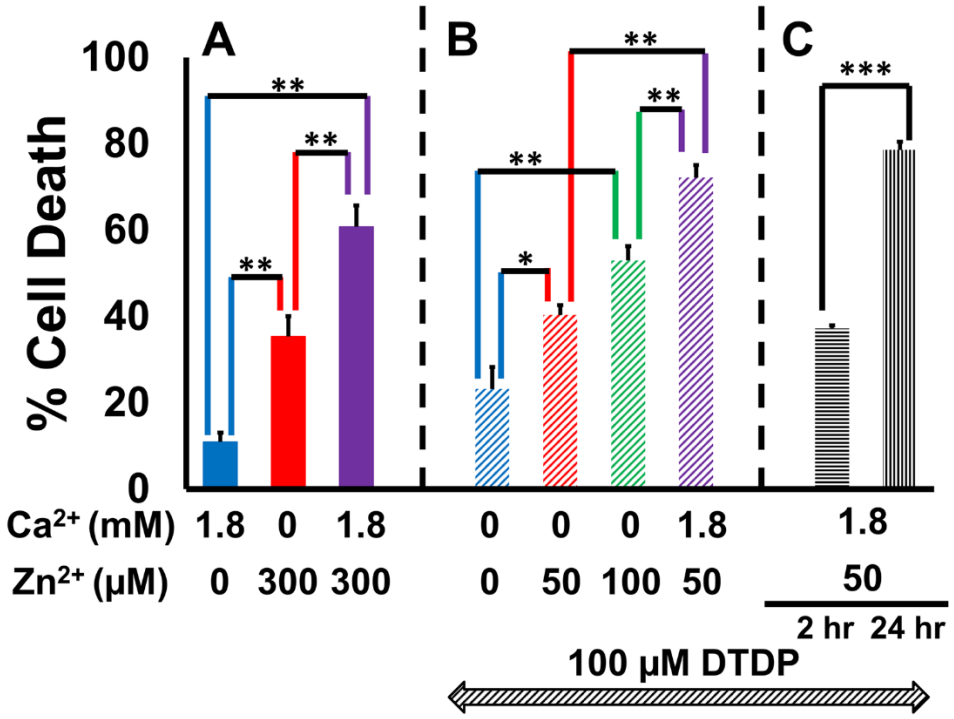

Figure 2.8. Mitochondrial Zn^{2+} accumulation contributes to neuron death.
Neurons were exposed to a sequence of 10 min DTDP (100 μM; in **B** only), 5 min high K^+/MK-801 exposures with Zn^{2+} and/or Ca^{2+} (concentration as shown), washed for 10 min, transferred to MEM + 25 mM glucose and returned to the incubator for 24 hrs (or 2 hrs; in **C** only), prior to assessing cell death via LDH efflux assay. Bars represent % cell death (see Material and methods), and represent mean ± SEM of 3 independent experiments, each consisting of 4 wells of cultured neurons (* indicates $p < 0.05$, ** indicates $p < 0.01$, *** indicates $p < 0.001$ by one-way ANOVA with Tukey post hoc [**A** and **B**] or by two-tailed t-test [**C**]).
A). Ca^{2+} and Zn^{2+} synergistically induce cell death: Note that while 300 μM Zn^{2+} induced more cell death than 1.8 mM Ca^{2+}, its impact was further exacerbated by the presence of Ca^{2+}.
B). Dose-dependency of Zn^{2+}-induced cell death with strong disrupted buffering: Note the dose-dependent increase in cell death with increased Zn^{2+} exposures, that was further enhanced by presence of Ca^{2+}.
C). Zn^{2+}-induced cell death occurs over hours: Note the significantly higher cell death at 24 hrs compared to 2 hrs.

CHAPTER 3

Zn^{2+} entry through the mitochondrial calcium uniporter: critical contributor to mitochondrial dysfunction and neurodegeneration

While prior studies discussed above have indicated that Zn^{2+} can also enter the mitochondria through the MCU, the specificity of the pore's role in Zn^{2+}-triggered injury is still debated. In this chapter, we use recently available MCU knockout mice to examine how the deletion of this channel impacts deleterious effects of Zn^{2+}. In cultured cortical neurons from MCU knockout mice, we find significantly reduced mitochondrial Zn^{2+} accumulation. Correspondingly, these neurons were protected from both acute and delayed Zn^{2+}-triggered mitochondrial dysfunction, including mitochondrial ROS generation, depolarization, swelling and inhibition of respiration. Furthermore, when toxic extramitochondrial effects of Ca^{2+} entry were moderated, both cultured neurons (exposed to Zn^{2+}) and CA1 neurons of hippocampal slices (subjected to prolonged oxygen glucose deprivation to model ischemia) from MCU knockout mice displayed decreased neurodegeneration.

Genetic deletion of MCU attenuates mitochondrial Zn^{2+} accumulation in cortical neurons

As prior studies of mitochondrial Zn^{2+} entry through the MCU have only used pharmacologic agents (as discussed above), using the MCU KO mice, we first sought to validate that Zn^{2+} can indeed enter the mitochondria through the MCU, with greater specificity than previously possible. Wildtype (**WT**) and MCU KO cultured neurons were

loaded with the low affinity cytosolic Zn^{2+} indicator Newport Green ($K_d \sim 1$ μM) in 0 mM Ca^{2+} HSS, and exposed to a sequence of 25, 75, and 300 μM exogenous Zn^{2+} (5 min each). Because VGCC are routes of exogenous Zn^{2+} entry through the plasma membrane that are more uniformly expressed across cortical neurons (in contrast to Ca-AMPAR, which are more selectively expressed in specific subsets of neurons), all Zn^{2+} exposures were performed in the presence of 90 mM K^+ ("**high K^+**"; to depolarize neurons, permitting Zn^{2+} influx through VGCC). MK-801 (10 μM), an NMDAR blocker used to prevent Ca^{2+} entry, was also added during Zn^{2+} exposures (even in Ca^{2+}-free conditions) in all experiments to eliminate any confounders caused by the channel activation. The dose-response curve consistently displayed greater Newport Green fluorescence rises (**ΔF**)—indicating higher cytosolic Zn^{2+} levels—in MCU KO neurons (**Fig 3.1 top**). After the Zn^{2+} exposures, the mitochondrial protonophore, carbonyl cyanide 4-(trifluoromethoxy)phenylhydrazone ("**FCCP**"; 1 μM, 5 min) was added. This dissipates the electrochemical gradient necessary for Zn^{2+} to be retained in mitochondria, leading to release of mitochondrial Zn^{2+} to the cytosol, and the consequent Newport Green ΔF estimates the degree of mitochondrial Zn^{2+} accumulation (Clausen et al., 2013; Ji and Weiss, 2018; Medvedeva et al., 2017; Sensi et al., 2003; Sensi et al., 2002). Note that FCCP increased Newport Green ΔF to similar peak levels in both genotypes, despite MCU KO displaying greater cytosolic Zn^{2+} levels during Zn^{2+} exposures, indicating attenuation of mitochondrial Zn^{2+} accumulation in the MCU KO neurons (**Fig 3.1 top**).

After validating Zn^{2+} uptake through the MCU with a spectrum of Zn^{2+} exposures alone, we next examined the role of the pore in permitting Zn^{2+} entry under more physiologic conditions, as may occur during homeostatic Zn^{2+} movement, by inducing

partial disruption of endogenous Zn^{2+} buffering and far lower extracellular Zn^{2+} entry. To do so, WT and MCU KO neurons were loaded with high affinity cytosolic Zn^{2+} indicator FluoZin-3 ($K_d \sim 15$ nM) in 0 mM Ca^{2+} HSS, and exposed to 2,2'-dithiodipyridine (**DTDP**), a thiol oxidant that disrupts Zn^{2+} binding to intracellular buffering proteins, at 60 μM, a concentration which induces partial intracellular Zn^{2+} mobilization (Ji and Weiss, 2018). Neurons were subsequently exposed to 1 μM Zn^{2+} + high K^+ with continued DTDP, followed by wash, and FCCP exposure as indicated (**Fig 3.1 middle**). As above, MCU KO neurons displayed significantly greater cytosolic Zn^{2+} levels in response to both intracellular Zn^{2+} mobilization alone as well as the subsequent low Zn^{2+} exposure. Furthermore, the lack of FluoZin-3 ΔF in response to FCCP in MCU KO indicates minimal mitochondrial Zn^{2+} accumulation, in contrast to the robust mitochondrial uptake occurring in WT.

While findings thus far support the notion that MCU facilitates mitochondrial Zn^{2+} entry, as Zn^{2+} exposures were carried out in the absence of Ca^{2+}, it is possible that the role MCU plays in Zn^{2+}-triggered mitochondrial dysfunction in pathophysiologic conditions (where Ca^{2+} is present) may be different. To address this, WT and MCU KO neurons loaded with Newport Green in 1.8 mM Ca^{2+} HSS were exposed to DTDP, 100 μM Zn^{2+} + high K^+, wash, and FCCP as indicated (**Fig 3.1 bottom**). This paradigm—combining both disruption of intracellular Zn^{2+} buffering and moderate exogenous Zn^{2+} exposure—was chosen, as it likely best reflects what may occur under pathophysiological conditions like ischemia. Similarly to findings in Ca^{2+}-free conditions, MCU KO neurons still displayed both higher cytosolic Zn^{2+} levels during Zn^{2+} exposure and reduced FCCP-induced mitochondrial Zn^{2+} release, further validating the critical role played by the MCU in permitting mitochondrial Zn^{2+} accumulation, whether from extracellular or intracellular sources.

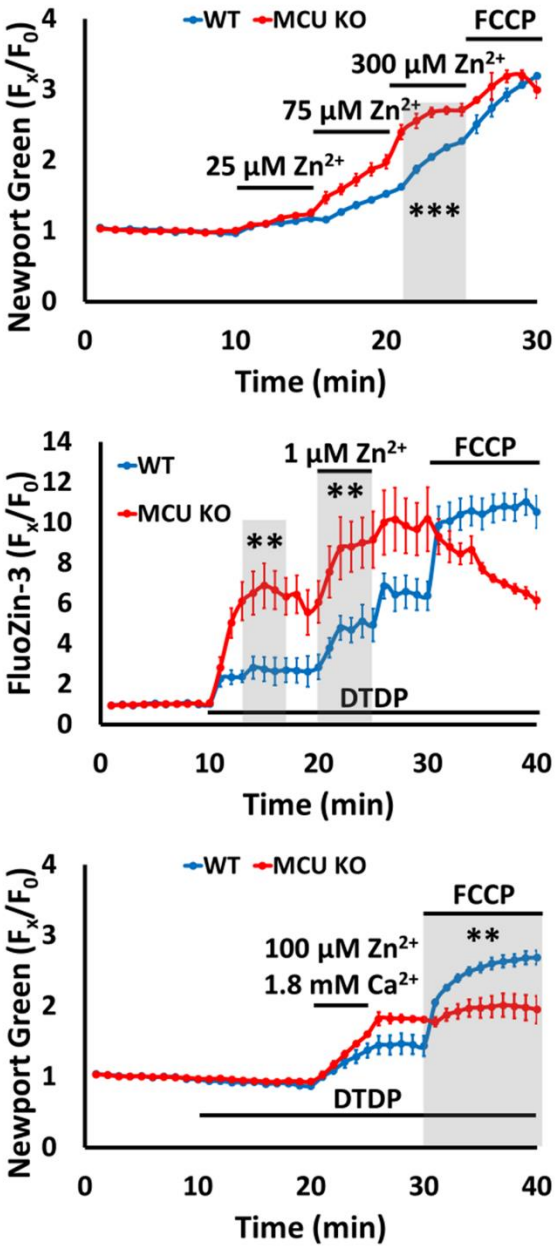

Figure 3.1. Mitochondrial Zn^{2+} accumulation is attenuated in mice with genetic deletion of MCU. WT (blue) and MCU KO (red) cultured cortical neurons were loaded with either low affinity cytosolic Zn^{2+} indicator Newport Green (**top and bottom**) or high affinity cytosolic Zn^{2+} indicator FluoZin-3 (**middle**), and exposed to indicated doses of exogenous Zn^{2+} with 90 mM K^+ ("**high K^+**", along with 10 μM MK-801 to inhibit Ca^{2+}-entry through the NMDAR). DTDP (60 μM; to disrupt cytosolic Zn^{2+} buffering) and FCCP (1 μM; to release mitochondrially sequestered Zn^{2+}) were added as indicated. Studies were carried out in HSS with either 0 mM Ca^{2+} (**top and middle**; to ensure observations of Zn^{2+} specifically) or 1.8 mM Ca^{2+} (**bottom**; to better model physiological condition). Traces show time course of indicator ΔF (background subtracted and normalized to baseline, [F_x/F_0]), and represent means ± standard error of the mean (**SEM**) of at least 6 experiments, consisting of ≥ 120 neurons. Grey bars indicate time points of comparison (** indicates $p < 0.01$, *** indicates $p < 0.001$, by two-tailed t-test). Note that MCU KO neurons consistently displayed greater ΔF in response to exogenous Zn^{2+} exposures and/or disrupted buffering, as well as reduced FCCP responses, both of which indicate the critical role that MCU plays in facilitating Zn^{2+} entry into mitochondria.

Zn^{2+}-triggered mitochondrial ROS production is specifically attenuated in MCU KO neurons

We next examined whether Zn^{2+}-triggered ROS production, long considered to be a critical contributor to downstream injury cascades (Ji et al., 2019), is also attenuated in MCU KO neurons. Indeed, as we have previously found that acute Zn^{2+}-induced ROS generation was almost entirely of mitochondrial origin (unlike Ca^{2+}-induced ROS, which had important contributions from both mitochondria and the cytosolic enzyme NADPH oxidase [**NOX**]) (Clausen et al., 2013), we expected minimal Zn^{2+}-triggered ROS generation in MCU KO, corresponding to the attenuated mitochondrial Zn^{2+} accumulation (as shown in **Fig 3.1**). Thus, WT and MCU KO neurons were loaded with Hydroethidine (**HEt**; a superoxide sensitive indicator whose fluorescence increase, ΔF, indicates total ROS production) (Bindokas et al., 1996; Clausen et al., 2013; Ji and Weiss, 2018) in 0 mM Ca^{2+} HSS, and exposed to DTDP (60 μM, 10 min), 100 μM Zn^{2+} + high K^+ (5 min), and wash as indicated (**Fig 3.2, Top**). In contrast to our expectation, there was no difference in HEt ΔF.

This appeared to contradict our prior finding that acute Zn^{2+}-triggered ROS is primarily of mitochondrial origin (Clausen et al., 2013). However, in light of previous studies which found that prolonged low level Zn^{2+} exposures could induce NOX activity (Noh and Koh, 2000), we hypothesized that the ROS generation in MCU KO could result from NOX upregulation secondary to the impaired mitochondrial Zn^{2+} buffering in the MCU KO, resulting in persistently higher cytosolic Zn^{2+} levels. To test this idea, the experiment was repeated in the presence of the NOX inhibitor, apocynin (500 μM), which almost completely eliminated Zn^{2+}-triggered ROS production in MCU KO neurons while having little effect in WT neurons (**Fig 3.2 Middle**). Repeating the experiment in physiological

(1.8 mM) Ca^{2+} HSS again revealed near elimination of Zn^{2+}-triggered ROS rise in MCU KO neurons with NOX inhibition (**Fig 3.2 Bottom**), further supporting the hypothesis that Zn^{2+}-triggered *mitochondrial* ROS generation is critically dependent upon entry through the MCU.

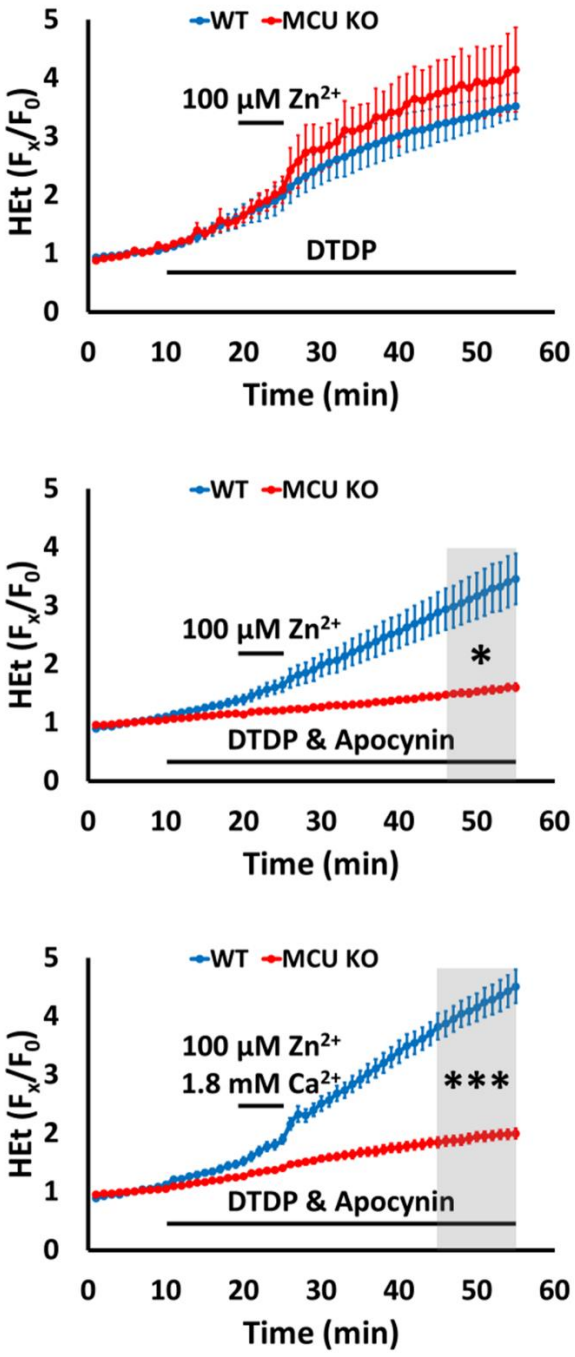

Figure 3.2. Zn^{2+}-triggered mitochondrial—but not cytosolic—ROS production is attenuated in MCU KO neurons.
WT (blue) and MCU KO (red) cultured neurons loaded with superoxide preferring ROS indicator Hydroethidine (**HEt**) in either 0 mM Ca^{2+} (**top and middle**) or 1.8 mM Ca^{2+} (**bottom**) HSS were exposed to 100 µM Zn^{2+} + high K^+, with DTDP (60 µM) and apocynin (500 µM) added as indicated. Traces display mean ± SEM F_x/F_0 values for HEt ΔF and represent ≥ 8 experiments consisting of ≥ 160 neurons. Grey bars indicate time points of comparison (* indicates $p < 0.05$, *** indicates $p < 0.001$, by two-tailed t-test). Despite the similar total ROS generation (**top**), note that Zn^{2+}-triggered ROS rise specifically from mitochondria (assessed via addition of NOX inhibitor apocynin to attenuate cytosolic ROS production) was significantly attenuated in MCU KO neurons (**top and bottom**).

Critical role of the MCU in acute and delayed Zn^{2+}-triggered mitochondrial dysfunction

We next examined the MCU dependence of other measures of Zn^{2+}-triggered mitochondrial dysfunction. As our goal was to better understand the pore's role in pathophysiologic conditions, we decided to use an exposure paradigm that models events likely to occur in pathological events like ischemia, incorporating both disruption of buffering and uptake of synaptic Zn^{2+} (henceforth termed the "**ischemic Zn^{2+} exposure**"; that parallels the paradigms used in **Fig 3.1 and 3.2 bottom** panels, and comprises 10 min pre-exposure to 60 μM DTDP, followed by 5 min 100 μM Zn^{2+} + high K^+ + DTDP and 3x wash into DTDP, all in 1.8 mM Ca^{2+} HSS; see Materials and methods).

We first examined the role of MCU in Zn^{2+}-triggered loss of mitochondrial membrane potential (**$\Delta\Psi_m$**) using Rhodamine 123 (**Rhod123**; 2 μM), a cationic indicator for which a cytosolic fluorescence increase (**ΔF**) indicates loss of $\Delta\Psi_m$ (see Materials and Methods). WT and MCU KO neurons loaded with Rhod123 were treated to the ischemic Zn^{2+} exposure, washed, and exposed to FCCP as indicated (**Fig 3.3A**). The lack of Rhod123 ΔF in MCU KO in response to the Zn^{2+} exposure (compared to the acute ΔF seen after addition of Zn^{2+} in WT neurons), indicates that the Zn^{2+} entry through the MCU is necessary to induce $\Delta\Psi_m$ loss (**Fig 3.3A**). FCCP, which causes maximal mitochondrial depolarization, increased Rhod123 ΔF to similar levels in both WT and MCU KO, indicating that the observed difference was not due to differences in the basal $\Delta\Psi_m$ between the two genotypes.

Next, we examined Zn^{2+} effects on mitochondrial energy production using the Seahorse assay, which measures oxygen consumption rate (**OCR**) at baseline and in response to sequential application of mitochondrial inhibitors (oligomycin, FCCP, and

antimycin A/rotenone), respectively indicating baseline respiration, ATP-linked respiration, maximum respiratory capacity, and extramitochondrial respiration. WT and MCU KO neurons were treated with either sham or the ischemic Zn^{2+} exposure, washed for 20 min, and incubated for 2 hrs prior to running the assay. Note the substantial preservation of mitochondrial respiration in MCU KO, in contrast to its significant inhibition in WT (**Fig 3.3B**).

Finally, we examined the long term effect of Zn^{2+} entry through the MCU on mitochondrial morphology. WT and MCU KO neurons were treated to the ischemic Zn^{2+} exposure, washed for 20 min, and after 12 hr incubation, cultures were loaded with the mitochondrial morphology marker, MitoTracker Green (200 nM) and examined under confocal microscopy (1000x; **Fig 3.3C left**). The length and the width of individual mitochondria were then measured blindly to determine their length/width (**L/W**) ratios, which were then collected to calculate the average L/W ratio of the mitochondria in a single neuron (**Fig 3.3C right**). Note that WT neurons showed multiple fragmented, swollen mitochondria (and a corresponding low L/W ratio), while MCU KO mitochondria preserved their morphology, maintaining their elongated structures with high L/W ratio (**Fig 3.3C**). These findings, showing significant protection from Zn^{2+}-effects in MCU KO over a spectrum of time, further validate the crucial role of the MCU in the induction of Zn^{2+} triggered mitochondrial dysfunction.

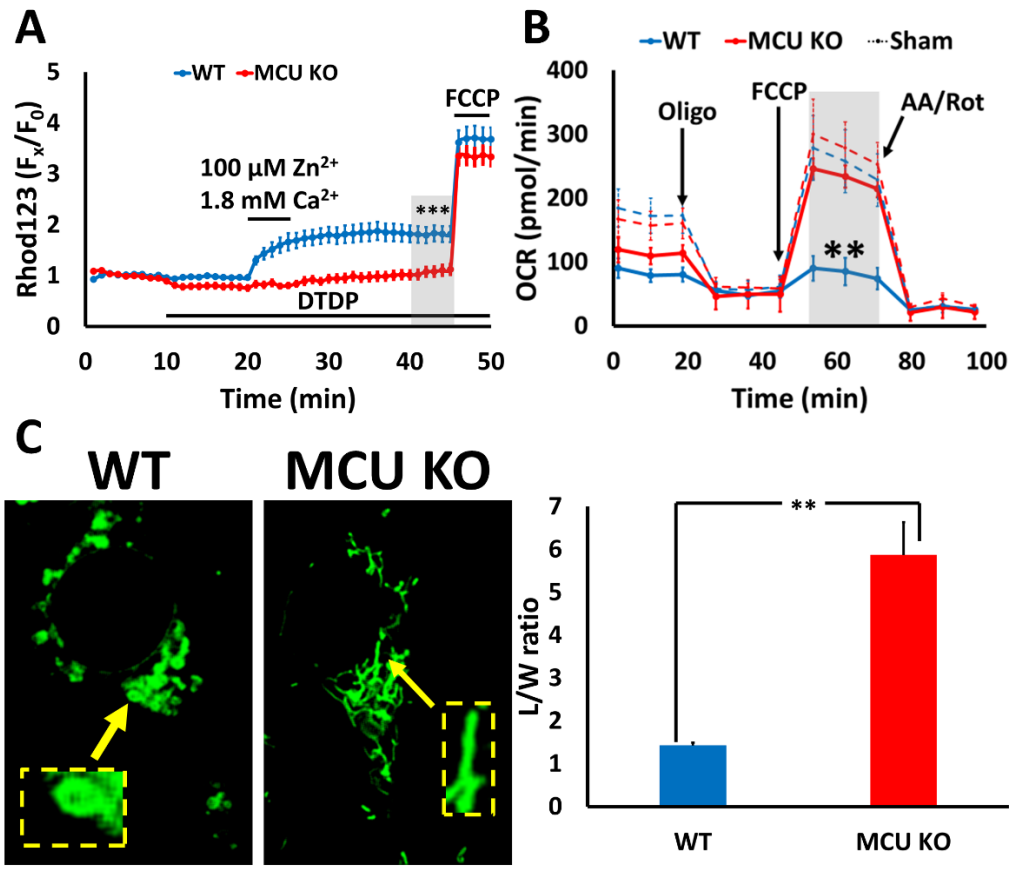

Figure 3.3. Genetic deletion of MCU confers prolonged protection from Zn^{2+}-triggered mitochondrial dysfunction.

WT (blue) and MCU KO (red) cultured neurons were exposed to the ischemic Zn^{2+} exposure (DTDP [60 μM; 10 min], 100 μM Zn^{2+} + high K^+ [5 min], followed by wash [20 min]). Grey bars indicate time points of comparison (** indicates $p < 0.01$, *** indicates $p < 0.001$, by two-tailed t-test).

A. Zn^{2+}-induced mitochondrial depolarization is attenuated in MCU KO neurons. WT and MCU KO neurons loaded with $\Delta\Psi_m$-sensitive indicator Rhodamine 123 (**Rhod123**) were treated to the ischemic Zn^{2+} exposure as indicated, followed by FCCP (1 μM; 5 min). Traces represent mean ± SEM F_x/F_0 values for Rhod123 ΔF and represent 8 experiments consisting of ≥ 160 neurons. Note the absence of Rhod123 ΔF in response to Zn^{2+} in MCU KO neurons, indicating protection from Zn^{2+}-induced mitochondrial depolarization.

B. Mitochondrial respiration is preserved after Zn^{2+} exposure in MCU KO neurons. WT and MCU KO neurons were treated to either sham (dashed lines) or the ischemic Zn^{2+} exposure (solid lines) as described above. After 2 hr incubation, cultures were placed in the Seahorse device, which measures O_2 consumption rate (**OCR**) during baseline and after sequential application of oligomycin (**Oligo**; 1 μM), FCCP (2 μM), and antimycin A/rotenone (**AA/Rot**; both 1 μM). Traces show time course of OCR and represent mean ± SEM of 3 separate experiments, each consisting of 3 – 4 wells of cultured neurons, with arrows indicating time point at which mitochondrial inhibitors were added. Note that mitochondrial respiration was preserved in MCU KO neurons in response to Zn^{2+}, compared to its dramatic inhibition WT.

C. MCU KO neurons are protected from Zn^{2+}-triggered disruption of mitochondrial morphology. 12 hrs after WT and MCU KO neurons were treated to ischemic Zn^{2+} exposure, mitochondria were labeled with MitoTracker Green and observed under confocal microscopy (1000x). Length/width ratio (**"L/W ratio"**) was calculated based on blinded measurement. Representative images (**left**) and average L/W ratios (**right**) for WT and MCU KO neurons are displayed. Bar graphs show mean + SEM of L/W ratio, each representing ≥ 5 experiments comprising ≥ 50 mitochondria. Note the significant mitochondrial fragmentation and swelling in WT neurons, compared to the elongated morphology maintained by MCU KO neuronal mitochondria, both of which correspond to their respective L/W ratios.

Zn^{2+}-specific contributions to neurotoxicity and ischemic neurodegeneration are attenuated in MCU KO neurons

Next, we sought to determine whether the beneficial effects observed in MCU KO neuronal mitochondria also extend to Zn^{2+}-triggered neurodegeneration. To this aim, WT and MCU KO neurons were exposed to the ischemic Zn^{2+} exposure (labeled as **Ca^{2+} & Zn^{2+}** exposure in **Fig 3.4A**), washed for 20 min, and returned to the incubator for 24 hrs prior to assessing cell death. Degree of neurodegeneration was quantified by lactate dehydrogenase (**LDH**) efflux assay and validated by morphological examination (see Materials and methods). To our surprise, in contrast to our findings on mitochondrial dysfunction, both WT and MCU KO neurons displayed similar degrees of neurodegeneration (**Fig 3.4A**). In light of prior reports that cells from MCU KO mice were not protected from Ca^{2+}-induced cell death (Nichols et al., 2017; Pan et al., 2013), we next sought to separately assess the Ca^{2+} and Zn^{2+} contributions to neurotoxicity in MCU KO neurons. When neurons were exposed to 1.8 mM Ca^{2+} + high K^+ alone (**Ca^{2+}** only exposure), MCU KO was not protective, and in fact markedly potentiated the Ca^{2+} dependent injury compared to WT neurons. However, with Zn^{2+} + high K^+ (with DTDP) and no Ca^{2+} (**Zn^{2+}** only exposure), MCU KO was protective compared to WT. To determine if MCU KO neurons would display neuroprotection if Ca^{2+} contributions were attenuated, cell death in WT and MCU KO neurons was quantified after the ischemic Zn^{2+} exposure (which includes both Zn^{2+} and Ca^{2+}) was repeated in the presence of the NOX inhibitor apocynin (as in **Fig. 2**, above), aiming to reduce the injury burden caused by cytosolic Ca^{2+} actions (including Ca^{2+}-induced NOX activation) (Brennan et al., 2009). Indeed, with NOX inhibition, we found significant neuroprotection from Zn^{2+}-induced injury in MCU KO neurons (**Fig 3.4A**),

supporting the hypothesis that targeting Zn^{2+} entry through the MCU specifically—unlike indiscriminate MCU blockade against both Ca^{2+} and Zn^{2+}—could be neuroprotective.

To test these findings in a model closer to *in vivo* injury, we next examined response to prolonged oxygen-glucose deprivation (**OGD**), as a model of ischemia, in acute hippocampal slices from MCU KO and WT mice. CA1 pyramidal neurons were loaded with low affinity, ratiometric cytosolic Ca^{2+} indicator Fura FF ($K_d \sim 6$ μM) (Medvedeva et al., 2009; Medvedeva and Weiss, 2014) and subjected to OGD (via perfusion with artificial cerebral spinal fluid [**ACSF**] bubbled with nitrogen gas to remove oxygen, and with glucose replaced by sucrose) with either physiologic (2 mM; **Fig 3.4B left**) or low Ca^{2+} levels (200 μM, to minimize Ca^{2+}-contributions to injury; **Fig 3.4B right**). Consistent with prior studies using pharmacologic MCU blockade (Medvedeva and Weiss, 2014), MCU KO slices displayed an accelerated onset of the lethal Ca^{2+} deregulation event in response to OGD with physiologic Ca^{2+} (**Fig 3.4B left**), possibly reflecting loss the of mitochondrial Ca^{2+} buffering capacity, and consequent increased cytosolic Ca^{2+} loading and activation of cytosolic Ca^{2+} dependent cell death pathways. However, when Ca^{2+} contributions to injury were attenuated (via lower Ca^{2+} levels), onset of Ca^{2+} deregulation was significantly delayed in MCU KO neurons (**Fig 3.4B right**). These data from hippocampal slices show that when extramitochondrial effects of Ca^{2+} are moderated, MCU deletion can confer significant protection against ischemic neurodegeneration. As the degree of this protection is similar to that conferred by Zn^{2+} chelation observed in prior studies (Medvedeva and Weiss, 2014), taken together with our current findings from cultured neurons, these observations support the hypothesis that attenuating mitochondrial Zn^{2+} accumulation through the MCU is neuroprotective.

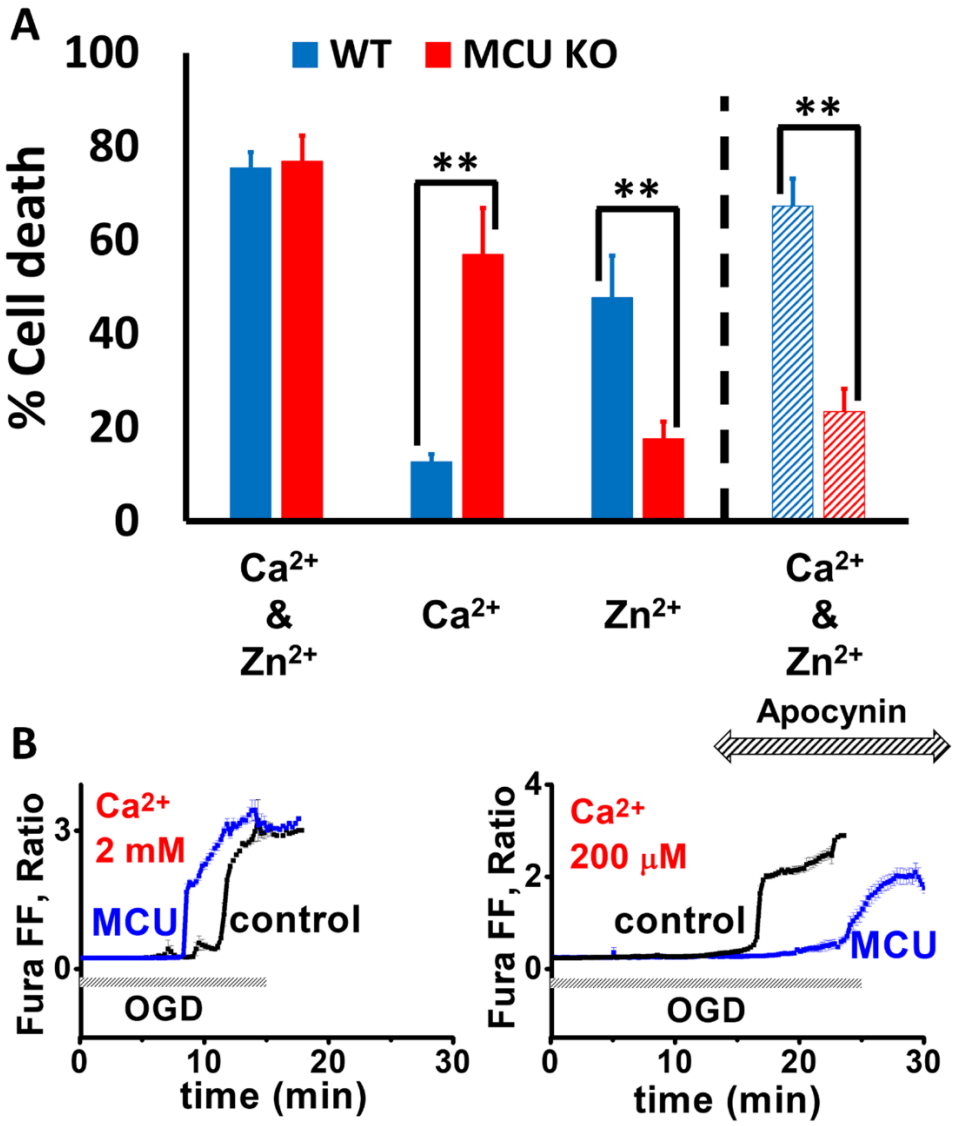

Figure 3.4. Zn^{2+}-specific contributions to neurotoxicity and ischemic neurodegeneration are attenuated in MCU KO cultured neurons and hippocampal slices.

A. Zn^{2+}-triggered neurotoxicity is attenuated in cultured MCU KO neurons. WT (blue) and MCU KO (red) neurons were exposed to a sequence of DTDP (10 min), Zn^{2+} and/or Ca^{2+} (all with high K^+; 5 min), and washed in DTDP ± Apocynin (500 µM) for 20 min. After 24 hr incubation, cell death was quantified with LDH efflux assay and validated with direct morphological examination. Concentrations used are indicated. Bars represent mean % cell death ± SEM of 6 independent experiments, each consisting of 4 wells of cultured neurons. Note that with attenuation of Ca^{2+}-contributions to injury (either via Ca^{2+}-free conditions or NOX inhibition), MCU KO neurons were significantly protected from Zn^{2+}-triggered neurotoxicity.

B. Ischemic neurodegeneration is delayed in MCU KO hippocampal CA1 neurons when Ca^{2+}-contributions are moderated. Individual CA1 pyramidal neurons in hippocampal slices from WT (black; "**control**") or MCU KO (blue; "**MCU**") were loaded with the cytosolic Ca^{2+} indicator Fura FF and subjected to prolonged OGD in artificial CSF containing either 2 mM (**left**) or 200 µM (**right**) Ca^{2+}. Traces show time course of ratio of Fura FF emissions upon excitation at 340 and 380 nm and represent mean ± SEM of ≥ 5 separate repetition. Note that while MCU KO CA1 neurons showed more rapid Ca^{2+} deregulation (as indicated by irreversible Fura FF signal rise) with physiologic (2 mM) Ca^{2+} (**left**; likely due to rapid, unbuffered cytosolic Ca^{2+} accumulation leading to more rapid catastrophic injury), when effects of Ca^{2+} were attenuated, ischemic neurodegeneration was significantly delayed (**right**).

CHAPTER 4

Delayed Zn^{2+} targeting interventions offers neuroprotective benefits

In this chapter, we applied the findings from the prior chapters to examine the potential utility of delayed interventions to attenuate both the mitochondrial dysfunction and neurodegeneration trigged by Zn^{2+}. In cultured neurons, we found that Zn^{2+} chelation after the high K^+/Zn^{2+} exposure attenuated both ROS production and neurodegeneration. Furthermore, we examine the therapeutic applicability of these findings, we added an MCU blocker after Zn^{2+} exposure in wildtype neurons (to induce post-insult MCU blockade) and on hippocampal slices after transient OGD. This significantly attenuated the delayed evolution of both mitochondrial dysfunction and neurotoxicity, supporting the potential utility of delayed interventions.

Delayed Zn^{2+}-chelation attenuates ROS generation and neurodegeneration

If mitochondrial Zn^{2+} accumulation does contribute to neurodegeneration *in vivo* (such as after transient ischemia), it would be valuable to determine whether targeted delayed interventions could abrogate its effects, yielding better outcomes. To begin to address this possibility, we used the membrane permeable Zn^{2+} chelator TPEN. Cultures were subjected to an exposure we had found to cause rapid mitochondrial swelling and extensive neurodegeneration (high K^+/50 μM Zn^{2+}/100 μM DTDP/MK-801 in 1.8 Ca^{2+} HSS, with apocynin added in HEt loaded cultures, as in **Fig 2.6, 2.8B**). We first examined effects of this exposure on ROS generation, which can contribute to subsequent neuronal damage. This exposure caused a rapidly increasing HEt ΔF that persisted for at least 30 min after the

5 min Zn^{2+} exposure (much as in **Fig 2.5C**). However, when TPEN (20 μM) was added immediately after washout of the high K^+/Zn^{2+} exposure, the HEt ΔF was markedly attenuated (**Fig 4.1A**). We then wondered whether this attenuation of ROS generation would be reflected by changes in subsequent neurodegeneration. To test this, cultures were exposed to high K^+/50 μM Zn^{2+}/100 μM DTDP/MK-801 in 1.8 Ca^{2+} HSS alone (as above; **Fig 2.8B**) or with TPEN (10 μM) added either 10 min before, during and after the Zn^{2+} exposure (**TPEN pre-treatment**), or only after the Zn^{2+} exposure (**TPEN post-treatment**; **Fig 4.1B**). While TPEN pre-treatment was markedly protective, validating the importance of Zn^{2+} to neuronal injury, it is notable that post-treatment was also modestly protective (**Fig 4.1B**). As the effect of Zn^{2+} chelation on cell death parallels that on ROS generation (**Fig 4.1A**), these findings support the idea that mitochondrial dysfunction contributes to neurodegeneration and suggest the potential utility of delayed interventions. In sum, these findings not only strengthen the hypothesis that slow Zn^{2+} translocation via VGCC in the presence of both disrupted cytosolic Zn^{2+} buffering and Ca^{2+} (as likely occur during pathologic conditions) can induce mitochondrial dysfunction and cell death, but also suggest the exciting possibility that delayed modulation of mitochondrial Zn^{2+} accumulation could provide some degrees of neuroprotection.

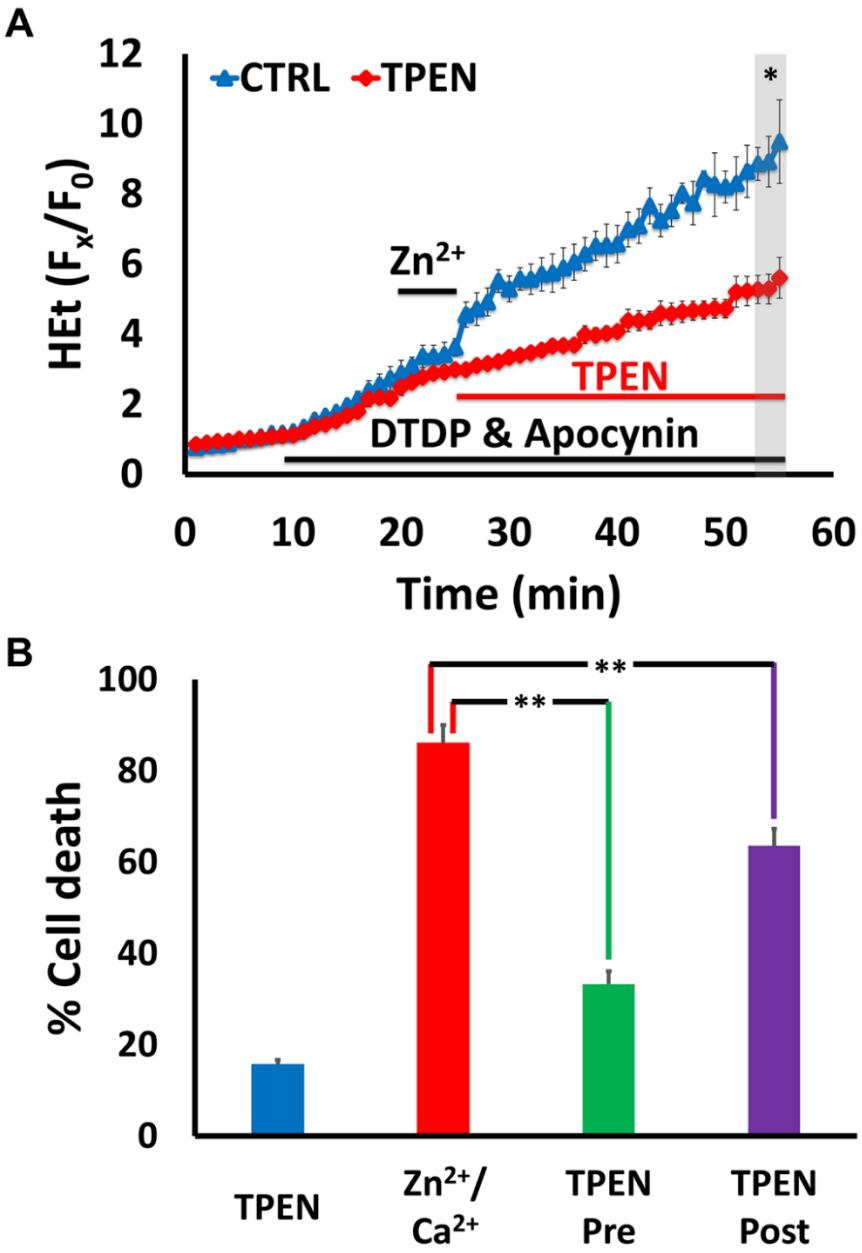

Figure 4.1. Delayed Zn^{2+} chelation attenuates mitochondrial ROS generation and neuron death. Neurons were exposed to high K^+/50 μM Zn^{2+}/MK-801, with DTDP (100 μM), and apocynin (500 μM, A only). TPEN was applied as indicated below. Traces (**A**) represent HEt F_x/F_0 and bars (**B**) represent % cell death after 24 hr; all values are mean ± SEM and represents ≥ 3 independent experiments. Grey bar (in **A**) indicates time points of comparison (* indicates $p < 0.05$, ** indicates $p < 0.01$, by two-tailed t-test [**A**] or by one-way ANOVA with Tukey post hoc [**B**]).

A). Delayed Zn^{2+} chelation attenuates Zn^{2+} triggered ROS production: Note the rapid rise in HEt ΔF that was largely attenuated by TPEN (20 μM), added after the Zn^{2+} exposure.

B). Zn^{2+} chelation attenuates cell death even when delivered after the Zn^{2+} exposure: Cultured neurons were exposed as described, with TPEN (10 μM) present either for 10 min before, during and 10 min after high K^+/Zn^{2+} exposure (TPEN pre), or only for 10 min after Zn^{2+} exposure (TPEN post). Cultures were then transferred to MEM + 25 mM glucose and returned to the incubator for 24 hrs, prior to assessing cell death via LDH efflux assay. Note that both the TPEN pre- and post-treatments attenuated neuron death.

Delayed MCU blockade attenuates Zn^{2+}-triggered mitochondrial dysfunction and cell death

To address whether findings of attenuated Zn^{2+}-triggered injury in MCU KO neurons might be applicable after cellular Zn^{2+} loading has already occurred, we examined the effects of delayed MCU blockade using the pharmacologic agent Ruthenium Red (**RR**). We first assessed changes in rapidly triggered mitochondrial dysfunction. WT neurons, loaded with either Rhod123 (**Fig 4.2A left**) or HEt (**Fig 4.2A right**), were treated with the ischemic Zn^{2+} exposure and washed into DTDP alone or DTDP + RR (10 μM), followed by FCCP in Rhod123-loaded cultures, as indicated. We found that delayed addition of RR attenuated both loss of $\Delta\Psi_m$ and ROS production even after initial mitochondrial Zn^{2+} loading had already occurred (**Fig 4.2A**).

We next set out to determine whether delayed MCU blockade by RR would provide prolonged preservation of mitochondrial morphology. WT neurons were exposed to the same paradigm above (the ischemic Zn^{2+} exposure followed by wash into DTDP ± RR for 20 min) and incubated for 12 hrs, after which mitochondria were labeled with MitoTracker Green and observed under confocal microscopy (as in **Fig 3C**). Note once again the preservation of elongated mitochondrial structure (corroborated by greater L/W ratio) in neurons treated with RR (**Fig 4.2B**). Finally, to test whether delayed MCU blockade could also have neuroprotective effects, the exposure was repeated and cell death assessed after 24 hr incubation (as above). The delayed but transient (20 min) MCU blockade produced a remarkable decrease in neurotoxicity (**Fig 4.2C**). These findings show that relatively brief MCU blockade after the insult can dramatically attenuate the downstream events that contribute to neuronal injury.

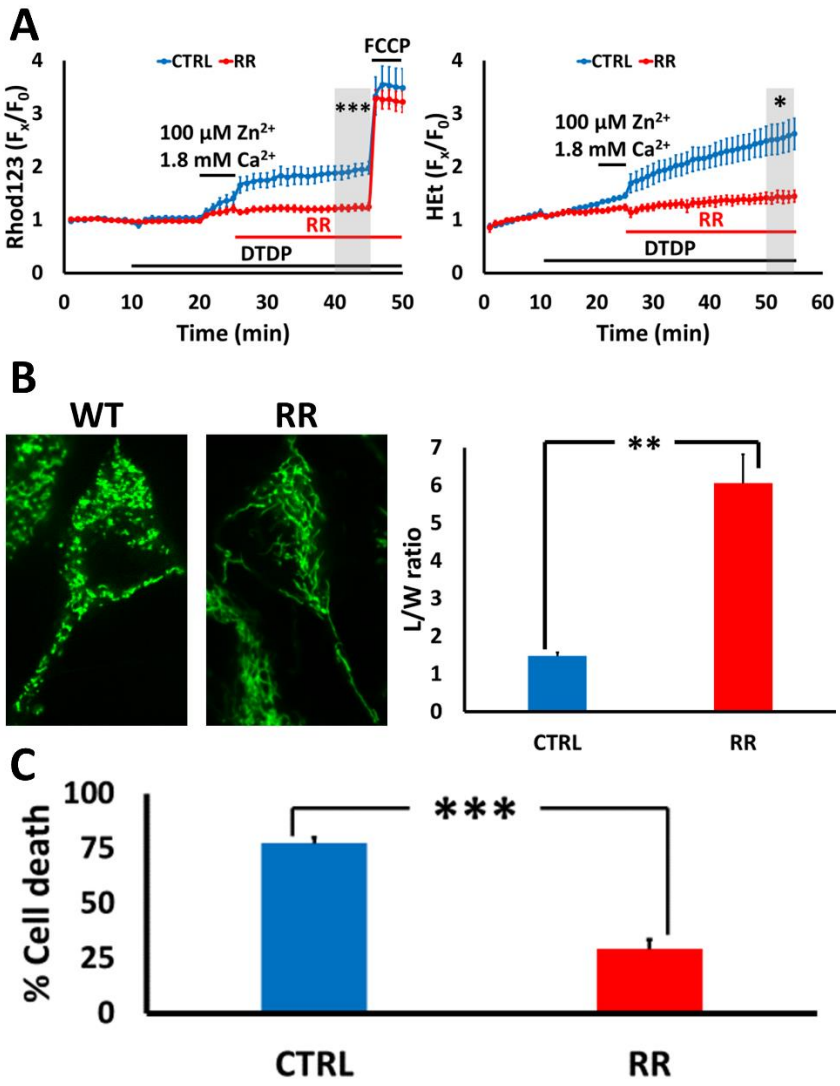

Figure 4.2. Delayed MCU blockade attenuates the Zn^{2+}-triggered mitochondrial dysfunction and neurodegeneration.

WT neurons were exposed to the ischemic Zn^{2+} exposure, followed by 20 min wash into DTDP alone (blue, "**CTRL**") or DTDP + 10 µM RR (red, "**RR**"). Traces represent mean ± SEM F_x/F_0 values for indicator ΔF (**A**) and represent 8 experiments consisting of ≥ 160 neurons. Bar graphs show mean + SEM of either L/W ratio (**B**) or % cell death (**C**), each representing ≥ 5 independent experiments. Grey bars indicate time points of comparison (** indicates $p < 0.01$, *** indicates $p < 0.001$, by two-tailed t-test).

A. Delayed MCU blockade attenuates acute Zn^{2+}-triggered mitochondrial dysfunction. Neurons loaded with either Rhod123 (**left**) or HEt (**right**) were treated as described above, with FCCP (1 µM) added in Rhod123 loaded neurons as indicated. Note that delayed RR attenuated both loss of $\Delta\Psi_m$ (**left**) and rise in ROS production (**right**) in response to Zn^{2+} exposure.

B. MCU blockade after Zn^{2+} exposure preserves mitochondrial morphology. WT neurons were treated to the ischemic Zn^{2+} exposures as described above. After 12 hr incubation, neuronal mitochondria were labeled with MitoTracker Green and observed under confocal microscopy (1000x), after which L/W ratio of mitochondria were calculated blindly. Note the preserved mitochondrial structure (indicated by their elongated morphology [**left**] and corroborated with high L/W ratio [**right**]) in RR-treated neurons.

C. Delayed MCU blockade attenuates neurodegeneration. WT neurons were treated to the ischemic Zn^{2+} exposures as described above. After 24 hr incubation, cell death was assessed via LDH efflux assay. Note that delayed MCU blockade (via transient RR treatment) significantly attenuated Zn^{2+}-triggered neurotoxicity.

Mitochondrial swelling after OGD in CA1 pyramidal neurons is attenuated by MCU blockade

To examine a possible consequence of the mitochondrial Zn^{2+} uptake in CA1, we used confocal imaging to assess changes in mitochondrial morphology ~1 h after sublethal OGD. Slices were exposed either to sham wash in oxygenated medium (as a control) or to a sublethal (~8.5 min) episode of OGD either alone or with RR applied 10 min after the end of the OGD for 15 min. One hour after OGD, slices were fixed and immunolabeled with antibody for the mitochondrial outer membrane marker TOM20. Slices were examined under confocal microscopy (1000×) and images were obtained in the CA1 pyramidal layer (**Fig 4.3**, top). For quantitative assessment, images were adjusted using ImageJ software to discriminate mitochondrial borders from background optimally and perinuclear regions were cropped from images and coded for blinded measurement of mitochondrial lengths and widths (see Materials and Methods). We found that OGD caused a marked "rounding up" of the mitochondria, with substantial decreases in their mean lengths, increases in their widths, and decreased length/width (L/W) ratios. We further found that delayed application of RR attenuated this effect, yielding an intermediate L/W ratio (**Fig 4.3**, bottom).

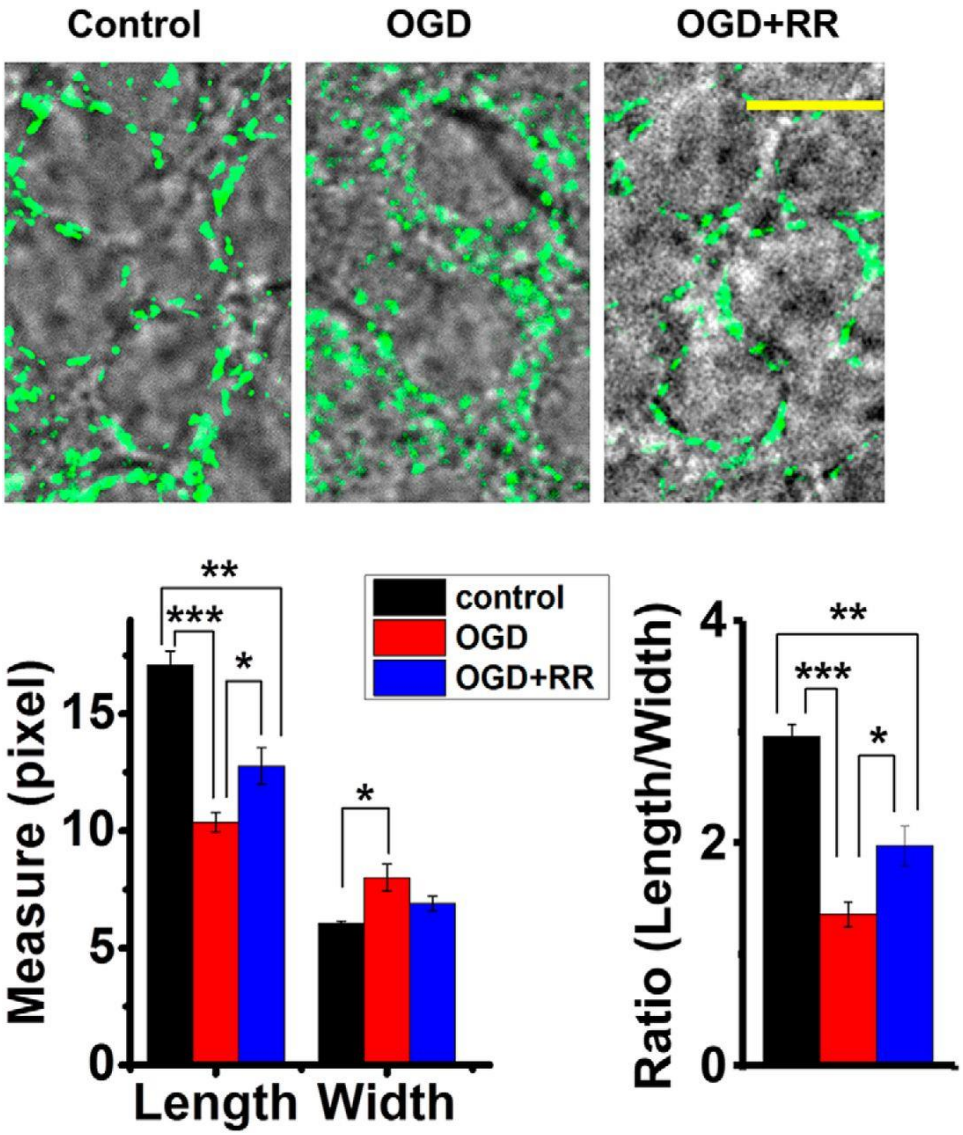

Figure 4.3. Mitochondrial swelling after OGD in CA1 pyramidal neurons is attenuated by MCU blockade.

Brain slices were subjected to sham wash in oxygenated medium (control) or were subjected to 8.5 min OGD either alone or with RR (10 μm, applied 10 min after termination of the OGD for 15 min). One hour after the end of the OGD, slices were fixed (with 4% PFA) and processed for immunostaining with TOM20 antibody. Top, Appearance of mitochondrial swelling. Representative merged images show the bright-field appearance of pyramidal neurons in the CA1 region overlaid with confocal fluorescence images of TOM-20-labeled mitochondria. Scale bar, 10 μm. Bottom, Quantitative measurements. Left, Mitochondrial measurements (length and width; obtained using ImageJ software, see Materials and Methods) after the indicated treatment. Graphs display mean values from 3–5 independently treated hippocampal slices comprising ≥18 neurons each condition and with 107 mitochondria measured in control (144 in OGD; 190 in OGD + RR; see Materials and Methods; length of control 1.4 ± 0.047 μm, OGD 0.8 ± 0.032 μm, p = 2.0 × 10−4 vs control; OGD + RR 1.0 ± 0.062 μm, p = 8 × 10−3 vs control, p = 0.04 vs OGD; width: control 0.49 ± 0.007 μm, OGD 0.64 ± 0.045 μm, p = 0.03 vs control; OGD + RR 0.55 ± 0.024 μm, p = 0.09 vs control, p = 0.1 vs OGD). Right, Mean L/W ratios observed after each treatment (based on the same data; control 2.9 ± 0.1, OGD 1.4 ± 0.11, p = 1.9 × 10−4 vs control; OGD + RR 2.0 ± 0.17, p = 7.9 × 10−3 vs control, p = 0.03 vs OGD). Note that OGD caused a "rounding up" of mitochondria, with a decrease in length and increase in width, and that this change was attenuated by delayed treatment with RR. *p < 0.05; **p < 0.01; ***p < 0.001.

CHAPTER 5

Summary and Conclusions

Summary of findings

In the present thesis, we sought to elucidate whether and how slow Zn^{2+} uptake via VGCC can impact the mitochondria to promote neuronal injury. We find that with disrupted buffering, as likely occurs in *in vivo* ischemia, brief exposure to low Zn^{2+} in depolarizing conditions (to elicit extracellular Zn^{2+} entry through the VGCC) acutely induced mitochondrial dysfunction, including loss of $\Delta\Psi_m$, ROS generation, mitochondrial swelling, and inhibition of respiration, as well as delayed neurodegeneration. The presence of physiologic levels of Ca^{2+} exacerbated these deleterious Zn^{2+} effects despite attenuating both cytosolic and mitochondrial Zn^{2+} accumulation, suggesting strong synergism between these two ions. While our findings do not prove that Zn^{2+} triggered mitochondrial dysfunction directly led to neurodegeneration, the strong correlation between the effects of Zn^{2+} on mitochondria and on cell death supports the hypothesis that mitochondrial Zn^{2+} accumulation—and the consequent dysfunction—is an important upstream contributor to neuronal injury.

We also used the recently available MCU KO mice to evaluate the role of MCU in Zn^{2+}-induced neuronal injury with greater specificity than was previously possible with pharmacological blockers. In cultured cortical neurons, genetic deletion of MCU attenuated mitochondrial Zn^{2+} accumulation, and consequently, diminished its deleterious effects on mitochondria, including loss of $\Delta\Psi_m$, inhibition of respiration, and swelling. While MCU KO surprisingly had little effect on the *total* cellular Zn^{2+}-triggered ROS generation, this

appeared to be due to an increased cytosolic NOX activity in the MCU KO neurons. Indeed, using the NOX antagonist apocynin, we found that *mitochondrial* ROS generation was nearly eliminated in the MCU KO neurons. In assessing the role of MCU on neurodegeneration 24 hrs after exposures to both Ca^{2+} and Zn^{2+}, we found genetic deletion of MCU was not protective. This death appeared to reflect primarily Ca^{2+} contribution, as further studies revealed accentuation of Ca^{2+}-induced cell death and attenuation of Zn^{2+}-triggered neurodegeneration in the MCU KO neurons. When a NOX antagonist was present during the combined Ca^{2+} and Zn^{2+} exposure, injury in the MCU KO was again significantly attenuated. These findings from cultured neurons were also reflected in the hippocampal slice OGD ischemia model. Whereas MCU KO accelerated OGD-induced cell death of CA1 pyramidal neurons when physiological levels of Ca^{2+} were present, when Ca^{2+} was lowered to abrogate its cytosolic effects, the neurodegeneration in the MCU KO pyramidal neurons was markedly delayed. These findings from the MCU KO cultured neurons and hippocampal slices further strengthen the notion that Zn^{2+} entry through the MCU is a critical contributor to mitochondrial dysfunction and the consequent neurodegeneration.

Finally, as therapeutic interventions in humans will generally entail application of drugs after an ischemic event has occurred, we tested effects of delayed administration of the Zn^{2+} chelator, TPEN, or the MCU antagonist, RR, after the Zn^{2+} exposure (again in presence of physiological Ca^{2+}). We found that Zn^{2+} chelation after Zn^{2+} loading attenuated both mitochondrial ROS generation and neuron death, further supporting that Zn^{2+} triggered mitochondrial dysfunction, and that the delayed RR diminished the induction of acute mitochondrial dysfunction ($\Delta\Psi_m$ and ROS), the gradual swelling, and subsequent cell

death. These findings provide further support to the possible therapeutic utility of delayed targeting of mitochondrial Zn^{2+} accumulation after ischemic episode can be protective.

Zn^{2+} triggered neurodegeneration: ongoing questions about sources and targets

In light of the debilitating consequences of ischemic stroke, there is a compelling need to develop a better understanding of neuronal injury mechanism in order to identify neuroprotective targets. While attention has long focused on Ca^{2+} as the critical ionic contributor to neuronal injury, emerging clues—including observations of cytosolic Zn^{2+} accumulation in neurons after ischemia and findings that selective Zn^{2+} chelation can be neuroprotective—have highlighted important contribution of Zn^{2+} (Calderone et al., 2004; Koh et al., 1996; Tonder et al., 1990). Indeed, most Ca^{2+} indicators also respond to Zn^{2+} with greater affinity than Ca^{2+}, and it is likely that some effects previously attributed to Ca^{2+} are actually due to Zn^{2+} (Cheng and Reynolds, 1998; Stork and Li, 2006).

Our understanding of Zn^{2+} mechanisms in ischemia has been in flux. It was first assumed that the toxic Zn^{2+} accumulation seen after ischemia or prolonged seizures resulted from presynaptic release (Assaf and Chung, 1984; Howell et al., 1984) and its translocation into post-synaptic neurons (Koh et al., 1996; Tonder et al., 1990) through routes including VGCC and Ca-AMPAR (Noh et al., 2005; Sensi et al., 2000; Yin et al., 2002). However, in studies using mice lacking presynaptic releasable Zn^{2+} (via knockout of the vesicular Zn^{2+} transporter, ZnT3) (Cole et al., 2000; Cole et al., 1999), prolonged seizures surprisingly still caused strong Zn^{2+} accumulation and Zn^{2+} dependent injury to CA1 pyramidal neurons, highlighting critical contributions from other sources (Lee et al., 2000). Further studies using ZnT3 knockouts as well as knockouts of the neuronal Zn^{2+} binding

protein, metallothionein-III (**MT-III**) (Erickson et al., 1997), provided compelling evidence for distinct contributions of Zn^{2+} to neuronal injury between CA1 and CA3 pyramidal neurons, with Zn^{2+} translocation, likely in large part through Ca-AMPAR, predominating in CA3, but mobilization from MT-III predominating in CA1 (Lee et al., 2000; Lee et al., 2003; Medvedeva et al., 2017). Thus, it is now apparent both synaptically released Zn^{2+} and Zn^{2+} mobilized from intracellular binding proteins (like MT-III) likely contribute to neuronal accumulation and injury in pathological conditions, although the respective contributions from these sources likely differ between populations of neurons.

Another unsettled question concerns the target(s) through which Zn^{2+} mediates injury. While it is apparent that Zn^{2+} can activate multiple pathways that contribute to neurodegeneration (Shuttleworth and Weiss, 2011), several lines of evidence led us to consider that mitochondria may be an important early target. Zn^{2+} has potent and complicated effects on isolated mitochondria, entering them through the mitochondrial Ca^{2+} uniporter (**MCU**), inhibiting electron transport and critically inhibiting their function through complex mechanisms, and triggering swelling via activation of mitochondrial permeability transition pore (**mPTP**), all of which lead to biphasic effects, with low levels increasing respiration and inhibiting ROS production while high levels induce opposite effects (Brown et al., 2000; Dineley et al., 2005; Gazaryan et al., 2007; Jiang et al., 2001; Link and von Jagow, 1995; Sensi et al., 2003; Skulachev et al., 1967; Wudarczyk et al., 1999). In cultured neurons, Zn^{2+} loading via rapid entry through Ca-AMPAR resulted in acute mitochondrial dysfunction, including rapid loss of $\Delta\psi_m$ and ROS production (Sensi et al., 1999a; Sensi et al., 1999b, 2000), supporting the idea that mitochondria may be important Zn^{2+} targets in neuronal injury.

However, not all studies support this idea. First, brief fairly high (300 μM) Zn^{2+} exposures to depolarized neurons (triggering slower Zn^{2+} translocation through VGCC) induced considerable delayed neurodegeneration but caused relatively little acute mitochondrial dysfunction (Pivovarova et al., 2014; Sensi et al., 1999a; Weiss et al., 1993). Furthermore, a recent study of isolated mitochondria in highly purified buffer reported that in contrast to Ca^{2+}, Zn^{2+} did not trigger mPTP opening and was a weak trigger of depolarization (Devinney et al., 2009). Thus, although Zn^{2+} appears to contribute to neurodegeneration after ischemia or prolonged seizures, there has been ongoing debate as to respective contributions of Zn^{2+} vs Ca^{2+} to mitochondrial dysfunction in these conditions.

Mitochondrial Zn^{2+} accumulation and its consequences

Despite evidence that both Zn^{2+} and Ca^{2+} contributed to neurodegeneration after ischemia or prolonged seizures, until recently there had been little attempt to discriminate their respective effects. To this aim, we carried out the first study seeking to track both ions simultaneously in single pyramidal neurons in hippocampal slices subjected to oxygen glucose deprivation (**OGD**) (Medvedeva et al., 2009), and found Zn^{2+} rises to precede and contribute to subsequent lethal Ca^{2+} overload; with Zn^{2+} chelation, the cell death was markedly delayed. Furthermore, the early Zn^{2+} effects appeared to depend upon its interaction with mitochondria (Medvedeva et al., 2009), with uptake of endogenous Zn^{2+} into mitochondria through the MCU contributing specifically to ROS production and neuronal cell death (Medvedeva and Weiss, 2014). Indeed, other studies have supported the idea that Zn^{2+} may contribute to mitochondrial dysfunction after *in vivo* ischemia, specifically promoting release of pro-apoptotic peptides from mitochondria and

contributing to the activation of large channels in the mitochondrial outer membranes (Bonanni et al., 2006; Calderone et al., 2004).

As noted above, despite some studies suggesting that Zn^{2+} may only weakly impact mitochondrial function (Devinney et al., 2009; Pivovarova et al., 2014), there has been a growing body of evidence that Zn^{2+}—as well as Ca^{2+}—can enter mitochondria and impact their function. While the nature of interactions between these ions on mitochondria has been little explored, prior studies have provided early clues for possible synergism between these ions. Specifically, combined application of Ca^{2+} and Zn^{2+} caused greater swelling of isolated mitochondria than Ca^{2+} or Zn^{2+} alone (Jiang et al., 2001), and Zn^{2+} entry through Ca-AMPAR yielded stronger and more persistent ROS generation when Ca^{2+} was also present (Sensi et al., 2000). Present studies extend these early clues via examination of effects of slower Zn^{2+} and Ca^{2+} entry through VGCC, and find potent synergism between Zn^{2+} and Ca^{2+} on multiple measures of mitochondrial dysfunction. These findings are particularly notable, as the presence of Ca^{2+} clearly resulted in a decreased amount of Zn^{2+} entering the neurons. While there has been consensus that Ca^{2+} influx through VGCC does not usually cause significant injury, our findings suggest that with Zn^{2+} present under pathophysiologic condition, these effects are dramatically enhanced and could be an important contributor to neuronal damage.

However, the nature of the interactions between Ca^{2+} and Zn^{2+} remains unclear and merits further study. One possibility is that the presence of Ca^{2+} may modify Zn^{2+} permeation through the MCU. While the MCU was previously considered to be quite selective for Ca^{2+}, Zn^{2+} can also enter mitochondria through this route (Clausen et al., 2013; Gazaryan et al., 2007; Jiang et al., 2001; Malaiyandi et al., 2005; Saris and Niva, 1994), and

Ca^{2+} was actually found to markedly facilitate Zn^{2+} entry through the MCU in isolated mitochondria (Saris and Niva, 1994). Yet, despite the ability to block both Ca^{2+} and Zn^{2+} uptake into mitochondria, therapeutic attempts using MCU blockers have been disappointing, showing evidence of neuroprotection in some cases, while worsening outcomes in others (Velasco and Tapia, 2000). The reasons for this are not completely clear, but it is possible that by preventing mitochondrial Ca^{2+} uptake, MCU blockade promoted excess cytosolic Ca^{2+} accumulation, leading to loss of cytosolic Ca^{2+} homeostasis that ultimately induced further neuronal injury (Murphy et al., 2014). Furthermore, as the pharmacologic MCU blockers have been characterized to lack full specificity for the MCU and exert numerous nonspecific effects (including VGCC blockade and antioxidant) (Meinicke et al., 1998; Tapia and Velasco, 1997), it was not possible to ascertain whether the effects—protective or not—were indeed specifically due to MCU blockade.

The recent identification of the MCU gene and its associated regulatory peptides (De Stefani et al., 2015; Kamer and Mootha, 2015; Marchi and Pinton, 2014) provided a major opportunity for breakthrough in the study of these channels. Interestingly, the regulatory subunits MICU1 and 2 appear to respond to Ca^{2+} to enable pore opening, preventing pore opening when Ca^{2+} low and opening it when Ca^{2+} rises – conferring a sigmoid shaped Ca^{2+} concentration, channel activation relationship (Kamer and Mootha, 2015; Marchi and Pinton, 2014; Murgia and Rizzuto, 2015). Thus, might some Ca^{2+} be needed for channel gating and Zn^{2+} entry, possibly accounting for the paucity of Zn^{2+} effects on isolated mitochondria carried out in purified Ca^{2+} free media (Devinney et al., 2009)? These findings may have implication for Zn^{2+} effects on mitochondria as well, especially in light of prior evidence that Ca^{2+} not only is necessary for Zn^{2+} effects in certain conditions (as

discussed above), but also enhances Zn^{2+} entry through the MCU (Saris and Niva, 1994). Furthermore, we et al., have observed evidence for synergism between Zn^{2+} and Ca^{2+} on mitochondria, with far greater effects of Zn^{2+} in presence of Ca^{2+} (Gazaryan et al., 2007; Ji and Weiss, 2018; Jiang et al., 2001; Sensi et al., 2000), which could be explained in part by Ca^{2+} dependence of the MCU pore opening.

The other unresolved issue concerns whether the levels of Zn^{2+} readily achieved in neurons in pathological conditions are likely to induce acute disruption of mitochondrial function, in light of observations (discussed above) that brief strong Zn^{2+} exposures to depolarized neurons caused little acute disruption of mitochondrial function (Pivovarova et al., 2014; Sensi et al., 1999a). However, although such relatively slow Zn^{2+} entry through VGCC does not cause the acute ROS production and strong loss of $\Delta\Psi_m$ seen with more rapid entry (through Ca-AMPAR), these exposures do result in persistent (at least 2 hrs) Zn^{2+} accumulation in mitochondria, contributing to partial loss of $\Delta\Psi_m$ and release of pro-apoptotic peptides (Jiang et al., 2001; Sensi et al., 2002). It is also notable that strong disruption of cytosolic Zn^{2+} buffering alone (in the absence of extracellular Zn^{2+}) results in sufficient intracellular Zn^{2+} mobilization to cause milder disruption of mitochondrial function and trigger delayed neurodegeneration (Aizenman et al., 2000; Bossy-Wetzel et al., 2004; Sensi et al., 2003). Thus, perhaps it is not surprising that in combination, even relatively slow Zn^{2+} entry under conditions of impaired cytosolic Zn^{2+} buffering can acutely disrupt mitochondrial function.

In past studies we found that strong disruption of buffering enhanced ROS production caused by relatively low levels of Zn^{2+} entry (Clausen et al., 2013). Present studies markedly extend the understanding of conditions that determine effects of cellular

Zn^{2+} loads on mitochondria. First, we find that even partial disruption of cytosolic Zn^{2+} buffering (that had little effect on its own), markedly increase mitochondrial disruption caused by low levels of Zn^{2+} entry, with Zn^{2+} levels even as low as 10 μM potently disrupting mitochondria. Secondly, we find that the effects are markedly enhanced by the presence of physiological levels of Ca^{2+} entry (and may be artificially inhibited under the non-physiological conditions of limited or absent Ca^{2+} in which many prior studies of Zn^{2+} were carried out). We further find that the enhanced disruption of mitochondria extends beyond the usual measures of loss of $\Delta\Psi_m$ and ROS production to include strong and progressive swelling and long lasting inhibition of respiration, effects that may be indicative of severe or irrecoverable disruption. Finally, we examine effects of the presence of Ca^{2+} and disrupted Zn^{2+} buffering not only on mitochondrial function but also on cell death as well. While we do not definitively demonstrate that the Zn^{2+} dependent mitochondrial disruption leads directly to cell death, we found strong correlation between the effects of the Ca^{2+} and disrupted Zn^{2+} buffering on mitochondrial function and on cell death. In light of our data that delayed Zn^{2+} chelation attenuated both acute mitochondrial ROS generation and delayed neurodegeneration, our study provides new support to the idea that Zn^{2+} triggered mitochondrial disruption is an important upstream event that contributes to delayed injury, and targeting it could be protective.

Delayed targeting of Zn^{2+} for protection against ischemia

Studies in hippocampal slice OGD models of ischemia have yielded important clues to how Zn^{2+} may contribute to ischemic neurodegeneration. Early studies clearly showed acute extracellular and intracellular Zn^{2+} rises (Li et al., 2001; Wei et al., 2004), but

interactions between Zn^{2+} and Ca^{2+} effects were unexplored. Thus, we carried out the first study monitoring Ca^{2+} and Zn^{2+} simultaneously in single CA1 HPNs, and found Zn^{2+} rises to precede and contribute to lethal Ca^{2+} deregulation. Furthermore, this seemed to depend upon Zn^{2+} uptake into mitochondria (Medvedeva et al., 2009). To test the relevance of these findings, we carried out *in vivo* global ischemia studies in rats, where after inducing transient cardiac arrest, we used the Timm's sulfide silver stain to label reactive Zn^{2+}, and observed neurons under electron microscopy to examine both subcellular localization of Zn^{2+} and mitochondrial morphology (Yin et al., 2019). We found evidence of delayed and progressive mitochondrial Zn^{2+} accumulation, with the degree of accumulation correlating with the extent of mitochondrial structural disruption. These findings in hippocampal slices and whole animal models support a critical role of mitochondrial Zn^{2+} accumulation as an early factor in ischemic neurodegeneration the targeting of which may yield protection.

To test the role of MCU in this injury cascade, pharmacologic blockers (RR or the more specific analogue Ru-360) were added prior to prolonged OGD in hippocampal slices, which surprisingly accelerated the lethal Ca^{2+} deregulation. As this may have been due to MCU blockers hastening cytosolic Ca^{2+} accumulation by inhibiting mitochondrial Ca^{2+} uptake, when Ca^{2+} level was lowered, the blocker became highly protective. Additional findings that the degree of protection from lowering Ca^{2+} was similar to that from Zn^{2+} chelation supported the idea that the protection from MCU blockers was due to antagonism of Zn^{2+} entry into mitochondria via the MCU (Medvedeva and Weiss, 2014). Present studies using the MCU KO slice model subjected to prolonged OGD further validate these prior results, supporting the idea that attenuating Zn^{2+} entry specifically through MCU can

provide neuroprotection. Yet, as these studies entailed either pretreatment with MCU blocker or genetic knockout, they are limited in utility for translation. Indeed, attenuating MCU activity prior to insult appears to exacerbate peak Ca^{2+} loading and worsens Ca^{2+} dependent injury, and as ischemic events cannot be predicted in patients, most opportunities for intervention are after the acute ischemic insult.

To address mechanisms of such delayed injury after transient ischemia, we subjected slices to sublethal episodes of OGD (in which OGD was aborted shortly prior to the expected time of Ca^{2+} deregulation). We found that mitochondrial Zn^{2+} entry was an early event in response to sublethal OGD in both CA1 and CA3 regions. However, CA1 neurons had prolonged (> 1hr) Zn^{2+} accumulation in mitochondria that progressed during the period after OGD, and which appeared to contribute to delayed mitochondrial swelling. In contrast, far less late mitochondrial Zn^{2+} accumulation was observed in the CA3 neurons. Given the particular vulnerability of CA1 neurons to delayed ischemic degeneration, it is possible that this early mitochondrial Zn^{2+} accumulation and prolonged sequestration is a key trigger of the persistent mitochondrial dysfunction, including mitochondrial swelling, CytC release and mitochondrial multi-conductance channel activation observed in some animal studies (Bonanni et al., 2006; Calderone et al., 2004; Sugawara et al., 1999). Late administration of the MCU blocker RR diminished both the delayed Zn^{2+} accumulation within the mitochondria and the consequent mitochondrial swelling 1 hr after sublethal OGD in CA1 HPNs (Medvedeva et al., 2017).

Present findings of protective effects of late RR after Zn^{2+} exposures to cultured cortical neurons provide further support to the idea that delayed mitochondrial Zn^{2+} accumulation contributes to mitochondrial dysfunction and delayed neurodegeneration

and supports the utility of late interventions. Although the available antagonists lack full specificity for this channel, and their other actions (including antioxidant effects) could contribute to their benefit, present findings with the MCU KO provide compelling support to the notion that antagonism of mitochondrial Zn^{2+} accumulation plays a crucial role. Indeed, late administration of these antagonists after the insult permits buffering of acute cytosolic Ca^{2+} loads by the mitochondria prior to MCU blockade and may abrogate the problem of enhanced cytosolic Ca^{2+} loading seen with pretreatment.

Neurodegeneration: The culmination of cascades of injury-promoting events

Cell death is multi-step process, occurring when a sequence of events leads to a state from which the cell cannot recover. As discussed above, ROS production has been strongly implicated as a trigger of the neurodegeneration occurring after excitotoxic Ca^{2+} loading, and downstream events have been identified, including activation of Poly (ADP-ribose) polymerase (**PARP**), a nuclear enzyme involved in DNA repair which becomes activated in response to ROS induced DNA damage. PARP utilizes NAD^+ as substrate, with strong activity leading to NAD^+ depletion, glycolytic and mitochondrial inhibition, and release of the apoptotic mediator, Apoptosis Inducing Factor (**AIF**) (Kauppinen and Swanson, 2007). Paralleling these studies of Ca^{2+} excitotoxicity, moderate Zn^{2+} exposures have also been found to cause ROS production (in part due to delayed induction of NOX and neuronal nitric oxide synthase) (Kim and Koh, 2002; Noh and Koh, 2000), resulting in PARP activation, that contributes to the evolving injury (Kim and Koh, 2002).

A number of pathways have also been described in which early Zn^{2+} signals can trigger more delayed neurodegeneration. Studies of the delayed neurodegeneration caused by strong intracellular Zn^{2+} mobilization (Aizenman et al., 2000) have implicated a distinct pathway, in which activation of p38 MAP kinase results in membrane insertion of Kv2.1 K^+ channels, resulting in K^+ efflux from neurons and consequent apoptosis (McLaughlin et al., 2001).

Notably, these mechanisms contributing to delayed degeneration in response to early Zn^{2+} signals represent later steps in cascades, the inciting steps of which are not always apparent. However, in light of our findings that mitochondrial accumulation of endogenous Zn^{2+} under ischemic conditions triggers rapid mitochondrial ROS production (Medvedeva and Weiss, 2014), ***perhaps mitochondrial ROS constitutes a critical upstream trigger of some of these downstream, neurodegeneration pathways*.** Indeed, Zn^{2+} triggered acute mitochondrial ROS could mediate DNA damage that underlies PARP activation, and has been implicated in the activation of p38 MAP kinase occurring upstream from the insertion of Kv2.1 K^+ channels (Bossy-Wetzel et al., 2004), raising the possibility that early targeting of mitochondrial Zn^{2+} may have both immediate and delayed therapeutic benefits.

Therapeutic potential of targeting mitochondrial Zn^{2+}: possible future directions

In summary, studies at multiple levels of complexity—ranging from isolated mitochondria and dissociated neurons, to hippocampal slice and *in vivo* models of

ischemia—indicate that Zn^{2+} is likely to contribute to mitochondrial dysfunction, ROS generation, and neurodegeneration in ischemia (and may well do so in prolonged seizures and brain trauma as well). Furthermore, emerging evidence supports the notion that the Zn^{2+} entry into mitochondria is an early event in the ischemic injury cascade (especially in hippocampal CA1), which, as it occurs upstream from onset of terminal Ca^{2+} deregulation, may not be adequately targeted by simply slowing neuronal Ca^{2+} entry (as via NMDAR blockade). We started with the comment that the available treatments for ischemia injury are inadequate, reflecting in part incomplete understanding of relevant targetable events. We wish to end by suggesting a new hypothesis: Early mitochondrial Zn^{2+} accumulation—and the consequent disruption of their function—is a critical and targetable event in the neurodegenerative sequence; this idea merits further investigation and examination for therapeutic utility.

With strong and prolonged ischemia, mitochondrial Zn^{2+} loading may result in rapid irreversible mitochondrial disruption and cell death (Medvedeva et al., 2009; Medvedeva and Weiss, 2014). However, with milder or transient ischemia, mitochondrial Zn^{2+} loading may contribute to the activation of downstream cell death pathways. Optimal interventions might well vary depending on the stage at which they are delivered. We believe that the targeting of specific events in the injury cascade has potential to yield benefit (see **Fig. 5.1**):

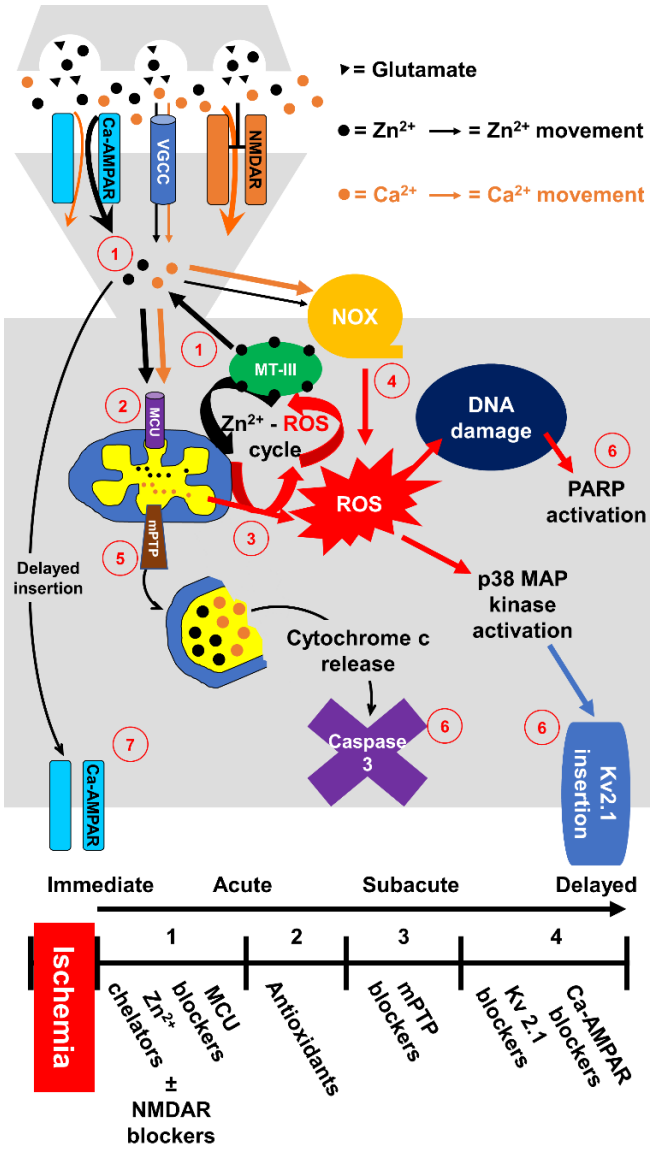

Figure 5.1. Zn^{2+}-induced mitochondrial dysfunction is a critical and targetable early contributor to ischemic neuronal injury.
During ischemia, Zn^{2+} accumulation in neurons reflects contributions from two primary sources: Zn^{2+} released from presynaptic vesicles that enters postsynaptic neurons (through Ca-AMPAR and VGCC), and Zn^{2+} released from MT-III (due to oxidative stress and acidosis) (**1**). This Zn^{2+} rapidly enters mitochondria through the MCU (**2**). An early consequence of mitochondrial Zn^{2+} accumulation is acute ROS generation, which can further disrupt cytosolic Zn^{2+} buffering, resulting in more mitochondrial Zn^{2+} entry and consequent dysfunction, thereby initiating a feedforward "*Zn^{2+}-ROS*" cycle. (**3**). In addition, Zn^{2+} can induce delayed activation of NOX, producing more ROS, and possibly further amplifying this Zn^{2+}-ROS cycle (**4**). This protracted Zn^{2+} influx into mitochondria triggers mPTP opening, leading to mitochondrial depolarization, swelling, and cytochrome C release (**5**). These Zn^{2+} effects on mitochondria (ROS generation and mPTP opening) can activate major downstream events, including direct oxidative damage to proteins and DNA (that can lead to PARP activation), activation of the apoptotic pathway via Caspase 3, and activation of p38 MAP kinase, promoting the delayed insertion of Kv2.1 K^+ channels (**6**). Furthermore, cytosolic Zn^{2+}, acting through incompletely defined mechanisms, can cause delayed insertion of Ca-AMPAR, further promoting delayed neurodegeneration (**7**). As these steps are temporally discrete, optimal therapeutic strategies will likely target a combination of them at different time points, as highlighted in timeline.

(1) Early mitochondrial Zn^{2+} accumulation: At the early stages, Zn^{2+} chelators or MCU blockers might provide benefit by lessening early mitochondrial Zn^{2+} accumulation. Indeed, delayed Zn^{2+} chelation and MCU blockade have each shown beneficial effects in recent *in vitro* studies (Ji and Weiss, 2018; Medvedeva et al., 2017; Slepchenko et al., 2017). Of note, these interventions could also act to promote injurious Ca^{2+} loading, possibly complicating efforts to use them for therapeutic benefit *in vivo*. Specifically, while diminishing mitochondrial Zn^{2+} accumulation, Zn^{2+} chelation attenuates physiological antagonism of NMDAR by synaptic Zn^{2+}, thereby increasing neuroexcitation (Cole et al., 2000; Dominguez et al., 2003; Vogt et al., 2000) and MCU blockade during acute stages of ischemia could diminish mitochondrial buffering of cytosolic Ca^{2+} loads (Velasco and Tapia, 2000), both effects that could exacerbate early injurious cytosolic Ca^{2+} loading and hasten Ca^{2+} deregulation. For this reason, in acute stages of ischemia, these agents could show greatest benefit when combined with maneuvers (such as NMDAR blockade) to abrogate rapid Ca^{2+} loading (Medvedeva and Weiss, 2014).

(2) Mitochondrial ROS generation: Antioxidants may provide benefit at slightly later stages, in two ways: **a.** By diminishing oxidative Zn^{2+} mobilization from buffers (thereby helping to prevent delayed oxidative feedforward amplification of Zn^{2+} triggered mitochondrial disruption), and **b.** By decreasing oxidative tissue damage and activation of oxidant triggered downstream pathways (including PARP and p38 MAP kinase).

(3) Opening of the mPTP: Mitochondrial Zn^{2+} loading may also act upstream to more delayed apoptotic forms of injury, with Zn^{2+} triggered mPTP opening (occurring up to several hours after the Zn^{2+} load) resulting in mitochondrial disruption and release of

apoptotic mediators like (cytochrome C and AIF), effects against which mPTP blockers (like cyclosporine A) might provide benefit.

(4) Downstream injury pathways: As noted above, Zn^{2+} signals have been found to contribute to delayed insertion of new ion channels that promote delayed neurodegeneration. Targeting of these channels (specifically Kv2.1 channels and Ca-AMPAR) may yield benefit from hours to several days after the episode (Aizenman et al., 2000; McLaughlin et al., 2001; Noh et al., 2005; Yeh et al., 2017).

In summary, accumulating evidence supports the notion that early mitochondrial Zn^{2+} accumulation after ischemia contributes to mitochondrial dysfunction and may well be a critical triggering event for a number of neurodegenerative cascades. The targeting of these Zn^{2+} triggered events in the post ischemic period has been largely unexplored, yet has potential to yield substantial benefit, and merits further study.

REFERENCES

1. Aizenman, E., Stout, A.K., Hartnett, K.A., Dineley, K.E., McLaughlin, B., Reynolds, I.J., 2000. Induction of neuronal apoptosis by thiol oxidation: putative role of intracellular zinc release. J Neurochem 75, 1878-1888.
2. Assaf, S.Y., Chung, S.H., 1984. Release of endogenous Zn2+ from brain tissue during activity. Nature 308, 734-736.
3. Ben-Ari, Y., Tremblay, E., Ottersen, O.P., 1980a. Injections of kainic acid into the amygdaloid complex of the rat: an electrographic, clinical and histological study in relation to the pathology of epilepsy. Neuroscience 5, 515-528.
4. Ben-Ari, Y., Tremblay, E., Ottersen, O.P., Meldrum, B.S., 1980b. The role of epileptic activity in hippocampal and "remote" cerebral lesions induced by kainic acid. Brain Res 191, 79-97.
5. Benjamin, E.J., Virani, S.S., Callaway, C.W., Chamberlain, A.M., Chang, A.R., Cheng, S., Chiuve, S.E., Cushman, M., Delling, F.N., Deo, R., de Ferranti, S.D., Ferguson, J.F., Fornage, M., Gillespie, C., Isasi, C.R., Jimenez, M.C., Jordan, L.C., Judd, S.E., Lackland, D., Lichtman, J.H., Lisabeth, L., Liu, S., Longenecker, C.T., Lutsey, P.L., Mackey, J.S., Matchar, D.B., Matsushita, K., Mussolino, M.E., Nasir, K., O'Flaherty, M., Palaniappan, L.P., Pandey, A., Pandey, D.K., Reeves, M.J., Ritchey, M.D., Rodriguez, C.J., Roth, G.A., Rosamond, W.D., Sampson, U.K.A., Satou, G.M., Shah, S.H., Spartano, N.L., Tirschwell, D.L., Tsao, C.W., Voeks, J.H., Willey, J.Z., Wilkins, J.T., Wu, J.H., Alger, H.M., Wong, S.S., Muntner, P., American Heart Association Council on, E., Prevention Statistics, C., Stroke Statistics, S., 2018. Heart Disease and Stroke Statistics-2018 Update: A Report From the American Heart Association. Circulation 137, e67-e492.

6. Bindokas, V.P., Jordan, J., Lee, C.C., Miller, R.J., 1996. Superoxide production in rat hippocampal neurons: selective imaging with hydroethidine. J Neurosci 16, 1324-1336.
7. Bonanni, L., Chachar, M., Jover-Mengual, T., Li, H., Jones, A., Yokota, H., Ofengeim, D., Flannery, R.J., Miyawaki, T., Cho, C.H., Polster, B.M., Pypaert, M., Hardwick, J.M., Sensi, S.L., Zukin, R.S., Jonas, E.A., 2006. Zinc-dependent multi-conductance channel activity in mitochondria isolated from ischemic brain. J Neurosci 26, 6851-6862.
8. Bossy-Wetzel, E., Talantova, M.V., Lee, W.D., Scholzke, M.N., Harrop, A., Mathews, E., Gotz, T., Han, J., Ellisman, M.H., Perkins, G.A., Lipton, S.A., 2004. Crosstalk between Nitric Oxide and Zinc Pathways to Neuronal Cell Death Involving Mitochondrial Dysfunction and p38-Activated K(+) Channels. Neuron 41, 351-365.
9. Brand, M.D., Nicholls, D.G., 2011. Assessing mitochondrial dysfunction in cells. The Biochemical journal 435, 297-312.
10. Brennan, A.M., Suh, S.W., Won, S.J., Narasimhan, P., Kauppinen, T.M., Lee, H., Edling, Y., Chan, P.H., Swanson, R.A., 2009. NADPH oxidase is the primary source of superoxide induced by NMDAR activation. Nature neuroscience 12, 857-863.
11. Brierley, G.P., 1967. Ion transport by heart mitochondria. VII. Activation of the energy-linked accumulation of Mg++ by Zn++ and other cations. J Biol Chem 242, 1115-1122.
12. Brown, A.M., Kristal, B.S., Effron, M.S., Shestopalov, A.I., Ullucci, P.A., Sheu, K.F., Blass, J.P., Cooper, A.J., 2000. Zn2+ inhibits alpha-ketoglutarate-stimulated mitochondrial respiration and the isolated alpha-ketoglutarate dehydrogenase complex. J Biol Chem 275, 13441-13447.

13. Brustovetsky, N., Brustovetsky, T., Jemmerson, R., Dubinsky, J.M., 2002. Calcium-induced cytochrome c release from CNS mitochondria is associated with the permeability transition and rupture of the outer membrane. J Neurochem 80, 207-218.
14. Buckman, J.F., Hernandez, H., Kress, G.J., Votyakova, T.V., Pal, S., Reynolds, I.J., 2001. MitoTracker labeling in primary neuronal and astrocytic cultures: influence of mitochondrial membrane potential and oxidants. Journal of neuroscience methods 104, 165-176.
15. Calderone, A., Jover, T., Mashiko, T., Noh, K.M., Tanaka, H., Bennett, M.V., Zukin, R.S., 2004. Late calcium EDTA rescues hippocampal CA1 neurons from global ischemia-induced death. J Neurosci 24, 9903-9913.
16. Cheng, C., Reynolds, I.J., 1998. Calcium-sensitive fluorescent dyes can report increases in intracellular free zinc concentration in cultured forebrain neurons. J Neurochem 71, 2401-2410.
17. Choi, D.W., 1987. Ionic dependence of glutamate neurotoxicity. J Neurosci 7, 369-79.
18. Choi, D.W., Koh, J.Y., Peters, S., 1988. Pharmacology of glutamate neurotoxicity in cortical cell culture: attenuation by NMDA antagonists. J Neurosci 8, 185-196.
19. Clausen, A., McClanahan, T., Ji, S.G., Weiss, J.H., 2013. Mechanisms of Rapid Reactive Oxygen Species Generation in response to Cytosolic Ca2+ or Zn2+ Loads in Cortical Neurons. Plos One 8, e83347.
20. Cole, T.B., Robbins, C.A., Wenzel, H.J., Schwartzkroin, P.A., Palmiter, R.D., 2000. Seizures and neuronal damage in mice lacking vesicular zinc. Epilepsy Res 39, 153-169.

21. Cole, T.B., Wenzel, H.J., Kafer, K.E., Schwartzkroin, P.A., Palmiter, R.D., 1999. Elimination of zinc from synaptic vesicles in the intact mouse brain by disruption of the ZnT3 gene. Proc Natl Acad Sci U S A 96, 1716-1721.
22. Colvin, R.A., Holmes, W.R., Fontaine, C.P., Maret, W., 2010. Cytosolic zinc buffering and muffling: their role in intracellular zinc homeostasis. Metallomics 2, 306-317.
23. De Stefani, D., Patron, M., Rizzuto, R., 2015. Structure and function of the mitochondrial calcium uniporter complex. Biochim Biophys Acta 1853, 2006-2011.
24. Devinney, M.J., 2nd, Reynolds, I.J., Dineley, K.E., 2005. Simultaneous detection of intracellular free calcium and zinc using fura-2FF and FluoZin-3. Cell Calcium 37, 225-232.
25. Devinney, M.J., Malaiyandi, L.M., Vergun, O., DeFranco, D.B., Hastings, T.G., Dineley, K.E., 2009. A comparison of Zn2+- and Ca2+-triggered depolarization of liver mitochondria reveals no evidence of Zn2+-induced permeability transition. Cell calcium 45, 447-455.
26. Dineley, K.E., Richards, L.L., Votyakova, T.V., Reynolds, I.J., 2005. Zinc causes loss of membrane potential and elevates reactive oxygen species in rat brain mitochondria. Mitochondrion 5, 55-65.
27. Dominguez, M.I., Blasco-Ibanez, J.M., Crespo, C., Marques-Mari, A.I., Martinez-Guijarro, F.J., 2003. Zinc chelation during non-lesioning overexcitation results in neuronal death in the mouse hippocampus. Neuroscience 116, 791-806.
28. Duchen, M.R., Surin, A., Jacobson, J., 2003. Imaging mitochondrial function in intact cells. Methods Enzymol 361, 353-389.

29. Dugan, L.L., Sensi, S.L., Canzoniero, L.M., Handran, S.D., Rothman, S.M., Lin, T.S., Goldberg M.P., Choi D.W., 1995. Mitochondrial production of reactive oxygen species in cortical neurons following exposure to N-methyl-D-aspartate. J Neurosci 15, 6377-6388.
30. Erickson, J.C., Hollopeter, G., Thomas, S.A., Froelick, G.J., Palmiter, R.D., 1997. Disruption of the metallothionein-III gene in mice: analysis of brain zinc, behavior, and neuron vulnerability to metals, aging, and seizures. J Neurosci 17, 1271-1281.
31. Frederickson, C.J., Hernandez, M.D., McGinty, J.F., 1989. Translocation of zinc may contribute to seizure-induced death of neurons. Brain Res 480, 317-321.
32. Frederickson, C.J., Rampy, B.A., Reamy-Rampy, S., Howell, G.A., 1992. Distribution of histochemically reactive zinc in the forebrain of the rat. J Chem Neuroanat 5, 521-530.
33. Frederickson, C.J., 1989. Neurobiology of zinc and zinc-containing neurons. Int Rev Neurobiol 31, 145-238.
34. Frederickson, C.J., Giblin, L.J., Krezel, A., McAdoo, D.J., Mueller, R.N., Zeng, Y., Balaji, R.V., Masalha, R., Thompson, R.B., Fierke, C.A., Sarvey, J.M., de Valdenebro, M., Prough, D.S., Zornow, M.H., 2006. Concentrations of extracellular free zinc (pZn)e in the central nervous system during simple anesthetization, ischemia and reperfusion. Exp Neurol 198, 285-293.
35. Frederickson, C.J., Hernandez, M.D., McGinty, J.F., 1989. Translocation of zinc may contribute to seizure-induced death of neurons. Brain Res 480, 317-321.
36. Freund, W.D., Reddig, S., 1994. AMPA/Zn(2+)-induced neurotoxicity in rat primary cortical cultures: involvement of L-type calcium channels. Brain Res 654, 257-264.

37. Friberg, H., Wieloch, T., 2002. Mitochondrial permeability transition in acute neurodegeneration. Biochimie 84, 241-250.
38. Gazaryan, I.G., Krasinskaya, I.P., Kristal, B.S., Brown, A.M., 2007. Zinc irreversibly damages major enzymes of energy production and antioxidant defense prior to mitochondrial permeability transition. J Biol Chem 282, 24373-24380.
39. Gee, K.R., Zhou, Z.L., Ton-That, D., Sensi, S.L., Weiss, J.H., 2002. Measuring zinc in living cells. A new generation of sensitive and selective fluorescent probes. Cell calcium 31, 245-251.
40. Gorter, J.A., Petrozzino, J.J., Aronica, E.M., Rosenbaum, D.M., Opitz, T., Bennett, M.V., Connor, J.A., Zukin, R.S., 1997. Global ischemia induces downregulation of Glur2 mRNA and increases AMPA receptor-mediated Ca2+ influx in hippocampal CA1 neurons of gerbil. J Neurosci 17, 6179-6188.
41. Granzotto, A., Sensi, S.L., 2015. Intracellular zinc is a critical intermediate in the excitotoxic cascade. Neurobiol Dis 81, 25-37.
42. Halestrap, A.P., 2006. Calcium, mitochondria and reperfusion injury: a pore way to die. Biochemical Society transactions 34, 232-237.
43. Howell, G.A., Welch, M.G., Frederickson, C.J., 1984. Stimulation-induced uptake and release of zinc in hippocampal slices. Nature 308, 736-738.
44. Hoyte, L., Barber, P.A., Buchan, A.M., Hill, M.D., 2004. The rise and fall of NMDA antagonists for ischemic stroke. Current molecular medicine 4, 131-136.
45. Ikonomidou, C., Turski, L., 2002. Why did NMDAR antagonists fail clinical trials for stroke and traumatic brain injury? The Lancet. Neurology 1, 383-386.

46. Ji, S.G., Medvedeva, Y.V., Wang, H.L., Yin, H.Z., Weiss, J.H., 2019. Mitochondrial Zn(2+) Accumulation: A Potential Trigger of Hippocampal Ischemic Injury. The Neuroscientist : a review journal bringing neurobiology, neurology and psychiatry 25, 126-138.
47. Ji, S.G., Weiss, J.H., 2018. Zn(2+)-induced disruption of neuronal mitochondrial function: Synergism with Ca(2+), critical dependence upon cytosolic Zn(2+) buffering, and contributions to neuronal injury. Exp Neurol 302, 181-195.
48. Jia, Y., Jeng, J.M., Sensi, S.L., Weiss, J.H., 2002. Zn2+ currents are mediated by calcium-permeable AMPA/kainate channels in cultured murine hippocampal neurones. J Physiol 543, 35-48.
49. Jiang, D., Sullivan, P.G., Sensi, S.L., Steward, O., Weiss, J.H., 2001. Zn(2+) induces permeability transition pore opening and release of pro-apoptotic peptides from neuronal mitochondria. J Biol Chem 276, 47524-47529.
50. Jiang, L.J., Vasak, M., Vallee, B.L., Maret, W., 2000. Zinc transfer potentials of the alpha - and beta-clusters of metallothionein are affected by domain interactions in the whole molecule. Proc Natl Acad Sci U S A 97, 2503-2508.
51. Kambe, T., Hashimoto, A., Fujimoto, S., 2014. Current understanding of ZIP and ZnT zinc transporters in human health and diseases. Cell Mol Life Sci 71, 3281-3295.
52. Kamer, K.J., Mootha, V.K., 2015. The molecular era of the mitochondrial calcium uniporter. Nature reviews. Molecular cell biology 16, 545-553.
53. Kauppinen, T.M., Swanson R.A., 2007. The role of poly(ADP-ribose) polymerase-1 in CNS disease. Neuroscience 145, 1267-1272.

54. Kerchner, G.A., Canzoniero, L.M., Yu, S.P., Ling, C., Choi, D.W., 2000. Zn2+ current is mediated by voltage-gated Ca2+ channels and enhanced by extracellular acidity in mouse cortical neurones. J Physiol 528 Pt 1, 39-52.
55. Kim, Y.H., Koh, J.Y., 2002. The role of NADPH oxidase and neuronal nitric oxide synthase in zinc-induced poly(ADP-ribose) polymerase activation and cell death in cortical culture. Exp Neurol 177, 407-418.
56. Kirino, T., 1982. Delayed neuronal death in the gerbil hippocampus following ischemia. Brain Res 239, 57-69.
57. Koh, J.Y., Choi, D.W., 1994. Zinc toxicity on cultured cortical neurons: involvement of N-methyl-D-aspartate receptors. Neuroscience 60: 1049-1057.
58. Koh, J.Y., Suh, S.W., Gwag, B.J., He, Y.Y., Hsu, C.Y., Choi, D.W., 1996. The role of zinc in selective neuronal death after transient global cerebral ischemia. Science 272, 1013-1016.
59. Koh, J.Y., Choi, D.W., 1987. Quantitative determination of glutamate mediated cortical neuronal injury in cell culture by lactate dehydrogenase efflux assay. Journal of neuroscience methods 20, 83-90.
60. Lafon-Cazal, M., Pietri, S., Culcasi, M., Bockaert, J., 1993. NMDA-dependent superoxide production and neurotoxicity. Nature 364, 535-537.
61. Lee, J.Y., Cole, T.B., Palmiter, R.D., Koh, J.Y., 2000. Accumulation of zinc in degenerating hippocampal neurons of ZnT3-null mice after seizures: evidence against synaptic vesicle origin. J Neurosci 20, RC79.

62. Lee, J.Y., Kim, J.H., Palmiter, R.D., Koh, J.Y., 2003. Zinc released from metallothionein-iii may contribute to hippocampal CA1 and thalamic neuronal death following acute brain injury. Exp Neurol 184, 337-347.
63. Lerma, J., Morales, M., Ibarz, J.M., Somohano, F., 1994. Rectification properties and Ca2+ permeability of glutamate receptor channels in hippocampal cells. Eur J Neurosci 6, 1080-1088.
64. Li, Y., Hough, C.J., Suh, S.W., Sarvey, J.M., Frederickson, C.J., 2001. Rapid translocation of Zn(2+) from presynaptic terminals into postsynaptic hippocampal neurons after physiological stimulation. Journal of neurophysiology 86, 2597-2604.
65. Link, T.A., von Jagow, G., 1995. Zinc ions inhibit the QP center of bovine heart mitochondrial bc1 complex by blocking a protonatable group. J Biol Chem 270, 25001-25006.
66. Malaiyandi, L.M., Dineley, K.E., Reynolds, I.J., 2004. Divergent consequences arise from metallothionein overexpression in astrocytes: zinc buffering and oxidant-induced zinc release. Glia 45, 346-353.
67. Malaiyandi, L.M., Vergun, O., Dineley, K.E., Reynolds, I.J., 2005. Direct visualization of mitochondrial zinc accumulation reveals uniporter-dependent and -independent transport mechanisms. J Neurochem 93, 1242-1250.
68. Marchi, S., Pinton, P., 2014. The mitochondrial calcium uniporter complex: molecular components, structure and physiopathological implications. J Physiol 592, 829-839.
69. Maret, W., 2015. Analyzing free zinc(II) ion concentrations in cell biology with fluorescent chelating molecules. Metallomics 7, 202-211.

70. Maret, W., 1995. Metallothionein/disulfide interactions, oxidative stress, and the mobilization of cellular zinc. Neurochemistry international 27, 111-117.
71. Maret, W., 2011. Redox biochemistry of mammalian metallothioneins. Journal of biological inorganic chemistry : JBIC : a publication of the Society of Biological Inorganic Chemistry 16, 1079-1086.
72. Maret, W., Vallee, B.L., 1998. Thiolate ligands in metallothionein confer redox activity on zinc clusters. Proc Natl Acad Sci U S A 95, 3478-3482.
73. McLaughlin, B., Pal, S., Tran, M.P., Parsons, A.A., Barone, F.C., Erhardt, J.A., Aizenman, E., 2001. p38 activation is required upstream of potassium current enhancement and caspase cleavage in thiol oxidant-induced neuronal apoptosis. J Neurosci 21, 3303-3311.
74. Medvedeva, Y.V., Ji, S.G., Yin, H.Z., Weiss, J.H., 2017. Differential Vulnerability of CA1 versus CA3 Pyramidal Neurons After Ischemia: Possible Relationship to Sources of Zn2+ Accumulation and Its Entry into and Prolonged Effects on Mitochondria. J Neurosci 37, 726-737.
75. Medvedeva, Y.V., Lin, B., Shuttleworth, C.W., Weiss, J.H., 2009. Intracellular Zn2+ accumulation contributes to synaptic failure, mitochondrial depolarization, and cell death in an acute slice oxygen-glucose deprivation model of ischemia. J Neurosci 29, 1105-1114.
76. Medvedeva, Y.V., Weiss, J.H., 2014. Intramitochondrial Zn(2+) accumulation via the Ca(2+) uniporter contributes to acute ischemic neurodegeneration. Neurobiol Dis 68, 137-144.

77. Meinicke, A.R., Bechara, E.J., Vercesi, A.E., 1998. Ruthenium red-catalyzed degradation of peroxides can prevent mitochondrial oxidative damage induced by either tert-butyl hydroperoxide or inorganic phosphate. Archives of biochemistry and biophysics 349, 275-280.
78. Murgia, M., Rizzuto, R., 2015. Molecular diversity and pleiotropic role of the mitochondrial calcium uniporter. Cell calcium 58, 11-17.
79. Murphy, E., Pan, X., Nguyen, T., Liu, J., Holmstrom, K.M., Finkel, T., 2014. Unresolved questions from the analysis of mice lacking MCU expression. Biochemical and biophysical research communications 449, 384-385.
80. Nicholls, D.G., Budd, S.L., 2000. Mitochondria and neuronal survival. Physiol Rev 80, 315-360.
81. Nichols, M., Elustondo, P.A., Warford, J., Thirumaran, A., Pavlov, E.V., Robertson, G.S., 2017. Global ablation of the mitochondrial calcium uniporter increases glycolysis in cortical neurons subjected to energetic stressors. Journal of cerebral blood flow and metabolism : official journal of the International Society of Cerebral Blood Flow and Metabolism 37, 3027-3041.
82. Noh, K.M., Koh, J.Y., 2000. Induction and activation by zinc of NADPH oxidase in cultured cortical neurons and astrocytes. J Neurosci 20, RC111.
83. Noh, K.M., Yokota, H., Mashiko, T., Castillo, P.E., Zukin, R.S., Bennett, M.V., 2005. Blockade of calcium-permeable AMPA receptors protects hippocampal neurons against global ischemia-induced death. Proc Natl Acad Sci U S A 102, 12230-12235.

84. Ogoshi, F., Weiss, J.H., 2003. Heterogeneity of Ca2+-permeable AMPA/kainate channel expression in hippocampal pyramidal neurons: Fluorescence imaging and immunocytochemical assessment. J Neurosci 23, 10521-10530

85. Ordy, J.M., Wengenack, T.M., Bialobok, P., Coleman, P.D., Rodier, P., Baggs, R.B., Dunlap, W.P., Kates, B., 1993. Selective vulnerability and early progression of hippocampal CA1 pyramidal cell degeneration and GFAP-positive astrocyte reactivity in the rat four-vessel occlusion model of transient global ischemia. Exp Neurol 119, 128-139.

86. Pan, X., Liu, J., Nguyen, T., Liu, C., Sun, J., Teng, Y., Fergusson, M.M., Rovira, II, Allen, M., Springer, D.A., Aponte, A.M., Gucek, M., Balaban, R.S., Murphy, E., Finkel, T., 2013. The physiological role of mitochondrial calcium revealed by mice lacking the mitochondrial calcium uniporter. Nature cell biology 15, 1464-1472.

87. Pivovarova, N.B., Stanika, R.I., Kazanina, G., Villanueva, I., Andrews, S.B., 2014. The interactive roles of zinc and calcium in mitochondrial dysfunction and neurodegeneration. J Neurochem 128, 592-602.

88. Randall, R.D., Thayer, S.A., 1992. Glutamate-induced calcium transient triggers delayed calcium overload and neurotoxicity in rat hippocampal neurons. J Neurosci 12, 1882-1895.

89. Reynolds, I.J., Hastings, T.G., 1995. Glutamate induces the production of reactive oxygen species in cultured forebrain neurons following NMDAR activation. J Neurosci 15, 3318-3327.

90. Rothman, S.M., Olney, J.W., 1986. Glutamate and the pathophysiology of hypoxic--ischemic brain damage. Ann Neurol 19, 105-111.

91. Saris, N.E., Niva, K., 1994. Is Zn2+ transported by the mitochondrial calcium uniporter? FEBS Lett 356, 195-198.

92. Sattler, R., Xiong, Z., Lu, W.Y., Hafner, M., MacDonald, J.F., Tymianski, M., 1999. Specific coupling of NMDAR activation to nitric oxide neurotoxicity by PSD-95 protein. Science 284, 1845-1848.

93. Sensi, S.L., Paoletti, P., Koh J.Y., Aizenman, E., Bush, A.I., Hershfinkel, M., 2011. The neurophysiology and pathology of brain zinc. J Neurosci 31, 16076-16085.

94. Sensi, S.L., Ton-That, D., Sullivan, P.G., Jonas, E.A., Gee, K.R., Kaczmarek, L.K., Weiss, J.H., 2003. Modulation of mitochondrial function by endogenous Zn2+ pools. Proc Natl Acad Sci U S A 100, 6157-6162.

95. Sensi, S.L., Ton-That, D., Weiss, J.H., 2002. Mitochondrial sequestration and Ca(2+)-dependent release of cytosolic Zn(2+) loads in cortical neurons. Neurobiology of disease 10, 100-108.

96. Sensi, S.L., Yin, H.Z., Carriedo, S.G., Rao, S.S., Weiss, J.H., 1999. Preferential Zn2+ influx through Ca2+-permeable AMPA/kainate channels triggers prolonged mitochondrial superoxide production. Proc Natl Acad Sci U S A 96, 2414-2419.

97. Sensi, S.L., Yin, H.Z., Weiss, J.H., 1999b. Glutamate triggers preferential Zn2+ flux through Ca2+ permeable AMPA channels and consequent ROS production. Neuroreport 10, 1723-1727.

98. Sensi, S.L., Yin, H.Z., Weiss, J.H., 2000. AMPA/kainate receptor-triggered Zn2+ entry into cortical neurons induces mitochondrial Zn2+ uptake and persistent mitochondrial dysfunction. The European journal of neuroscience 12, 3813-3818.

99. Shuttleworth, C.W., Weiss, J.H., 2011. Zinc: new clues to diverse roles in brain ischemia. Trends Pharmacol Sci 32, 480-486.

100. Siesjo, B.K., 1988. Historical overview. Calcium, ischemia, and death of brain cells. Ann N Y Acad Sci 522, 638-661.

101. Skulachev, V.P., Chistyakov, V.V., Jasaitis, A.A., Smirnova, E.G., 1967. Inhibition of the respiratory chain by zinc ions. Biochemical and biophysical research communications 26, 1-6.

102. Slepchenko, K.G., Lu, Q., Li, Y.V., 2017. Cross talk between increased intracellular zinc (Zn2+) and accumulation of reactive oxygen species in chemical ischemia. American journal of physiology. Cell physiology 313, C448-C459.

103. Sloviter, R.S., 1985. A selective loss of hippocampal mossy fiber Timm stain accompanies granule cell seizure activity induced by perforant path stimulation. Brain Res 330, 150-153.

104. Stork, C.J., Li, Y.V., 2006. Intracellular zinc elevation measured with a "calcium-specific" indicator during ischemia and reperfusion in rat hippocampus: a question on calcium overload. J Neurosci 26, 10430-10437.

105. Sugawara, T., Fujimura, M., Morita-Fujimura, Y., Kawase, M., Chan, P.H., 1999. Mitochondrial release of cytochrome c corresponds to the selective vulnerability of hippocampal CA1 neurons in rats after transient global cerebral ischemia. J Neurosci 19, RC39.

106. Suh, S.W., Chen, J.W., Motamedi, M., Bell, B., Listiak, K., Pons, N.F., Danscher, G., Frederickson, C.J., 2000. Evidence that synaptically-released zinc contributes to neuronal injury after traumatic brain injury. Brain Res 852, 268-273.

107. Tanaka, S., Kondo, S., Tanaka, T., Yonemasu, Y., 1988. Long-term observation of rats after unilateral intra-amygdaloid injection of kainic acid. Brain Res 463, 163-167.

108. Tapia, R., Velasco, I., 1997. Ruthenium red as a tool to study calcium channels, neuronal death and the function of neural pathways. Neurochemistry international 30, 137-147.

109. Thibault, O., Landfield, P.W., 1996. Increase in single L-type calcium channels in hippocampal neurons during aging. Science 272, 1017-1020.

110. Tonder, N., Johansen, F.F., Frederickson, C.J., Zimmer, J., Diemer, N.H., 1990. Possible role of zinc in the selective degeneration of dentate hilar neurons after cerebral ischemia in the adult rat. Neurosci Lett 109, 247-252.

111. Ueno, S., Tsukamoto, M., Hirano, T., Kikuchi, K., Yamada, M.K., Nishiyama, N., Nagano, T., Matsuki, N., Ikegaya, Y., 2002. Mossy fiber Zn2+ spillover modulates heterosynaptic N-methyl-D-aspartate receptor activity in hippocampal CA3 circuits. The Journal of cell biology 158, 215-220.

112. Velasco, I., Tapia, R., 2000. Alterations of intracellular calcium homeostasis and mitochondrial function are involved in ruthenium red neurotoxicity in primary cortical cultures. Journal of neuroscience research 60, 543-551.

113. Vogt, K., Mellor, J., Tong, G., Nicoll, R., 2000. The actions of synaptically released zinc at hippocampal mossy fiber synapses. Neuron 26, 187-196.

114. Wang, G.J., Thayer, SA., 1996. Sequestration of glutamate-induced Ca2+ loads by mitochondria in cultured rat hippocampal neurons. J Neurophysiol 76, 1611-1621.

115. Wei, G., Hough, C.J., Li, Y., Sarvey, J.M., 2004. Characterization of extracellular accumulation of Zn2+ during ischemia and reperfusion of hippocampus slices in rat. Neuroscience 125, 867-877.

116. Weiss, J.H., Hartley, D.M., Koh, J.Y., Choi, D.W., 1993. AMPA receptor activation potentiates zinc neurotoxicity. Neuron 10, 43-49.

117. Weiss, J.H., Sensi, S.L., Koh, J.Y., 2000. Zn(2+): a novel ionic mediator of neural injury in brain disease. Trends Pharmacol Sci 21, 395-401.

118. White, R.J., Reynolds, I.J., 1997. Mitochondria accumulate Ca2+ following intense glutamate stimulation of cultured rat forebrain neurones. J Physiol 498 (Pt 1), 31-47.

119. Wudarczyk, J., Debska, G., Lenartowicz, E., 1999. Zinc as an inducer of the membrane permeability transition in rat liver mitochondria. Archives of biochemistry and biophysics 363, 1-8.

120. Yao, J., Irwin, R.W., Zhao, L., Nilsen, J., Hamilton, R.T., Brinton, R.D., 2009. Mitochondrial bioenergetic deficit precedes Alzheimer's pathology in female mouse model of Alzheimer's disease. Proc Natl Acad Sci U S A 106, 14670-14675.

121. Yeh, C.Y., Bulas, A.M., Moutal, A., Saloman, J.L., Hartnett, K.A., Anderson, C.T., Tzounopoulos, T., Sun, D., Khanna, R., Aizenman, E., 2017. Targeting a Potassium Channel/Syntaxin Interaction Ameliorates Cell Death in Ischemic Stroke. J Neurosci 37, 5648-5658.

122. Yin H.Z., Sensi S.L., Carriedo S.G., Weiss J.H., 1999. Dendritic localization of Ca(2+)-permeable AMPA/kainate channels in hippocampal pyramidal neurons. J Comp Neurol 409, 250-260.

123. Yin, H., Turetsky, D., Choi, D.W., Weiss, J.H., 1994. Cortical neurones with Ca2+ permeable AMPA/kainate channels display distinct receptor immunoreactivity and are GABAergic. Neurobiology of disease 1, 43-49.

124. Yin, H.Z., Sensi, S.L., Ogoshi, F., Weiss, J.H., 2002. Blockade of Ca2+-permeable AMPA/kainate channels decreases oxygen-glucose deprivation-induced Zn2+ accumulation and neuronal loss in hippocampal pyramidal neurons. J Neurosci 22, 1273-1279.

125. Yin, H.Z., Wang, H.L., Ji, S.G., Medvedeva, Y.V., Tian, G., Bazrafkan, A.K., Maki, N.Z., Akbari, Y., Weiss, J.H., 2019. Rapid Intramitochondrial Zn2+ Accumulation in CA1 Hippocampal Pyramidal Neurons After Transient Global Ischemia: A Possible Contributor to Mitochondrial Disruption and Cell Death. Journal of neuropathology and experimental neurology 78, 655-664.

126. Yin, H.Z., Weiss, J.H., 1995. Zn(2+) permeates Ca(2+) permeable AMPA/kainate channels and triggers selective neural injury. Neuroreport 6, 2553-2556.